Material Science and Technology Division

Propulsion Materials Program
Quarterly Progress Report for
April through June 2011

David P. Stinton
Technical Project Manager

Prepared for
U.S. Department of Energy
Assistant Secretary for Energy Efficiency and Renewable Energy
Office of Vehicle Technologies Program
VT 05 04 000

Prepared by the
OAK RIDGE NATIONAL LABORATORY
Oak Ridge, Tennessee 37831-6066
Managed by
UT-Battelle, LLC
for the Department of Energy
Under contract DE-AC05-00OR22725

CONTENTS

Project 18516 – Materials for Hybrid and Electric Drive Systems

Agreement 23279 - Improved Organics for Power Electronics and Electric Motors *(ORNL)*

Agreement 23278 - Low-Cost Direct Bonded Aluminum (DBA) Substrates *(ORNL)*

Agreement 19201 – MBD Non-Rare Earth Magnetic Materials *(ORNL)*

Project 18518 – Materials for High Efficiency Engines

Agreement 11752 – Materials for HCCI Engines *(ORNL)*

Agreement 13329 – Design Optimization of Piezoceramic Multilayer Actuators for Heavy Duty Diesel Engine Fuel Injectors *(ORNL)*

Agreement 15050 – Evaluation of Materials via ACERT Engine *(ORNL)*

Agreement 16303 – Materials for High Pressure Fuel Injection Systems *(ORNL)*

Agreement 16304 – Materials for Advanced Engine Valve Train *(ORNL)*

Agreement 17257 – Materials for Advanced Turbocharger Design *(ORNL)*

Agreement 17894 – NDE for ACERT Engine Components *(ANL)*

Agreement 18570 – Engine Materials Compatibility with Alternate Fuels *(ORNL)*

Agreement 18571 – Materials Issues Associated with EGR Systems *(ORNL)*

Agreement 19202 – Titanium Friction and Wear *(ORNL)*

Agreement 23284 – Friction Reduction Through Surface Modification *(ORNL)*

Agreement 23285 - Efficiency Implications of Advanced Materials in Advanced Combustion Internal Engines *(ORNL)*

Project 18519 – Materials for Exhaust and Energy Recovery

Agreement 9130 – Catalyst Characterization *(ORNL)*

Agreement 10461 – Durability of Diesel Engine Particulate Filters *(ORNL)*

Agreement 10635 – Catalysts via First Principles *(ORNL)*

Agreement 19214 - Biofuels Impact on Diesel Particulate Filters *(ORNL)*

Agreement 20091 – Electrically Regenerated DPF Material *(ORNL)*

<u>Project 18865 – Materials by Design</u>

Agreement 9105 – Characterization of Catalyst Microstructures *(ORNL)*

Agreement 14957 – Thermoelectric Mechanical Reliability *(ORNL)*

Agreement 16308 – MBD - Thermoelectrics Theory and Structure *(ORNL)*

Agreement 23279: Improved Organics for Power Electronics and Electric Motors

A. A. Wereszczak, C. W. Ayers, R. H. Wiles, M. K. Ferber, and H. Wang
Oak Ridge National Laboratory

Objective/Scope

Identify lower-cost and better-performing organic compounds for dielectric and thermal management applications in power electronics and electric motors. Candidate and new organic compounds (e.g., epoxy molded compounds or EMCs) will be characterized and developed to promote low-cost fabrication, volume reduction, mechanically resilience, and improved and alternative thermal management exploitation. They include compounds presently used in dielectrics in power electronic devices, potting compounds used with capacitors, and pottings used in motors. For dielectrics, improved performance represents a higher-temperature capability and the sustainment of dielectric and gel-like mechanical damping properties under thermal cycling and vibratory conditions. For potting compounds used with capacitors or motors, interest exists to identify alternatives that have higher thermal conductivity (or that enhance the thermal conductivity of existing compounds) or that benefit structural or damping performance without compromising thermal performance.

Technical Highlights

The thermal conductivities were measured with a wide variety of organic molding and casting compounds from motor housings, film capacitors, and the exteriors of power modules. A hot disk thermal constants analyzer was used. A measured thermal conductivity of approximately 0.3 W/mK was typical for all those materials.

A finite element model was constructed of a film capacitor where the thermal conductivity of its surrounding (exterior) epoxy was varied to examine what the internal temperature was for a fixed Wattage of heat generation. Increasing the thermal conductivity by one order of magnitude (e.g., 0.5 to 5 W/mK) produced a large temperature decrease in the interior. This result was informative because it gave our project a goal to seek for thermal conductivity increase. Similar thermal models are being constructed for epoxy compounds for motors and the exterior of a power electronic module, and a similar observation is anticipated for both those components.

A computer program was completed that constructs an image of particle-containing matrix or an epoxy molding compound. An arbitrary or measured particle size distribution and particle volume fraction are inputted. The image is inputted into ORNL's µ-FEA software to create an ANSYS input file that enables the reconstruction of the composite in ANSYS. A transient thermal analysis is then run and the composites thermal diffusivity and thermal conductivity are estimate. This analysis is assisting our efforts in examining the roles of particle size distribution and volume fraction on thermal conductivity and their optimizations to produce maximum thermal conductivity.

A new epoxy molding compound containing (elemental) silicon as the filler is under development. An invention disclosure has been filed. SolEpoxy, an epoxy molding

compound manufacturer with a long history, is under contract to make Si-EMCs for this project. Completed systems should be available in Q4 and thermal properties will be measured.

Status of FY 2011 Milestones

1. Establish baselines by measuring thermal properties of unused and serviced organics of each of three classes of organics. [Jun11] *Will be completed in Q4 because initial funding commenced during Q2.*
2. Develop test methods that representatively thermal cycle each of the three classes of organic materials. [Sep11] *On schedule.*

Communications/Visits/Travel

- A poster describing this project was presented 11 May 2011 at the DOE Annual Merit Review, Arlington, VA.
- Wereszczak visited SolEpoxy (Olean, NY) on 14 June 2011 to discuss potential collaborations.
- Several technical discussions have occurred with Mossey Creek's J. Carberry about epoxy molding compounds.
- Numerous discussions held with NTRC staff members (Ayers, Wiles, and Marlino).

Problems Encountered

Funding for project did not begin until Q2.

Publications/Presentations/Awards

An invention disclosure was filed. A. A. Wereszczak and J. Carberry, "Thermally-Conductive, Electrically-Insulating, Silicon-Containing Epoxy Molding Compounds (Si-EMCs)," DOE S-Number S-124,118, Invention Disclosure Number 201102561, February 28, 2011.

References

None.

Agreement 23278: Low-Cost Direct Bonded Aluminum (DBA) Substrates

H. -T. Lin and A. A. Wereszczak
Oak Ridge National Laboratory

Objective/Scope

This project seeks to develop low-cost, high quality, and thermomechanically robust direct-bonded aluminum (DBA) substrates. Low-cost DBA substrates will lessen the cost of the inverter insulated gate bipolar transistor (IGBT) power modules while concomitantly sustaining or improving thermal management and improving thermomechanical reliability. Compared to copper and DBC substrates, aluminum has a lower elastic modulus so it imparts a lower stress on the ceramic substrate it sandwiches, and this contributes to improved mechanical reliability of the entire substrate. Wire and ribbon for bonding in power electronic modules tends to be aluminum, so the apparent coefficient of thermal expansion of DBAs is compatible with them unlike DBCs. The use of a DBA substrate will also lessen the weight up to 50% compared to presently used DBC substrates, and this would contribute to the weight reduction goals of the inverter and converter in the APEEM program as well.

Technical Highlights

Microstructure characterizations of commercially available direct-bonded aluminum (DBA) and direct bonded copper (DBC) substrates were completed during this quarterly reporting period. Figure 1 shows the typical microstructure of DBA substrates acquired from two commercial companies (designated as DBA-A and DBA-B) in Japan. Both substrates have the aluminum sheets that are cladded on both sides of the aluminum nitride (AlN) substrate, and the interface is very intact and coherent without any type of defects. At a higher magnification the commercial DBA-A substrate shows the presence of an interfacial layer (~20 µm) with random distribution of Al-Si particles between the Al and AlN (Fig. A2), suggesting the use of Al-Si alloy for the bonding manufacturing process. On the other hand, the presence of Al-Si layer is not very apparent in the commercial DBA-B substrate (Fig. B2). Note that the light secondary phase in the AlN ceramic substrate is with the chemical elements of Y, Al, and O, consistent with the Y_2O_3 and Al_2O_3 additives typically used in the sintering of AlN ceramics. Figure 2 shows the microstructure of a commercial DBC substrate. There is a distinctive interfacial layer (~50 µm) between Cu and AlN ceramic with chemical composition of Ag, Cu, Al, and Mg, which suggests the use of Ag-containing material for the bonding of this DBC. Specimens of these commercial DBA and DBA substrates will be prepared and tested under a specified thermal cycle condition (e.g., between -50°C and 200°C) to provide a database for reference.

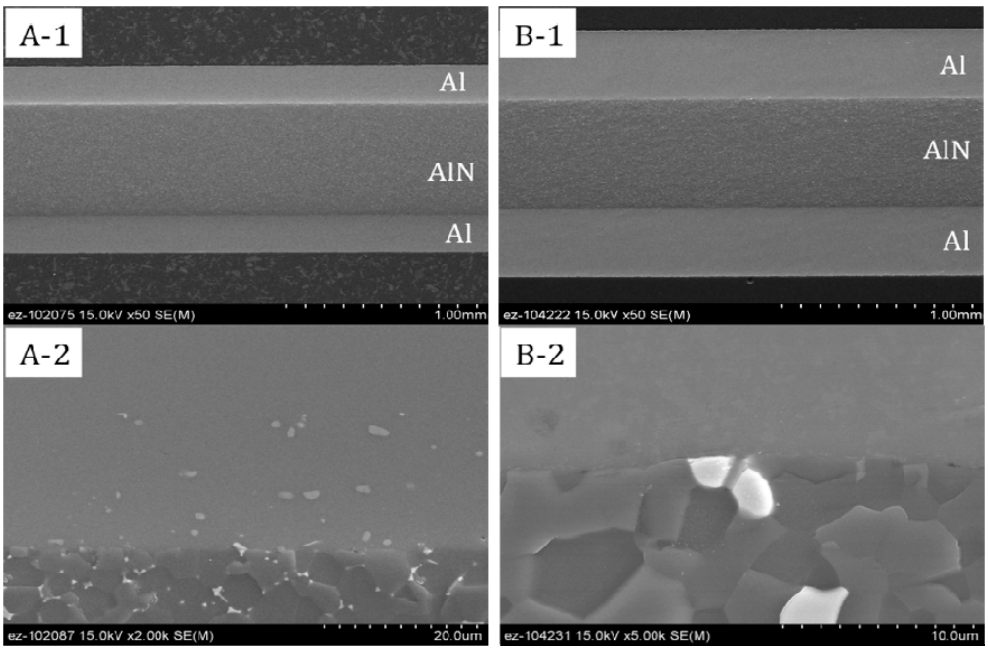

Figure 1. SEM micrographs of polished cross-section of commercially available DBA substrates. Note aluminum is cladded on both sides of an aluminum nitride ceramic substrate.

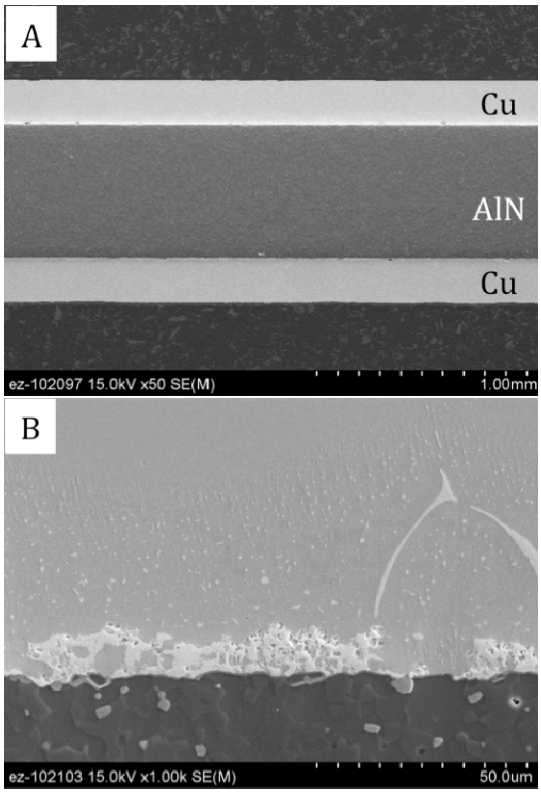

Figure 2. SEM micrographs of polished cross-section of commercially available DBC substrate. Note copper is cladded on both sides of an aluminum nitride ceramic substrate.

The coefficient of thermal expansion (CTE) of commercial Al_2O_3 and AlN substrate was measured and analyzed. These physical properties would be used for modeling the temperature profile and thermomechanical stress under simulated application condition and thus probabilistic reliability prediction. The measured CTE of commercial Al_2O_3 and AlN substrate is 7.5 x 10^{-6}/°C and 4.5 x 10^{-6}/°C, respectively, which are consistent to the reported values of 8.2 x 10^{-6}/°C and 4.5 x 10^{-6}/°C. In addition, results showed that the CTE values of Al_2O_3 were insensitive to the substrate thickness (between 0.64 mm and 53 mm) investigated in this study, suggesting the reproducibility of the data and consistency of the quality of Al_2O_3 material substrates. Properties of Young's modulus and Poisson ratio would be measured and reported in the next quarterly period.

A preliminary trial run to bond the aluminum to both Al_2O_3 and AlN substrates was performed in this reporting period. A commercial Al-12Si brazing paste (designated as DayBraze 729) inquired from Johnson Manufacturing Company, Princeton, Iowa was employed for the preliminary bonding experiment. The Al_2O_3/Al and AlN/Al specimens with Al-12Si brazing paste were hot pressed at 640°C and 15 MPa for 30 minutes in flowing argon environment. Figure 3 shows the photo of the two samples after bonding process. Polished cross sections of both specimens will be prepared and characterized in detailed via SEM/EDAX analysis. Results will be described in the next quarterly report.

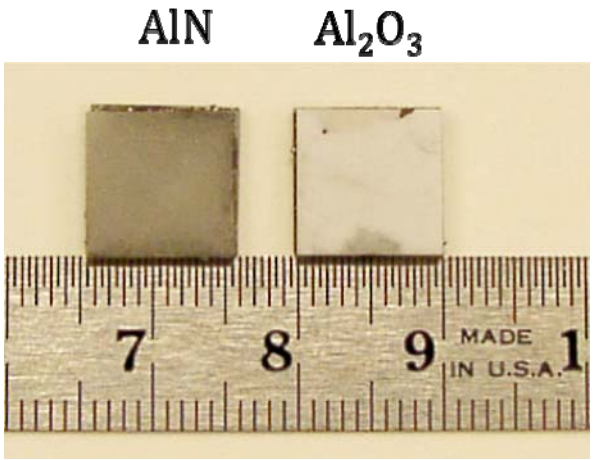

Figure 3. Photograph of Al_2O_3/Al and AlN/Al specimens after preliminary bonding trial run.

Status of FY 2011 Milestones

1. Survey conventional and alternative processing methods to directly bond Al to Al_2O_3 (and AlN). [**April 11**] – On schedule.
2. Down-select processing method most likely to produce high strength bonding. [**Sep 11**] – On schedule.

Communications/Visits/Travel

- Several discussions have occurred with ORNL/NTRC, USCAR EETT, General Motors, and NREL staff members about the plans for this project.

- H. T. Lin attended and presented the poster on this project at DOE Annual Merit Review, Arlington, VA, May 11, 2011.

Problems Encountered

None.

Publications/Presentations/Awards

Poster on this project was presented at DOE Annual Merit Review, Arlington, VA, May 11, 2011

References

None.

Agreement 19201: Non-Rare Earth Magnetic Materials

Michael A. McGuire
Oak Ridge National Laboratory

Objective/Scope

We will examine rare-earth-free chemical systems which hold promise for the discovery of new high-temperature ferromagnets with the large magnetic moments and strong anisotropies required for technologically useful permanent magnet materials. This research will focus on the development of new rare-earth free permanent magnet materials. Understudied chemical systems which are likely to contain materials with properties required for useful ferromagnets (large moments, high Curie temperatures, strong magnetic anisotropy) will be synthesized and characterized. First principle calculations will be performed to aid in the identification of promising target materials and to guide chemical tuning of magnetic properties through element substitutions and alloying. The focus will be on materials based on elements, such as Mn, Fe and Cr, suitable for application in vehicles.

The primary challenge in this work is to obtain high magnetic anisotropy without rare-earth elements, while maintaining high saturation magnetization. The two main sources of anisotropy are magneto-crystalline anisotropy and shape anisotropy. Magneto-crystalline anisotropy is an intrinsic property determined by energy required to rotate a magnetic moment relative to the crystal lattice. Shape anisotropy is an extrinsic property related to the domain structure of individual crystallites. We are targeting intermetallic compounds with large magneto-crystalline anisotropy, which could then be further enhanced by materials processing to optimize magnetic domain configurations. To obtain anisotropic magnetic properties, heavy transition metal elements will be incorporated instead of rare earths.

Technical Highlights

Study of Hf_2Co_{11} based melt-spun materials continued in this Quarter. Samples have been prepared for electron microscopy studies, and magnetization data were collected at high temperatures on several compositions. The results of the high temperature magnetization measurements are shown below in Figure 1.

The results indicate some component of the ribbons has a Curie temperature above 1000 K. Likely this is cobalt metal (T_{Cuire} = 1388 K). Curie temperatures for the “main” phases are seen to be near 800 K, with some variation with composition. Zr containing specimens have the largest magnetization per gram, due in part to the smaller mass of Zr relative to Hf. However, the Hf samples have shown better demagnetization behavior at near room temperature. These results show that study of alloys like $ZrHfCo_{11}$ may be warranted.

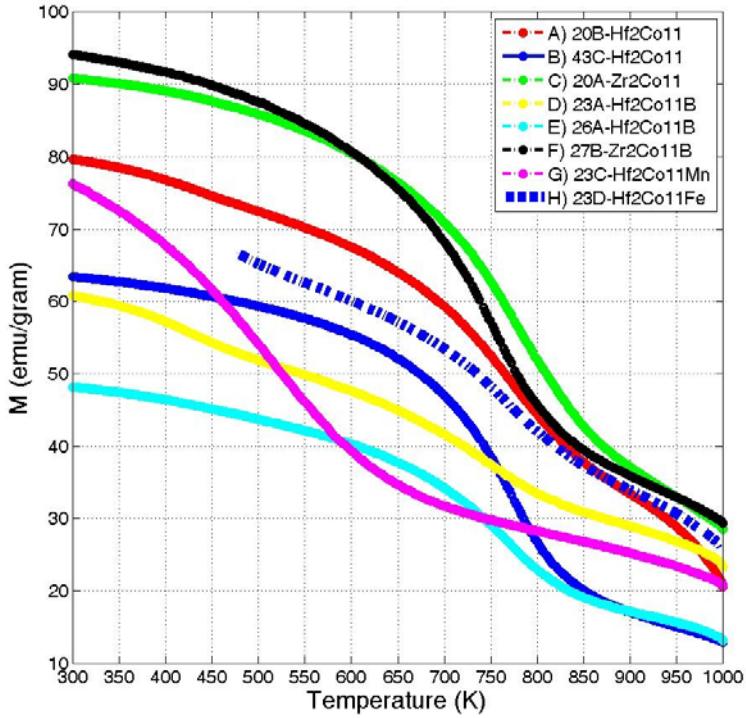

Figure 1. Magnetization vs. temperature for melt-spun ribbons of Hf_2Co_{11}-based materials from 300 – 1000K. The applied field is 3 Tesla.

In other work, following the successful growth of single crystals of materials containing Hf/Zr and Co from molten metal solvents in last Quarter, we have examined many ternary systems using the same technique. The products are still being analyzed; however, promising results have already been observed, including preliminary evidence for a new Fe-rich ternary intermetallic. These efforts will continue into FY2012.

Status of FY 2011 Milestones

Analysis of (Hf/Zr)-(Co/Fe) systems: on schedule. High temperature magnetization measurements further our understanding of these materials.

Interstitial nitrogen in iron compounds: on schedule. For this report, work related to this task focused on crystal growths containing other related light elements and pnictogens.

Communications/Visits/Travel

2011 DOE Hydrogen and Fuel Cells Program and Vehicle Technologies Program Annual Merit Review, May 9-13, 2011.

Problems Encountered

The physical moving of equipment into new laboratories slowed progress during this Quarter.

Publications/Presentations/Awards

Oral presentation at Annual Merit Review, May 11, 2011.

References

None

Agreement 11752: Materials for High Efficiency Engines

Govindarajan Muralidharan, Rick Battiste, and Bruce G. Bunting
Oak Ridge National Laboratory

Objective/Scope

To identify and catalog the materials operating conditions in the HCCI engines and utilize computational design concepts to develop advanced materials for such applications. The primary emphasis of this project is the identification and development of advanced

Technical Highlights

In this quarter, work was continued on Ni-based alloys for valve applications. As reported earlier, using thermodynamic modeling, microstructure evaluation, and mechanical property evaluation, high temperature fatigue was identified as a property of critical interest in Ni-based alloy valve materials for the next generation automotive engines. In order to develop relationships between the microstructures of the alloys and their mechanical properties, high-temperature fatigue property data were obtained on all down-selected alloys as a part of the project. Using the approximate correlation between the fatigue lives obtained using the rotating beam and fully reversed fatigue testing techniques several alloys with required microstructures have been identified as candidates for high temperature valve applications.

Using the microstructures of these alloys as a guide, computational thermodynamics was used to identify additional alloys with microstructure similar to the commercial alloys with desirable properties. In contrast to the commercially available alloys with high Nickel contents (> 75%), the Ni-content in these alloys ranges from about 30 wt. % to 45 wt. % with the potential to achieve comparable properties. This implies that the alloys will be of lower cost but comparable mechanical properties.

Results from the fatigue tests on newly developed alloys HCCI-9 and HCCI-16 showed that new alloys with greater strength levels were required to perform at 870oC and stress levels of 35 Ksi. In this quarter, work continued in designing and fabricating new alloys aimed at increasing the strength levels. Table 1 shows the newly developed alloys and their measured yield strengths at 870°C in the aged condition.

Alloy Designation	**Nickel wt. %**	**Yield Strength at 870°C (Ksi)**
HCCI-41M	~ 40 wt. % Ni	56.3
HCCI-66	~ 44 wt.% Ni	52.7
HCCI-67	~ 44 wt. % Ni	59.2

Results from HCCI-41M and HCCI-67 show that a larger Nickel content is required along with increased content of strengthening elements. Nickel levels of 45-50 wt. % will be targeted in the following alloy development work.

Status of FY 2011 Milestones:

- Present progress detailing results on the high temperature tensile testing and fatigue testing of new ORNL-developed alloys at the Annual Merit Review
    - Completed on time
- Identify a path for the further development of exhaust valve alloys (7/2011)
    - Completed on time.

Communications/Visits/Travel

None

Problems Encountered

None

Publications/Presentations/Awards

None at this time

References

None

Agreement 13329: Design Optimization of Piezoceramic Multilayer Actuators for Heavy Duty Diesel Engine Fuel Injectors

H.-T. Lin, H. Wang, K.-W. Zhang, A. A. Wereszczak,
Oak Ridge National Laboratory

R. Stafford and D. Memering
Cummins Inc.

Objective/Scope

Enable confident utilization of piezo stack actuator in fuel injectors for heavy vehicle diesel engines. The use of such actuators in diesel fuel injectors has the potential to reduce injector response time, provide greater precision and control of the fuel injection event, lessen energy consumption, and reduce emissions. Though piezoelectric function is the obvious primary function of lead zirconate titanate (PZT) ceramic stacks for fuel injectors, their mechanical reliability can be a performance and life limiter because PZT is brittle, lacks high strength, and is susceptible to fatigue and thus slow crack growth process. However, that brittleness, relatively low strength, and fatigue susceptibility can be overcome with the use of appropriate probabilistic ceramic component design methods.

Technical Highlights

1. Mechanical Testing and Characterization of PZT Ceramics

Ball-on-ring (BoR) setup was used to test single-layer PZT materials. The BoR testing is a part of proposed technical tasks to generate the input mechanical data for reliability design of PZT stack in target electric field, temperature, and humidity environments. As reported previously, an oil bath/container has been designed and fabricated to include electronic fluid (FC-40) as a working environment of ball-on-ring setup. The inclusion of FC-40 allows the application of high electric field to the PZT due to the enabled control of the partial discharge. Results on the mechanical strength of KCI at the electric field as high as 2 times of the coercive field revealed no significant difference as compared to the no-electric field (or referred to as open circuit) case. The effects of both FC-40 and the electric field were proposed to be confirmed.

On the other hand, the focus of Cummins on EPCOS piezo stack demands more data on tape-cast PZT. The supply of single-layer PZT specimens by the manufacturer has not been shown to be feasible so far. As a result, alternative approaches have been pursued in this project for PZT mechanical strength characterization. (1) Use Pieso Systems, Inc. (PSI) PZT as a substituting material, particularly, PSI 5A4E and 5H4E. Note these piezoelectric ceramics were also tape-cast, and characterized extensively in

the early stage of this project.[1] The PZT sheets are commercially available and the technique of specimen preparation from the sheets has been well developed. (2) Use 10-layer short PZT stacks or PZT plates extracted from the EPCOS piezo stacks. The desired PZT plates are not readily available again. Chemical dissolving of the supplied PZT stack was demonstrated to be effective for the previous PZT stacks (7mm x 7mm x 30mm) offering a sound base for the current PZT stacks.

PSI PZT specimens from old purchases were used in this task. In the second quarter reporting period, the BoR tests under OC (open circuit) were conducted on PSI 5H4E specimens that had a nominal size of 10mm x 10mm x 0.267mm. The experimental data showed that the aged 5H4E (sheet 4) did not exhibit any degradation in mechanical strength as compared to the as-received fresh specimens (sheet 3). The insensitivity of mechanical strength of PSI 5H4E on aging is distinctly different from the results previously obtained on PSI 5A4E.[2]

Continual efforts were made on testing aged the PSI 5H4E specimens. Study on the effect of electric field on flexure strength under BoR configuration was carried out in this reporting quarter period. New experimental features introduced into the BoR tests include a modified Sawyer-Tower circuit for the in-situ monitoring of electric displacement during the electric loading. The field levels of +/-2Ec (+/-1.6 kV/mm) were tested. Responses of PZT specimens under 10-g preload were measured by the output of the Sawyer-Tower circuit as shown in Fig. 1. The abrupt increase of the output shows the substantial domain activities occurring when the electric field was applied against the poling direction [Fig. 1(b)].

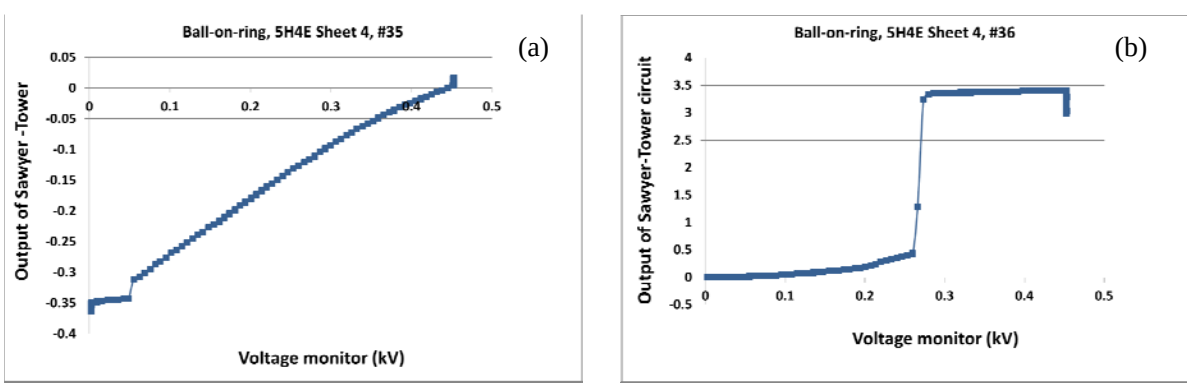

Fig. 1 Electric displacement measured by modified Sawyer-Tower circuit versus input voltage for (a) the applied field is identified in the original poling direction, and (b) the applied field is against the poling direction. The measurement was conducted in ball-on-ring (BoR) setup for PSI 5H4E specimens.

The applied electric field significantly enhanced the flexure strength of the aged PZT as demonstrated in Fig. 2. The increase from around 110 MPa to 150 MPa after the application of +/-2Ec signifies the considerable de-aging effect. The fractography analysis, as shown in Figs. 3 and 4, shows the failure origins feature a mixed mode of intergranular and transgranular fractures that typically initiate from the surface pore or large grain agglomerate.

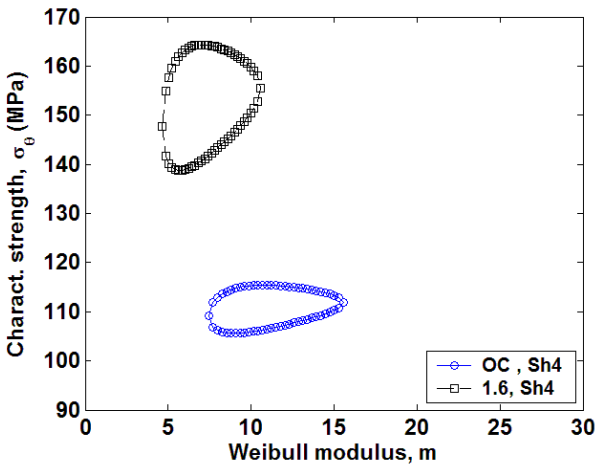

Fig. 2 (a) Confidence ratio rings in 95% confidence level. Data points were obtained for PSI 5H4E (sheet 4) using BoR setup with electric field applied. The setup consists of a steel loading ball of diameter 6.35 mm and steel support ring of 7.44 mm. Displacement rate of the cross head was 0.001 mm/s. The PZT ceramics was on-shelf more than 54 months.

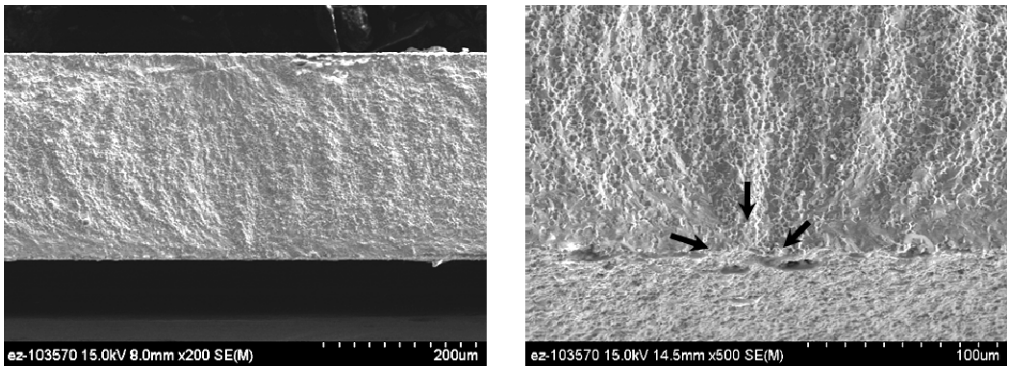

Fig. 3 Images of the failure origin at X200 (left) and X500 (right). Specimen 22 (PSI-5H4E) tested under OC, failure stress 124.887 MPa, transgranular mixed with intergranular fracture near origin (porous region type).

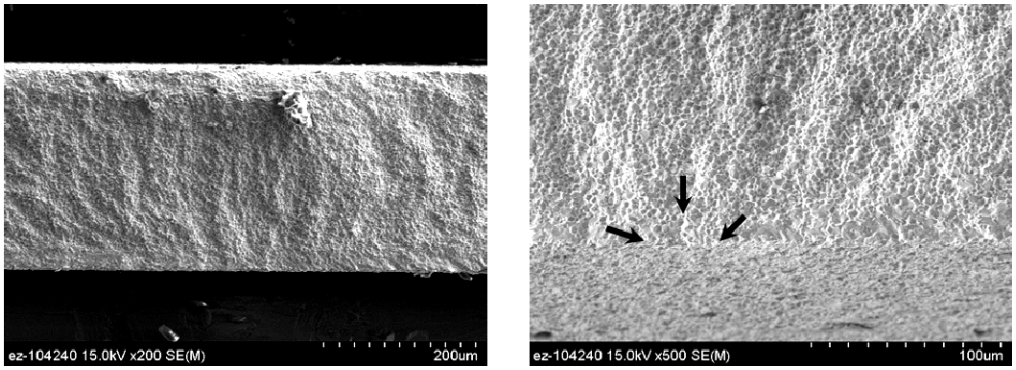

Fig. 4 Images of the failure origin at X200 (left) and X500 (right). Specimen 44 (PSI-5H4E) tested under 2Ec (1.6 kV/mm), failure stress 148.988 MPa, transgranular fractures mostly at origin but intergranular fractures in far field (agglomerate type).

The BoR tests with concurrently applied electric fields were also performed on the aged PSI-5A4E in this quarter of the project. These 5A4E specimens were prepared and obtained in the same period as the 5H4E tested in this and last quarters; namely they were aged more than 54 months before testing.

A controlled loading path was used in electric loading. All the tested specimens were loaded electrically to -3Ec and then to the specified target electric field levels. These target fields include -3Ec, -Ec, -0.0Ec, +1.2Ec, +2.4Ec, and +3.6Ec. The tests were performed in the open air. The previous tests with same setup on the as-received PZT specimens indicated that these tests shall be performed as designed without any significant dielectric breakdown.[2] After the stabilization of electric loading, the mechanical loading was initiated. The results shown in Fig. 5 demonstrate that the effect of electric loading is statistically significant among some data sets. It can be seen that the flexure strength was raised to 165MPa at -3.6 kV/mm and 195MPa at 3.6 kV/mm, respectively. Thus, the level of mechanical strength enhancement at -3Ec is different from that at +3Ec. This observation is somehow different from previous results.[2] Detailed fractographical study and analysis will be conducted to quantify the involved fracture mechanisms.

On the other hand, as the Dynasol 750 did not work effectively in solving individual 10-layer PZT plates, alternatives are under investigation to remove the 10-layer PZT from the supplied stack, including machining. Bomas Machine Specialties, Inc. was contacted for this job in earlier June. They proposed using the method of slicing to cut the 10-layer plates (each sized with 12mm x 12mm x 0.760mm) out of the whole stack (12mm x 12mm x 54 mm). The blade used in their workshop is 0.500mm, which obviously is too thick for slicing the target plates. The search for the effective removal method of individual plates is still undergoing.

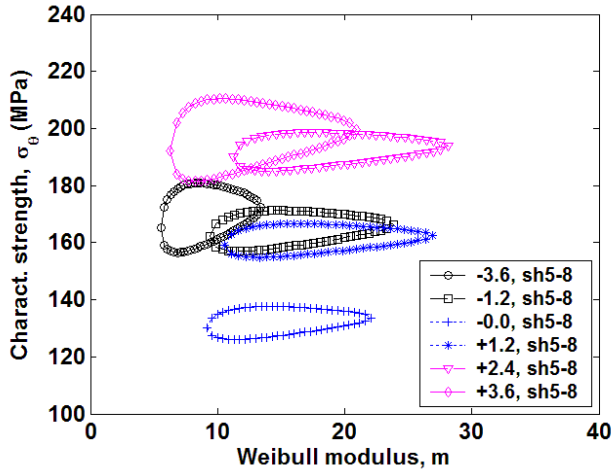

Fig. 5 Confidence ratio rings in 95% confidence level using BoR. The setup consists of a steel loading ball of diameter 6.35 mm and steel support ring of 7.44 mm. Displacement rate of the cross head was 0.001 mm/s. The PZT ceramics was on-shelf more than 54 months. The PZT specimens were loaded to -3Ec and then held at -3Ec or increased to -2Ec, 0 , Ec, 2Ec, and 3Ec.

2. Piezoelectric Testing and Characterization of PZT Stacks

The CRADA meeting held between Cummins and ORNL on 5/24/2011 further confirmed the critical need for testing down-selected PZT stacks manufactured by EPCOS. The stacks are sized with 12mm x 12mm x 54 mm and have a nominal capacitance of 16.15 μF at standard measurement condition, demanding a lot on driving electronics. It was also discussed in the meeting if the Cummins can lend the ORNL a PZT driver for such testing.

One alternative would be to test low-profile PZT actuators, particular double layer or triple layer PZT because these actuators will have a smaller capacitance. As a result, the fatigue can be carried out using the current PZT drivers such as Trek 350M/S. Additional advantage of this alternative is that the test setup can be accomplished using the piezodilatmeter due to the similar geometrical features of test specimens. Understanding obtained from these low-profile PZT actuators can thus be imaged back to the prototype stack in fuel injection system.

Currently, Piezo System, Inc. has 2-piezo layer extenders that can be used for such purpose. Their product T215-A4-NO-303X has a configuration of 2-piezo layer with 3 wire X-poled. It will be PSI-5A4E, single layer 0.005" thick, without reinforcement shim. The plane size will be 303 type: 0.500"x1.25", and total thickness of 2-layer is less than 0.015". The company was contacted for such application also in earlier June. However, they are quite reluctant to provide the products because the middle wire is susceptible to

the short circuit because of the thin individual layers (0.005"). It seems that other approaches need to be studied in order to obtain the required test specimens.

Status of FY 2011 Milestones

Measure and compare reliability of competing commercially available piezoactuators under consideration for use in diesel fuel injectors, *on schedule*.

Communications/Visits/Travel

Communications with Cummins, Inc. were made on CRADA update.

H. T. Lin presented the talk on “Design Optimization of Piezoceramic Multilayer Actuators for Heavy Duty Diesel Engine Fuel Injectors” at the 2011 DOE Annual Merit Review, May 9-12, Arlington, VA.

Publications/Presentations/Awards

1. Wang, H., Matsunaga, T., Lin, H.-T., and Mottern, A. M., Piezoelectric and dielectric performance of poled lead zirconate titanate in electric cyclic fatigue, in review
2. Wang, H., Matsunaga, T., and Lin, H.-T., Effects of temperature and electric field on mechanical strength of single-layer PZT plate, in preparation.

References

1. Wang, H. and Wereszczak, A. A., Effects of electric field on the biaxial strength of poled PZT, Ceram. Eng. Sci. Proc., 28 (8), 2007, 57-67.
2. Wang, H., Lin, H.-T., and Wereszczak, A. A., Strength properties of poled PZT subjected to biaxial flexural loading in high electric field, J. Am. Ceram. Soc., 93 (9), 2010, 2843-2849.

Agreement 15050: Evaluation of Materials via ACERT Engine

Michael Kass, Brian Kaul, Norberto Domingo, Robert M. Wagner,
K. Dean Edwards, H. T. Lin, and D. Ray Johnson
Oak Ridge National Laboratory

Objective/Scope

This project is focused on improving the performance, emissions and efficiency of heavy-duty diesel engines through the application of materials enabled technologies. The range of material systems is comprehensive and includes 1) improved structural materials to accommodate higher cylinder pressures and temperatures, 2) improved durability and corrosion resistance, 3) low inertial components to improve transient response, 4) improved emissions control performance, and 5) waste heat recovery systems.

To date a dynamometer engine research cell was constructed for use with heavy-duty engines. A 2004 C15 ACERT Caterpillar engine was provided by the Caterpillar materials research staff for materials-based efficiency evaluations. The engine was instrumented for combustion and thermal assessment. During FY09, the engine performance was assessed according to thermal availability and opportunities for efficiency improvements were identified. ORNL also completed a WFO with Caterpillar to evaluate a novel turbo concept. The novel turbo design was found to deliver efficiency and thermal improvements over the baseline turbo design. At the conclusion of these efforts, several materials-related efficiency improvement concepts were discussed and debated. The decision was to consider advanced alloy utilization in key components and emission control technologies. For FY 2011, projects involving valve material durability and high-temperature exhaust manifold performance were proposed.

Progress This Quarter (April – June 2011)

Caterpillar provided ORNL with a set of valves that composed of a novel high-temperature nickel-based alloy for improved durability. The valves durability study called for the engine to be run for 200 hours according to the transient cycle shown in Figure 1. The 200-hour engine runtime for this study was completed in May of 2011. The transient cycle consists of several high load settings and idle engine operation. In addition, the valve lash was measured for the untested condition and periodically in the course of the engine operation. The lash results are shown in and do not indicate a significant difference in the valve recession for those composed of the nickel-based alloy compared to the standard valves.

Caterpillar has also provided ORNL with stainless-steel alloy exhaust manifolds to test in comparison to the baseline ductile iron material. The test protocol for this study will consist of subjecting the manifolds to thermal cycling by operating the engine at high load until a target temperature is reached, then returning to idle with additional cooling air blowing on the manifolds until they have cooled off. This will be repeated for 2000 cycles, after which time the manifolds will be removed to inspect for cracking. The target temperatures are currently being determined through preliminary experiments with the

baseline iron manifold installed, after which testing of the stainless steel alloy manifolds will commence.

The nickel-alloy exhaust valves will remain in the engine during the exhaust manifold experiments to accumulate more hours. After completion of the exhaust manifold testing, the manifolds and valves will be removed, and the valve and manifold material performance will be evaluated by a team of materials researchers from ORNL and Caterpillar.

Publications/Presentations/Awards

None reported during this quarterly period.

Plans for Next Reporting Period

Complete engine evaluation for exhaust manifold materials.

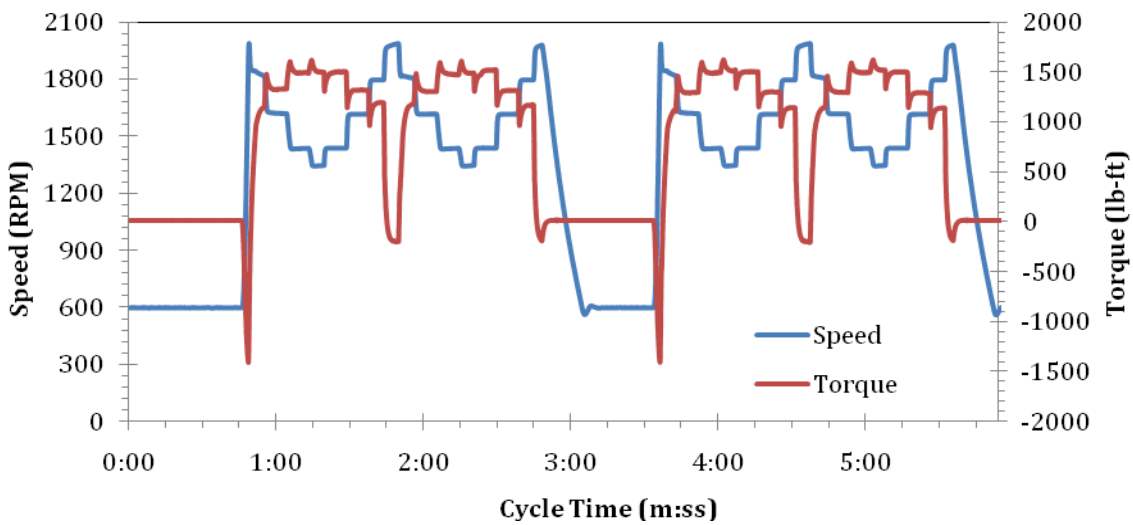

Figure 1 – Schematic of transient test cycles used to evaluate valve performance

Table 1 – Valve lash measurements

Cylinder #	Exhaust Valve Material	Valve #	0 hours	30 hours	50 hours	77 hours	200 hours
1	Ni Alloy	1	0.030	0.028	0.028	0.028	0.028
		3	0.030	0.028	0.028	0.028	0.028
2	Standard	5	0.030	0.028	0.028	0.028	0.028
		7	0.030	0.028	0.028	0.028	0.028
3	Ni Alloy	9	0.030	0.028	0.028	0.028	0.028
		11	0.030	0.028	0.028	0.028	0.028
4	Standard	13	0.030	0.028	0.027	0.027	0.027
		15	0.030	0.028	0.027	0.027	0.027
5	Ni Alloy	17	0.030	0.029	0.028	0.028	0.028
		19	0.030	0.028	0.028	0.028	0.028
6	Standard	21	0.030	0.028	0.027	0.027	0.027
		23	0.030	0.028	0.027	0.027	0.027

Agreement 16303: Materials for High Pressure Fuel Injection Systems

Peter J. Blau and Amit Shyam
Oak Ridge National Laboratory
and
Nan Yang
Caterpillar Corporation

Objective/Scope

The objective of this Cooperative Research and Development Agreement (CRADA) between UT-Battelle, LLC and Caterpillar Corporation is to investigate and understand the performance limitations of current alloy steels for high-pressure diesel engine fuel injector nozzles.

During recent decades, fuel efficient, low-emissions diesel engine designs for heavy trucks have relied upon increasing fuel injection pressures to optimize combustion characteristics. Precise fuel metering is required. This key functional requirement has raised concerns over the ability of spray holes to be machined to sufficiently close tolerances to provide desired spray patterns and for the materials of construction to withstand hundreds of millions of high-pressure pulses without succumbing to fatigue damage. The data and analyses obtained in the course of this three-year effort are expected to provide vital information for designers and material selectors for high-performance fuel systems for energy-efficient diesel engines.

A three-pronged approach has been developed. It involves: (1) characterization of current fuel injector hole geometry and alloy metallurgy, (2) measuring the residual stress in nozzle tips near spray holes, and (3) development and use of specialized fatigue test methods to address the special requirements of the next generation of high-pressure fuel injectors.

Technical Highlights

*Fatigue testing on fuel injector materials***.** A dual-pronged approach for characterizing the effects of small holes on the fatigue life and crack growth mechanisms of fuel injector alloys has been implemented. A procedure for the determination of small fatigue crack propagation threshold was developed by modification of the ASTM test standard E647. The small fatigue crack propagation threshold for the material with no heat treatment and the through-hardened material were determined to be 3.50 and 8.77 MPa√m, respectively. Figure 1 shows the small crack propagation behavior of the investigated material in various experimental conditions. At an equivalent value of stress intensity range, the cracks propagate at a lower rate for the through hardened material compared to the material with no heat treatment. Moreover, the hardened material does not show an effect of maximum stress on the crack propagation rates so a linear elastic fracture mechanics characterization is appropriate for this material.

The measured small crack propagation thresholds were applied to model the effect of notch size on the fatigue limit by application of the well-known Newman-Raju solutions. The effect of notch size on the predicted fatigue limit for both heat treatments is summarized in Figure 2. The generated experimental information can be applied to

implement a damage tolerant design for fuel injector materials. Such a design approach is expected to improve the reliability and improve the functional performance of diesel fuel injectors.

Plans for the Next Quarter

1) Continue to investigate the axial fatigue life and fatigue crack propagation behavior for fuel injector steels containing controlled flaws.

2) Investigate approaches for residual stress measurements at the scale of fuel injector orifices.

2) Conduct experiments to investigate the effects of diesel fuel environment on smooth specimen axial fatigue failures.

Status of FY 2011 Milestones

1) Complete baseline fatigue tests on smooth specimens without artificial flaws. **(3/31/2011) Status:** *Completed*.

2) Complete fatigue tests on steel specimens containing EDM holes in the presence of diesel fuel and prepare a final report. **(9/30/2011) Status**: *On-going*.

Communications/Visits/Travel

Amit Shyam travelled to Berlin, Germany to participate in the Fifth International Conference on Very High Cycle Fatigue. While there, he presented a paper on the very high cycle fatigue behavior of tool steel materials and also served as chairperson in one of the sessions. This paper was published in the proceedings (see below).

Problems Encountered

A delay in the receipt of specimens and the resulting decrease in spending rate over the last year required a no-cost extension to move the end date of the CRADA from mid-July to mid-October 2011. This extension has been approved by both parties.

Publications/Presentations/Awards

P. J. Blau, J. Y. Howe, D. Coffey, R. M. Trejo, L. R. Walker, B. C. Jolly, and N. Wang, "Microstructure, Morphology, and Nanomechanical Properties Near Fine Holes Produced by Electro-Discharge Machining," in preparation for the journal *Materials Engineering and Performance* (2011).

A. Shyam, P. J. Blau, T. Jordan, N. Yang and M. J. Pollard, "The Very High Cycle Fatigue behavior of Tool Steel Materials" in the Proceedings of the Fifth International Conference on High Cycle Fatigue, Eds. C. Berger and H.-J. Christ, DVM, 2011, pp. 525-530.

A. Shyam, P. Blau, T. Jordon and N. Yang, "The fatigue behavior of alloy steels," in preparation for ASM Materials Science and Technology Conference and Expo, Columbus, OH (October 16-20, 2011).

References

None

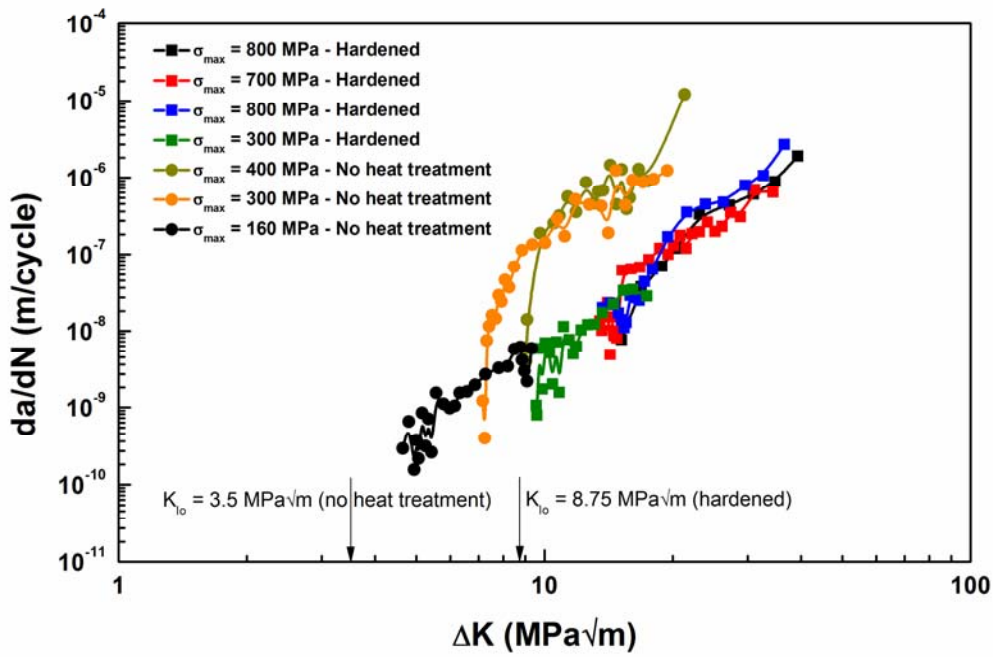

Figure 1. The effect of heat treatment on fatigue crack propagation behavior of a tool steel material. The material without a heat treatment has a fatigue crack propagation threshold of 40% of the through hardened material.

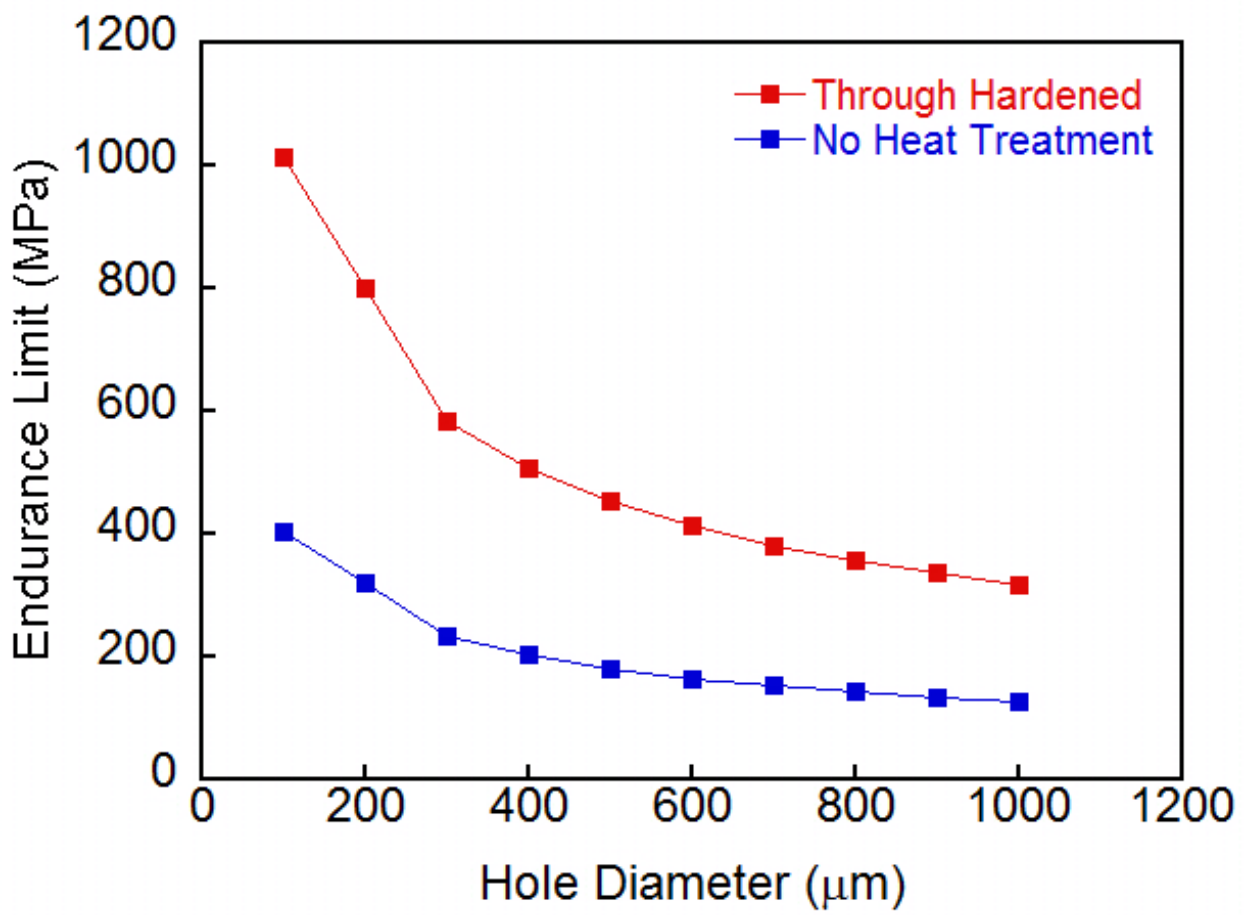

Figure 2: The effect of hole diameter on the predicted endurance limit for both the heat treatments.

Agreement 16304: Materials for Advanced Engine Valve Train

P.J. Maziasz and N.D. Evans
Oak Ridge National Laboratory
and
M.D. Veliz
Caterpillar, Inc.

Objective/Scope

This is an ORNL CRADA project with Caterpillar, NFE-07-00995 and DOE OVT Agreement 16304, which was extended for 24 months last year, and is now scheduled to end in Dec. 2012. This CRADA project focused on addressing the wear and failure modes of current on-highway heavy-duty diesel exhaust valves and seats, and then evaluated changes in valve-seat design or advanced alloy selection. Advanced alloy selection will enable higher temperature capability, as well as better performance and durability. Requests for more detailed information on this project should be directed to Caterpillar, Inc.

Highlights

Caterpillar, Inc.

Caterpillar completed very high temperature wear-rig tests of new prototype exhaust valves made from upgrade Ni-based superalloys with higher temperature capability than standard 31V superalloy valves. Additional testing included variations in seat-alloys in combination with the new upgraded Ni-based superalloys.

ORNL

ORNL has completed some of the initial creep-rupture testing at 816 - 871°C of specimens from the same upgrade Ni-based superalloys used to make new prototype exhaust valves for testing at Caterpillar. Both Ni-based alloys 1 and 2 show higher temperature capability and performance compared to the standard 31V superalloy. ORNL is characterizing prototype valves of Ni-based alloys 1 and 2 that have been wear-rig tested by Caterpillar.

Technical Progress, 3rd Quarter, FY2011

Background

This OVT Agreement 16304 is an ongoing ORNL CRADA project with Caterpillar, NFE-07-00995, which will last for about 5.5 years, after last year's new 24 month extension. This CRADA project has addressed the wear and failure modes found for current on-highway heavy-duty diesel exhaust valves and seats. It then identified changes in valve-seat advanced alloys that will enable higher temperature capability, as well as better performance and durability. The need for such upgraded valve-seat alloys is driven by the demand to meet new emissions and fuel economy goals, which continue to push diesel exhaust component temperature higher. The CRADA was extended for 24 more months due to outstanding technical progress and success at mitigating wear between

exhaust valves and seat-inserts at above 800°C. Requests for more detailed information on this project should be directed to Caterpillar, Inc.

Approach

Caterpillar provides the baseline wear and mechanical behavior characteristics of engine-exposed standard valves and seats, and provides exposure of similar components from simulation-rig testing at Caterpillar. ORNL provides more in-depth characterization and microcharacterization of those valves and seats, and provides knowledge and understanding of the full range of commercially available heat-resistant alloys, to select those most suitable for upgraded valve performance. ORNL and Caterpillar have developed an understanding of the underlying degradation mechanisms at seating surfaces, which is the technical basis for selecting and testing alternate valve and seat alloys with upgraded performance and temperature capability. Caterpillar and ORNL are working with Caterpillar's various component and materials suppliers, to enable prototype production of upgraded exhaust valves and seats for evaluation in Caterpillar's wear-test rig, and parallel testing and characterization of the same advanced alloys at ORNL.

Technical Progress – Caterpillar, Inc.

Caterpillar previously obtained new prototype exhaust valves from a major valve supplier, forged from two heats of advanced, alternate Ni-based superalloys with upgraded high-temperature properties. These new upgrade Ni-based superalloys have improved performance and higher temperature capability compared to the standard 31V alloy. Last quarter, Caterpillar completed some of the initial testing and evaluation of Ni-based 1 and 2 alloys in the wear-test rigs with the standard Co-based seat alloys, and this quarter included testing with alternate seat alloys as well. A summary of all the testing done to date at 850°C is shown in Figure 1. Ni-based alloy 1 had 2.7 times better seat-valve wear life at 850°C than the standard production 31V valve alloy, and is better than Ni-based alloy 2. Similar data on testing of the various valve and seat alloys at 740°C will be summarized next quarter. Additional wear-rig testing of Ni-based alloys 1 and 2 is planned, and Caterpillar is also obtaining more new prototype valves of these Ni-based 1 and 2 alloys engine-testing. Caterpillar has sent some of the new alloy valves to ORNL for characterization, and has added the seats of various alloys tested against those valves.

Technical Progress – ORNL

ORNL previously obtained new forged valves and various mechanical properties test specimens from one of Caterpillar's exhaust valve suppliers of two alternate alloys, Ni-based 1 and 2. Both Ni-based alloys have more temperature capability and performance than the standard 31V alloy. Previously it was shown that both alternate Ni-based alloys have higher tensile yield strength (YS) of 90-100 ksi when tested at 816°C (1500°F) in the age-hardened condition with no service, compared to the YS of about 70 ksi for the standard 31V alloy. The initial creep-rupture tests run at 816°C and 30 ksi (207 MPa) were completed last quarter, and data shown previously indicated that Ni-based alloy 1 had much better creep-resistance than the standard 31V alloy. Ni-

based 1 alloy was also several times better than Ni-based 2 alloy. This quarter, the initial creep-rupture testing done at 871°C and 15 ksi (104 MPa) was completed, and is

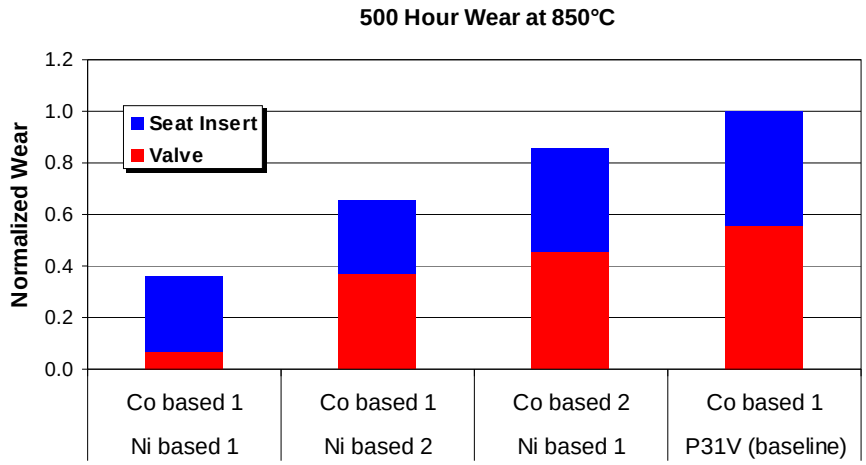

Figure 1 – Summary of Caterpillar wear-rig testing data, showing the separate wear of seat and valve components, and the cumulative wear (valve and seat-insert), for standard 31V alloy exhaust valves and new Ni-based 1 and 2 superalloy prototype valves at 850°C in air. The Ni-based 1 alloy is 2.7x better in total wear life with the standard Co-based seat alloy (1) compared to the standard 31V valve alloy.

shown in Figure 2. Again, both Ni-based alloys 1 and 2 have much better creep-resistance than standard 31V, and Ni-based alloy 1 has significantly better creep-resistance than Ni-based alloy 2. The differences in creep-rupture life among the various alloys is much larger than their differences in YS. Creep-testing of these various alloys at 816°C at a lower stress continued this quarter.

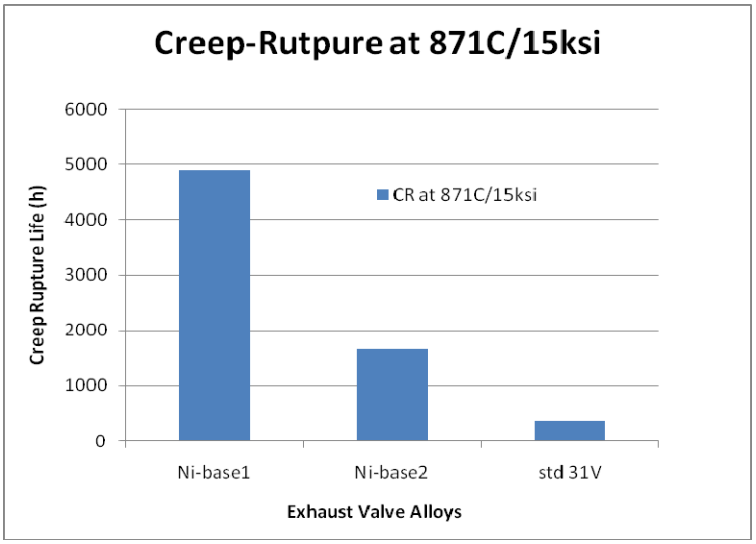

Figure 2 – Creep-rupture life of the standard 31V exhaust valve alloy and two alternate upgrade Ni-based superalloys, for creep tests run in air at 871°C (1600°F) and 15 ksi (104 MPa).

Tensile/creep specimens of these alloys were also being aged at 800 and 850°C for 5000h, and that was completed this quarter. Tensile and creep-rupture testing of these aged specimens began this quarter and will continue next quarter.

Microcharacterization of the rig-tested valves from Caterpillar continued this quarter, and the new method of nano-hardness profiling directly beneath the wear-seating surface of the standard 31V and new Ni-based alloys 1 and 2 began this quarter. Preliminary analysis shows significant surface hardening is occurring for Ni-base alloy 1 that is not found for the other alloys, so that this is a factor in the wear-resistance observed in Figure 1. This work will continue next quarter.

Communications/Visits/Travel

Detailed team communications between ORNL and Caterpillar occur regularly in multi-party conference calls. Caterpillar has extended team discussions to include their commercial seat-insert supplier as well as one of their exhaust valve suppliers.

Status of Milestones (ORNL for DOE)

Milestone for Caterpillar rig-testing of prototype valves and seats of new advanced alloys (Nov., 2010) was completed last quarter. Milestone for completing the initial creep-rupture testing of new Ni-based superalloys with upgraded performance at ORNL (Feb., 2011) was mainly satisfied this quarter.

Publications/Presentations/Awards

None

Agreement 17257: Materials for Advanced Turbocharger Designs

P.J. Maziasz and A. Shyam
Oak Ridge National Laboratory
and
K. Pattabiraman
Honeywell Turbo Technologies

Objective/Scope

This ORNL CRADA project with Honeywell, NFE-08-01671 (DOE/EERE/OVT Agreement 17257) began last year, and is scheduled to last for about 3 years. This CRADA project addresses the limitations of lifetime or use-temperature for the various components (casing, wheel, shaft, bearings) of both the turbine and compressor parts of the turbocharger system. As exhaust temperatures increase, to provide higher engine efficiency and lower emissions, turbocharger component temperatures also increase, so the need for more heat-resistant materials must be addressed. Requests for more detailed information on this CRADA project should be directed to Honeywell, Inc.

Highlights

Neutron-scattering experiments at ORNL to measure residual-stresses in critical locations of wheel/shaft assemblies and turbine housings were completed this quarter. Long-term creep-testing of cast CF8C-Plus austenitic stainless steel at 600°C continued this quarter, and aged specimen became available for testing next quarter. Assessments of the oxidation-resistance of CF8C-Plus steel relative to other exhaust component cast-irons and steels continued this quarter.

Technical Progress, 3rd Quarter, FY2011

Background

This CRADA project began last year, and will extend for 3 years, and covers several different tasks. The first task was to assess and prioritize the various components that need or would most benefit from materials upgrades to increase temperature capability and performance, as well as durability and reliability. The next tasks examine current performance and degradation modes of wheel/shaft assemblies for turbines and compressors, housings for turbines and compressors, and bearings. These tasks may then obtain and test new materials with upgraded performance, and provide the results to Honeywell for designing advanced turbocharger systems, or for manufacturing of new prototype components for testing and evaluation.

Approach

This CRADA project began early last year. This project is comprised of six tasks, which will span the next 36 month period. Activity began with ORNL and Honeywell discussing the priority of the various turbocharger components for materials upgrades. A turbocharger system includes the hot (turbine) end, driven by exhaust gas from the engine, a cold (compressor) end to increase air pressure into the combustion changer, and a transition region that connects these two ends. The turbine and compressor wheels are connected to a common shaft, supported by bearings. For the first task, the turbine wheel-shaft assembly was chosen as the first component for consideration, with analysis focused on residual stresses near the weld-joint of the Ni-based superalloy wheel to the steel shaft, which can upset balance during service. Another task of this new CRADA project continues previous work between ORNL and Honeywell on testing of the new CF8C-Plus cast stainless steel as a significant performance upgrade for the turbine housings relative to standard SiMo or Ni-resist cast irons. This CRADA project for turbine housings covers a broad range of other high temperature properties, including creep and fatigue strength, and includes turbine housing applications for passenger vehicle gasoline engines.

Technical Progress

For Task 1, Honeywell identified neutron-scattering experiments to measure residual stresses in welded wheel/shaft assemblies as one of their highest priority items. For Task 2, these experiments were defined, and neutron scattering experiments at the HFIR Residual Stress User- Facility began last quarter. Figure 1 shows a typical Honeywell wheel/shaft assembly. Preliminary neutron-scattering experiments for diffraction analysis of the steel shaft began previously, and additional experiments on wheel/shaft assemblies with variations in processing parameters continued and were completed this quarter. The Neutron Residual Stress Facility 2 (NRSF2) at HFIR is shown in Figure 2.

For Task 3, ORNL continued long-term creep-rupture tests at 600°C of the cast CF8C-Plus stainless steel this quarter, with one test at a higher stress rupturing after 7,300 h, and another test at a lower stress continuing beyond about 9500 h. ORNL completed aging of as-cast CF8C-Plus tensile/creep specimens at 700 and 800°C to 2500 h this quarter, and mechanical properties testing of the aged specimens began this quarter and will continue next quarter. ORNL also identified additional longer-term creep-rupture testing at 700-800°C that will add to previous creep-rupture data on CF8C-Plus and HK30-Nb steels, which will begin next quarter. Honeywell is addressing the next steps necessary to commercially produce some prototype turbocharger housing using CF8C-Plus steel for certain turbocharger models. This is the next step required so that new housings can be evaluated and tested on engines.

Figure 1 – Honeywell turbocharger wheel/shaft assembly used for neutron-scattering experiments, consisting of a Ni-based superalloy turbine wheel welded to a steel shaft.

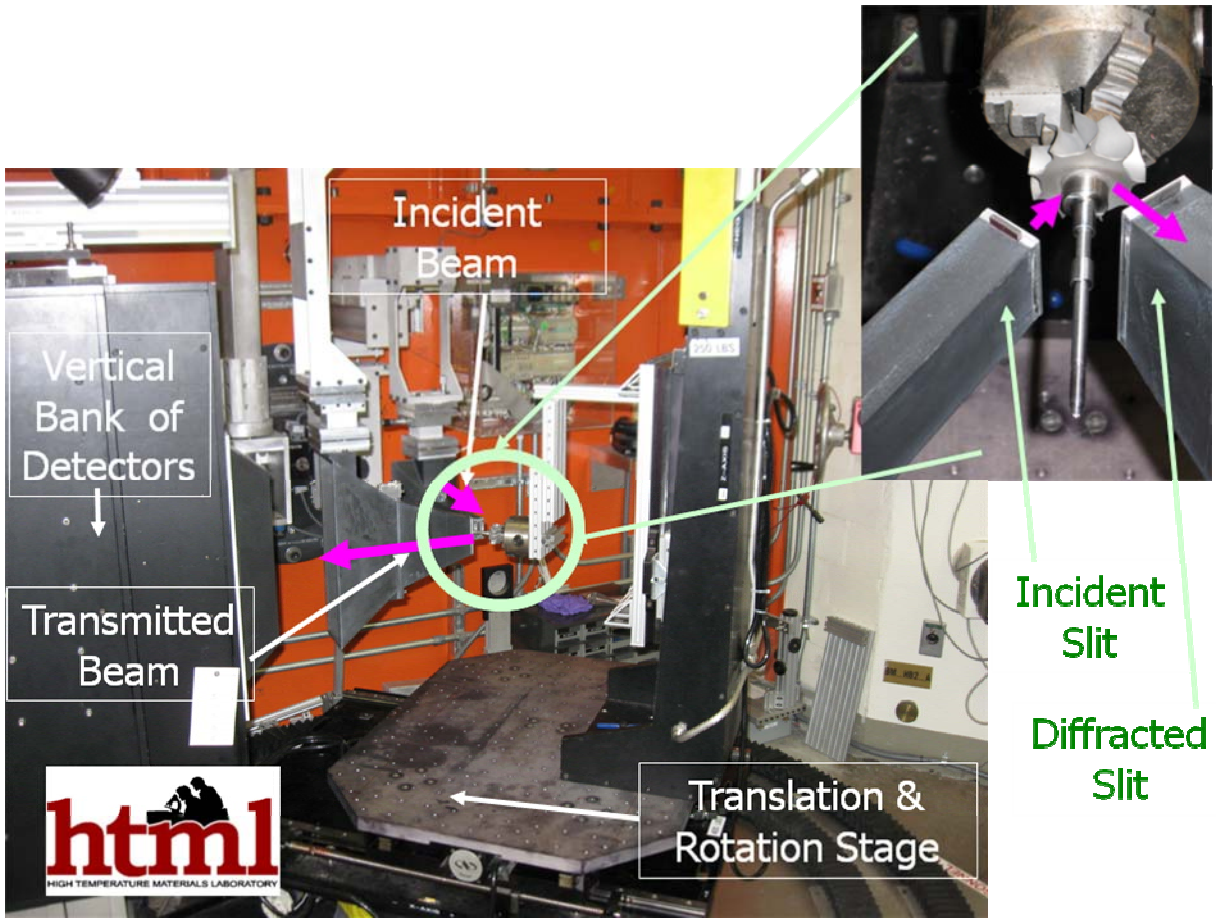

Figure 2 – The Neutron Residual-Stress Facility 2 (NRSF2) at the HFIR beam port, with the specific neutron scattering geometry used for the Honeywell turbocharger wheel/shaft assembly shown in the magnified inset. The NRSF2 is part of the High Temperature Materials Laboratory (HTML) at ORNL, and these experiments were run by Tom Watkins and Cam Hubbard of the Residual Stress User Center.

Oxidation experiments to assess the oxidation-resistance of cast CF8C-Plus relative to several cast-irons used for conventional turbochargers and exhaust system components began last quarter, and continued this quarter.

Communications/Visits/Travel

Periodic conference calls are held between ORNL and Honeywell Turbo Technologies, and email communications help to coordinate the work.

Status of Milestones (ORNL for DOE)

The FY2011 milestone to begin initial neutron-scattering residual-stress measurements on wheel/shaft assemblies for turbochargers (12/2011) was achieved, and the other milestones for FY2011 are on-track.

Publications/Presentations/Awards

None

Agreement 17894: NDE for ACERT^{TM} Engine Components

J. G. Sun and Mark Veliz*
Argonne National Laboratory
***Caterpillar Inc.**
Technical Center

Objective/Scope

Applications of advanced materials in diesel engines may enhance combustion and reduce parasitic and thermal losses, thereby improving engine efficiency. Engine components developed from advanced materials, however, require rigorous assessment to assure their reliability and durability in more stringent operating conditions. The objective of this work is to develop and assess various nondestructive evaluation (NDE) methods for characterization of advanced engine components in a CAT heavy-duty ACERT^{TM} experimental engine at ORNL. NDE technologies established at ANL, including optical scanning, infrared thermal imaging, ultrasonics, and X-ray computed tomography (CT), will be further developed for detection of volumetric, planar, and other types of flaws that may limit the performance of these components. NDE development will be focused on achieving higher spatial resolution and detection sensitivity. Current efforts are directed in applications of optical methods for valvetrain components, X-ray and ultrasonic for joinings, and thermal imaging for thermal barrier coatings (TBC).

Technical Highlights

Work during this period (April-June 2011) focused on synchrotron X-ray CT characterization of TiAl turbine wheel casts and on ultrasonic development for characterization of friction-welded joints between TiAl turbine wheel and Ti-6Al-4V shaft.

1. Synchrotron X-ray CT Characterization of TiAl Turbine-Wheel Casts

During this period we continued X-ray CT characterization of voids/porosity within TiAl turbine wheel casts received from Dr. Nan Yang of Caterpillar. For these casts, two types of flaws are of interest: one is micro and macro porosities located in the cast core region and the other is surface-opening shallow voids in the blade-root region (see Fig. 1a). In the previous period synchrotron X-ray CT was investigated for detection of these casting defects for a TiAl turbine-wheel cast shown in Fig. 1a. It was found that, because of the large blade diameter, X-ray transmission through the wheel was very weak so a long scanning time was required. As a result, the experiment produced only limited CT slices with strong artifacts due to a low signal-to-noise ratio. To overcome this difficulty, two cast wheels, one as-cast and one after HIPing, were machined into cylindrical core samples with a diameter of 2” as shown in Fig. 1b. Each sample contains both the core and the blade-root regions that are of interest for the NDE examination. Because of the smaller sample diameter, X-ray scanning time was reduced significantly and the signal-to-noise ratio in the acquired data was improved simultaneously.

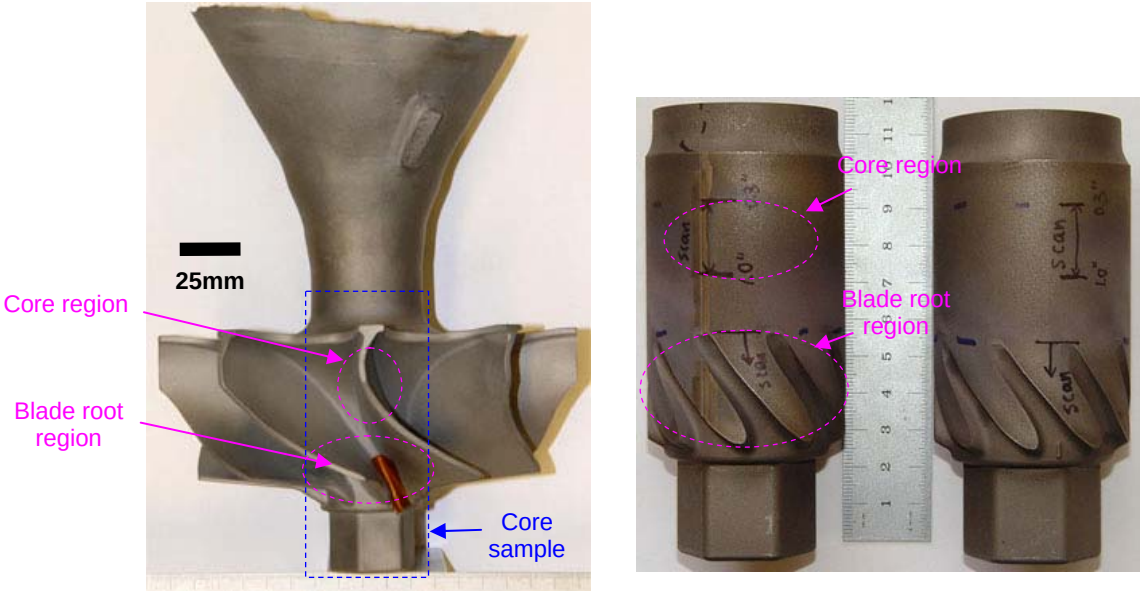

(a) (b)

Fig. 1. (a) A cast and (2) two machined cylindrical core samples of TiAl turbine wheels.

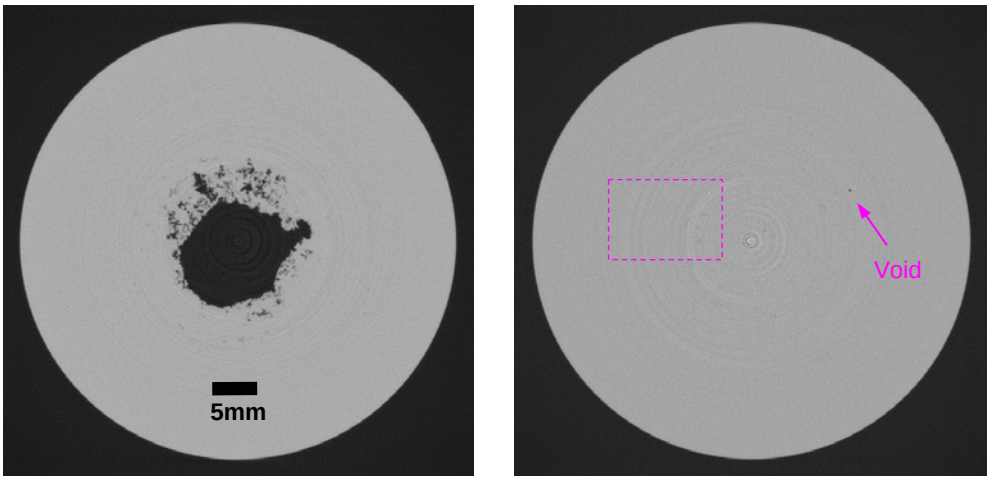

(a) (b)

Fig. 2. Typical X-ray CT slices for the as-cast cylindrical core sample: (a) within the core region and (b) within the blade-root region.

Figure 2 shows two X-ray CT slices of the as-cast sample: one located within the core region and the other within the blade-root region (see locations as illustrated in Fig. 1b). A large void of ~12mm in diameter was detected at the center of the core region (Fig. 2a). Adjacent to this large void, the material is porous with distributed voids of various sizes. The cast material is generally dense outside this porous central region, although small voids may still be found. Small voids may also be found within the blade-root region, as seen in Fig. 2b. Many of these voids are partially filled with material (not completely empty), as seen from the enlarged image in Fig. 3 (from the region marked in Fig. 2b). Figure 3 also shows the ring artifacts. If these ring artifacts are removed or

reduced in their significance, flaws can be identified more easily. Development of imaging processing algorithms to remove the ring artifact is continued in this period.

All cross-section slices acquired for the as-cast cylindrical core sample were composed together into a 3D volume data and sliced in the axial direction. Figure 4 is an axial CT slice. In this image, the axial size and geometry of the voids are clearly visualized.

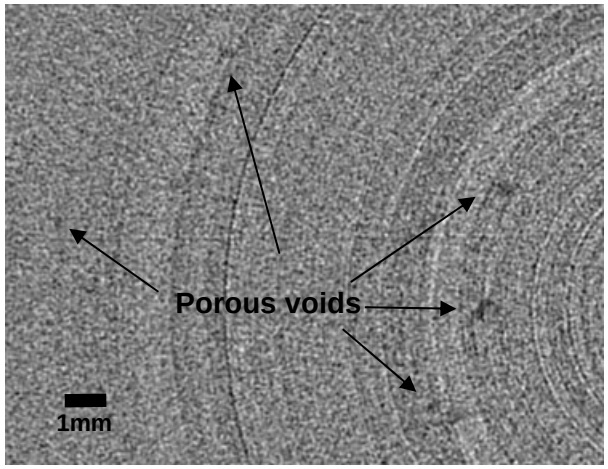

Fig. 3. An enlarge and re-scaled image of the CT slice shown in Fig. 2b.

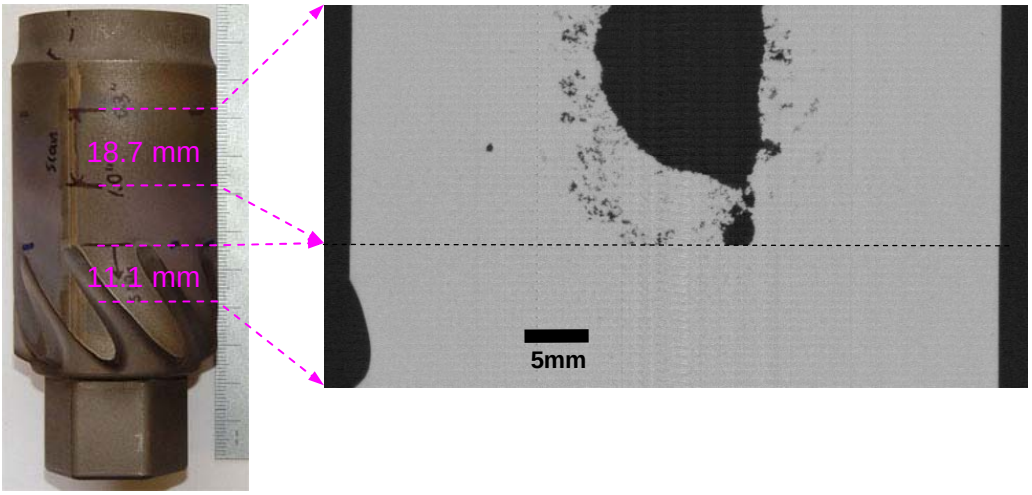

Fig. 4. Reconstructed axial CT slice image for the as-cast cylindrical core sample.

2. Ultrasonic Characterization of Friction-Welded Joints

Although synchrotron X-ray CT may detect all significant flaws within the friction-welded joints, this technology cannot be used in industrial facilities to inspect manufactured components. Industrial inspections rely on low-cost and fast inspection technologies. For weld inspection, ultrasonic technology is widely used (also used in Caterpillar [Yang et al. 2005]). Because flaw detection by X-ray CT is based on transmission contrast while by ultrasonic is based on reflection, detection sensitivity for these two technologies can be different. It is therefore necessary to establish a detection-sensitivity correlation between them for various flaw types and sizes. In addition,

because X-ray CT data can provide accurate information on the flaw size, geometry, orientation, and location within a component, the correlation may also aid for quantitative interpretation of ultrasonic data especially for complex flaw configurations.

Because ultrasonic detection is based on reflection, it is important to align the ultrasonic probe in a direction so a reflection from a flaw may return to the probe. In this investigation, the welding crack oriented along the weld plane is examined using a phased-array probe. A schematic system setup is shown in Fig. 5a and a photograph of the experimental system is in Fig. 5b. As illustrated in Fig. 5a, the phased-array probe scans the welding plane in both radial and circumferential directions, resulting in 2D scan images of the weld plane. This system, although in principle may not detect cracks perfectly aligned along the weld plane, should be able to detect real cracks that normally have imperfect crack plane.

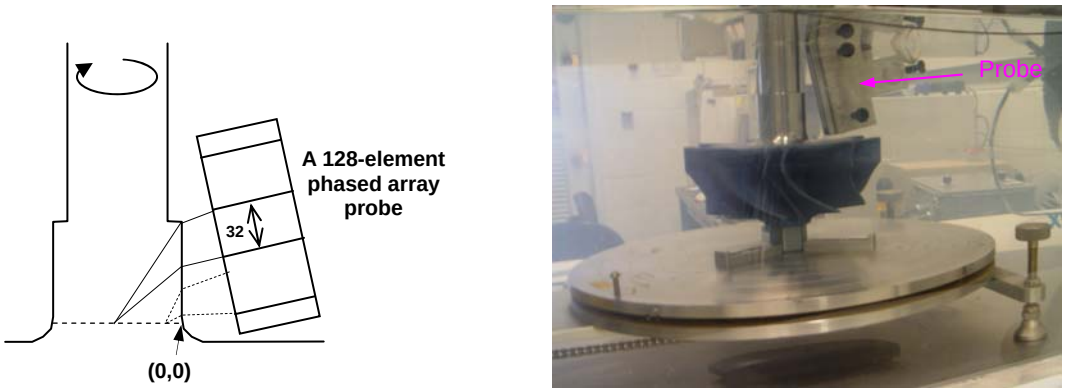

(a) (b)

Fig. 5. (a) Schematic and (b) photograph of an ultrasonic system to detect welding cracks in a TiAl turbocharger rotor.

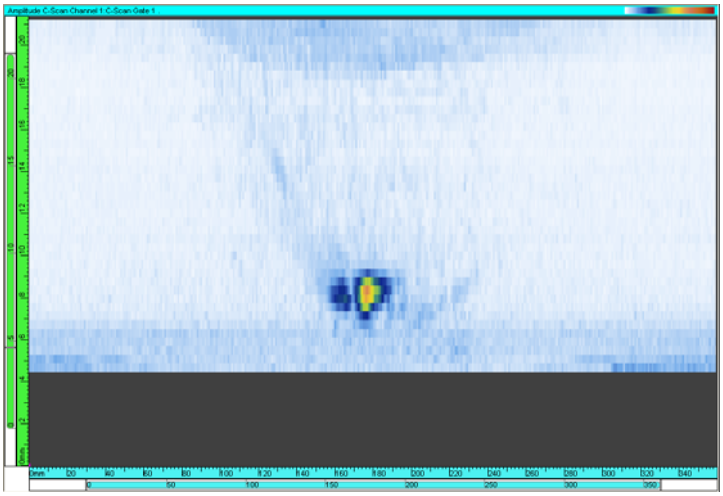

Fig. 6. C-scan image of a weld interface, showing a weld defect at ~180º and nominally 7-9 mm from the outer edge of the shaft.

Figure 6 is a C-scan image of the region ±3 mm from the nominal weld interface of a defective weld sample, plotted as a function of radial distance from the outer edge on the vertical axis and angular position on the horizontal. This image shows a weld defect at ~180º and nominally 7-9 mm from the outer edge of the shaft. The defect appears to be composed of two separate features. This defect has been confirmed from X-ray CT data; detailed correlation will be provided in the next report. It is noted that the current setup does not scan the outer ~4mm region of the weld interface, which can be corrected with further system optimization.

Status of FY 2010 Milestones

Current ANL milestones are on schedule.

Communications/Visits/Travel

J.G. Sun presented an invited talk "NDE of composite materials" at the Composite Workshop organized by United Technologies Research Center, East Hartford, CT, April 8, 2011.

J.G. Sun presented an invited talk "Nondestructive evaluation for ceramic materials" at the High-Efficiency Gas Turbine Workshop organized by DOE ARPA-E in Worcester, MA, May 2, 2011.

J.G. Sun attended the DOE Vehicle Technologies Program Annual Merit Review Meeting at Washington, DC, May 9-13, 2011.

J.G. Sun plans to present a paper entitled "Synchrotron X-ray CT characterization of friction-welded joints in TiAl turbocharger components" and a presentation entitled "Quantitative thermal tomography imaging of complex material structures" at the 38th Annual Review of Progress in Quantitative Nondestructive Evaluation in Burlington, VT, July 17-22, 2011.

Problems Encountered

None this period.

Publications/Presentations/Awards

None this period.

References

Nan Yang, et al., "Development of Titanium Alloys for Heavy-Duty Diesel Engines," Quarterly Progress Report for April through June 2005, Heavy Vehicle Propulsion Materials Program.

Agreement 18570: Engine Materials Compatibility with Alternate Fuels

S. J. Pawel
Oak Ridge National Laboratory

Objective/Scope

The purpose of this Cooperative Research and Development Agreement (CRADA) between Oak Ridge National Laboratory and USCAR is to systematically evaluate compatibility between engine materials and ethanol fuel blends over a range of temperatures consistent with engine operation. Four primary tasks are included in the overall program:

1) surface analysis of materials exposed in field and lab exposures
2) in-situ extraction of gas and/or fluid from the engine
3) development of electrochemical testing protocols
4) laboratory corrosion exposures of coupon materials

Technical Highlights

Emphasis in the third quarter of FY11 was placed on redesign of the main experiment to incorporate a testing apparatus with multiple reaction chambers and lower test volumes. Primarily, these changes improve safety associated with high temperature experiments intended to encourage reaction(s) between ethanol fuel blends and various materials and enable the detection of the onset of reactions (as signaled by fluctuations in temperature or pressure) more readily due to a greatly reduced thermal mass/volume of test solution and autoclave containment. The new apparatus consists of six reaction vessels each capable of containing approximately 50 mL of a biofuel blend and is shown in Figure 1. A close up view of a single reaction vessel is shown in Figure 2. Construction of the apparatus is planned for mid-July and testing will commence immediately thereafter.

Having several test stations will enable a more nimble approach to rapidly target experimental test conditions that are most conducive to ethanol degradation and/or corrosive to aluminum and its alloys. Test conditions that will be adjusted with each experimental iteration include temperature (ambient to ~200°C), pressure (atmospheric to 250 psig), amount of ethanol in the fuel blend, concentration of contaminants in the fuel blend including water, salts, and acids, and dissolved oxygen. Additionally, corrosion experiments will be conducted by making galvanic couples with the alloy as well as modifying its surface properties. It is anticipated that after gathering data from several of these experiments that a clearer picture will emerge on the specific mechanisms of ethanol and aluminum corrosion.

Other activities this quarter included finalizing plans with USCAR partners to perform in-situ engine measurements. The location for the capillary tubes has been defined and all of the engine hardware has been appropriately modified to allow access for the capillary tubes.

One engine is expected to be assembled for use in the capillary sampling test in the third quarter of calendar 2011, with initial testing completed during the third and fourth quarters.

Status of FY2011 Milestones
Ongoing.

Communications/Visits/Travel
Routine electronic mail and regular telephone contact (bimonthly conference calls) is being maintained between the USCAR Partners and the ORNL team. Recent work was presented at the DOE Annual Merit Review in Washington D.C. on May 9-13, 2011.

Problems Encountered
Shipping delays for critical experimental apparatus components

Publications/Presentations/Awards
None

References
None

Figure 1. Experimental apparatus including six independent reaction vessels where test conditions can be rapidly modified in successive experimental iterations.

Figure 2. Close up view of a single reaction vessel.

Agreement 18571: Materials Issues Associated with Exhaust Gas Recirculation Systems

M. J. Lance, C. S. Sluder and J. M. E. Storey
Oak Ridge National Laboratory

Objective/Scope

Provide information to industry specialists about fouling deposit properties so as to enable improved models and potential design improvements to reduce fouling and its impact on the performance of EGR (exhaust gas recirculation) coolers.

Technical Highlights

All remaining samples provided by the EGR team were imaged using neutron tomography at HFIR (High-Flux Isotope Reactor). Dr. Jens Gregor at the University of Tennessee has developed new code to reconstruct the 3-D tomographic sets from the raw images that helps to reduce the number of artifacts. Fig. 1 shows one slice taken through two EGR sections using the previous commercially available reconstruction code that produces lines emanating from the corners of the samples. Using a new PSIRT reconstruction code, Dr. Gregor has successfully eliminated these artifacts as shown in Fig.2 .

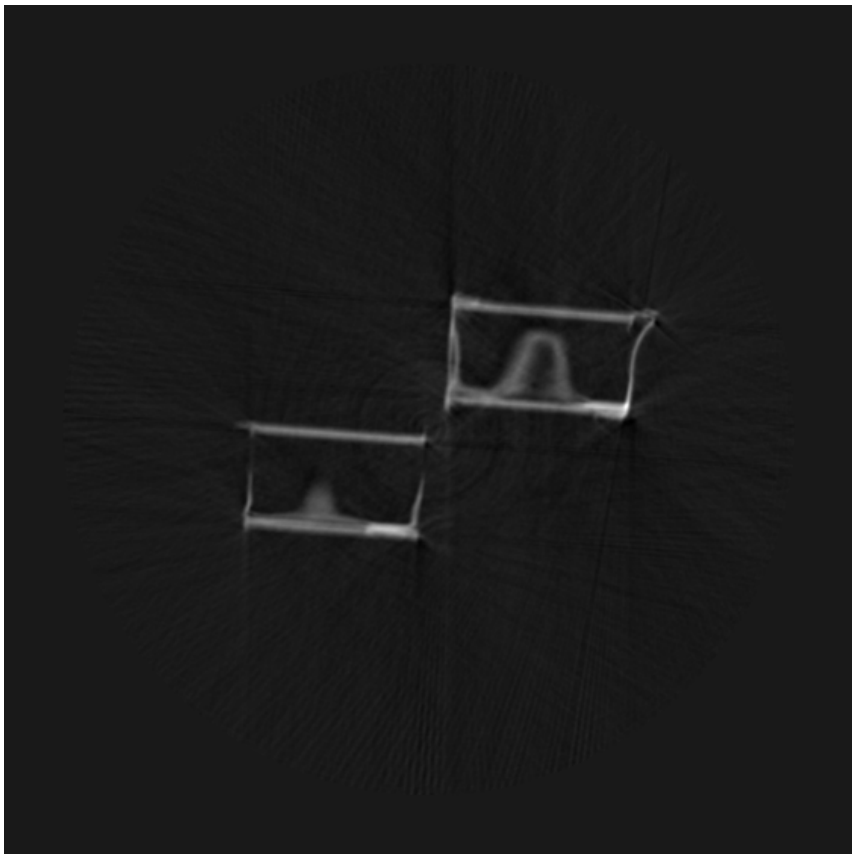

Figure 1. Two EGR sections imaged using neutron tomography. These slices were reconstructed using a Feldkamp algorithm which results in streaks in the image.

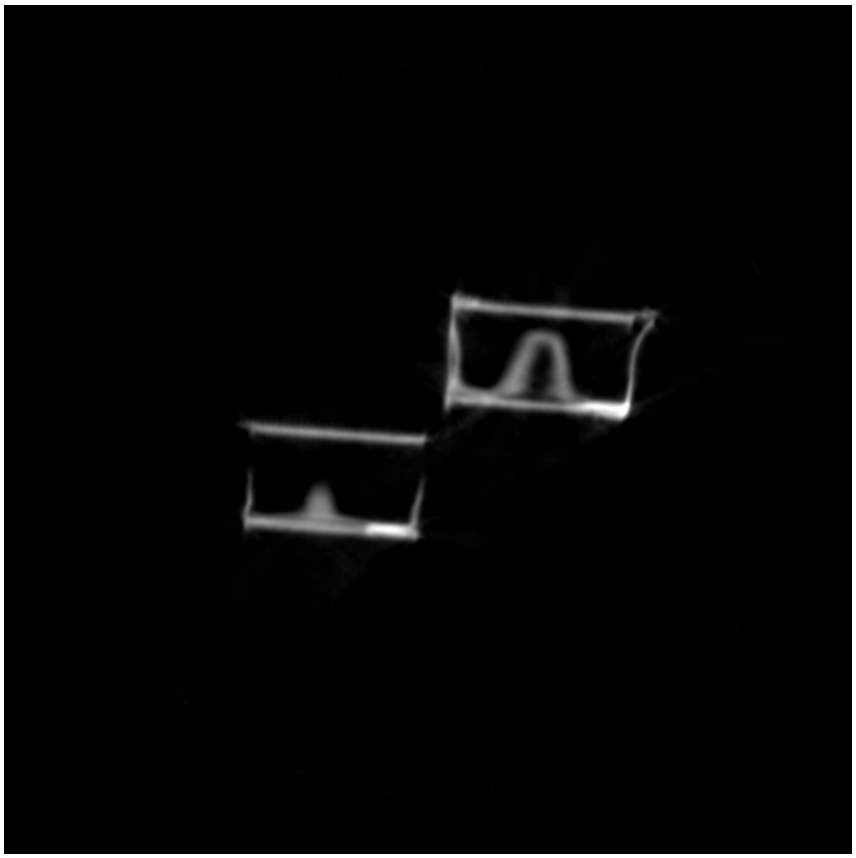

Figure 2. The same slices in Fig. 1 except reconstructed using the PSIRT reconstruction algorithm.

The bench-top reactor is now completely assembled and all devices are integrated with Labview software (see Fig. 3). The maximum temperature achievable out of the furnace is ~280°C which will be increased by flowing the gas through a quartz tube filled with SiO_2 chips to aid in heat transfer. Six tubes that have deposits within them have been formed using the 1.9L GM diesel engine.

Seven coolers have arrived for the second round of forensic deposit analysis from the industry consortium of EGR technicians.

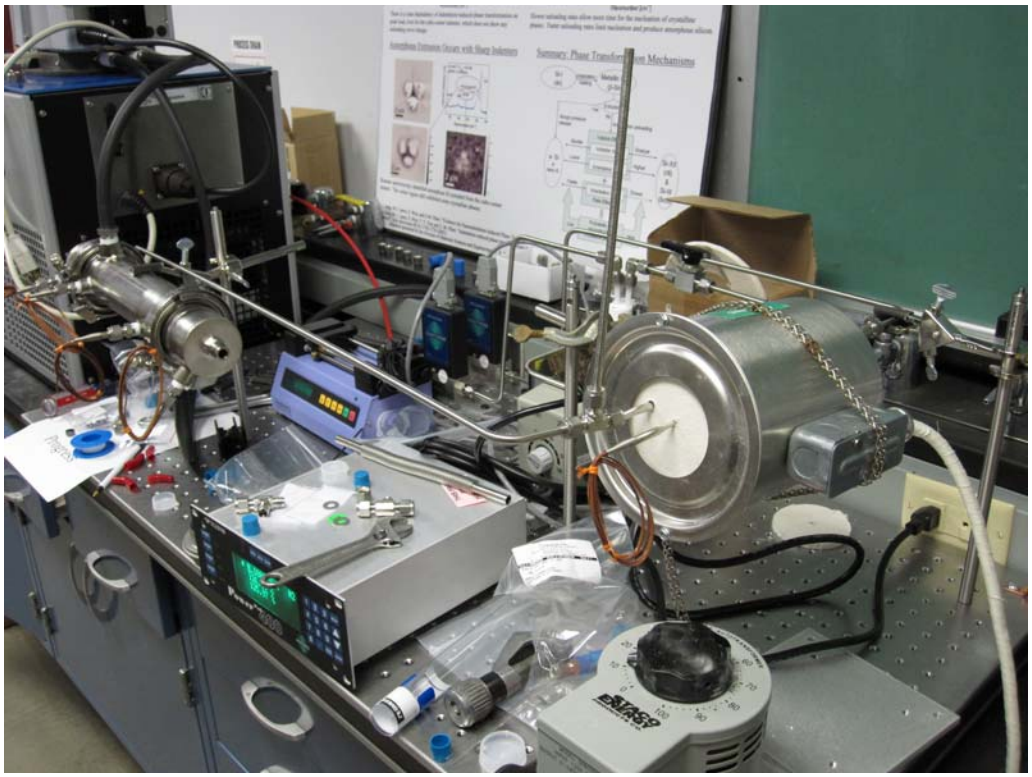

Figure 3. Bench-top tube reactor showing the furnace for heating the gas and the heat exchanger for cooling the deposit.

Status of FY2011 Milestones

1. Assemble and test sampling system for controlled deposit formation. (10/10) *On Schedule.*
2. Generate fouling deposits using an engine and sampler tube system and age them in controlled environments to investigate changes in deposit properties. (09/11) *On Schedule.*

Communications/Visits/Travel

None.

Problems Encountered

None.

Publications/Presentations/Awards

None.

References

None.

Agreement 19202: Titanium Friction and Wear (Surface Engineering of Bearing Components)

Peter Blau and Dinesh Bansal
Oak Ridge National Laboratory

Objective/Scope

The energy efficiency and durability of internal combustion engines (ICEs), whether fueled by conventional or alternative fuels, benefit from the use of lightweight materials. Examples include polymer composites and alloys of aluminum, magnesium, and titanium. While such materials offer attractive efficiency gains, their use also presents technical and economic challenges. One class of ICE applications involves tribological aspects: that is, those which concern friction, wear, and lubrication. Studies in the United States, Japan, and the United Kingdom have shown that mechanical losses comprise about fifteen percent of the energy dissipation from fuel in a typical ICE, and that of those, energy losses by friction comprise about eighty percent. The two major subsystems, in terms of engine frictional losses, are the piston ring/cylinder interface and the crankshaft bearings, including those on the connecting rods. Past research at ORNL has focused on the piston ring/cylinder interface. The current project which began in FY 2010 not only addresses the connecting rod bearings, but it also demonstrates how surface engineering and coating technologies that could benefit other friction- and wear-critical applications as well.

The objective of this project is to *enable the use of strong, lightweight titanium (Ti) alloys for wear and friction-sensitive engine components like connecting rods (CRs) and crankshafts.* The goal is to identify the most promising surface engineering methods, whether commercialized or experimental, to reduce friction and wear of Ti alloys under engine-like conditions. This work compliments recent developments in Ti processing technology that is aimed at reducing raw materials cost. It utilizes the experience of ORNL tribology staff to effect changes in surface-critical properties via a variety of potential treatments and combinations of treatments. The phases of this planned three-year effort are: 1) *Friction and wear baseline screening* of multiple surface treatments and coatings for titanium using ASTM test methods to down-select leading performers for more rigorous year 2 evaluation, 2) *Design and construction of a computer-controlled, variable load bearing tester* (VLBT) to simulate the contact pressure and lubricant regime excursions experienced by connecting rod bearings, and 3) *Development of a prototype diesel engine Ti-based connecting rod concept* using surface-engineered Ti bearing surfaces.

Technical Highlights

Down-selection of candidate surface treatments is completed. As reported in previous reports, nineteen candidate materials, including combinations of experimental and commercial coatings and surface treatments, were screened using an ASTM standard test method for reciprocating friction and wear behavior under lubricated conditions. Eight passed the dual criteria of (1) having friction coefficients less than 0.15 (placing them in the boundary or mixed lubrication regime). and (2) lasting for the full 400 m of

sliding distance without excessive noise or vibration. During the third quarter of FY 2011, these results were presented at the International Conference on Wear of Materials in Philadelphia (see **Publications and Presentations**, below).

Construction of the Variable Load Bearing Test System (VLBT). The final stages of construction of the VLBT were completed with the installation of twin load cells, the load actuator, and a modified shaft specimen holder to reduce run-out and improve alignment. The data acquisition system was upgraded to improve performance and enable integration of the test controls with the data acquisition function. A close-up of the specimen fixtures is shown in Figure 1. A robust, three-phase variable speed motor, controlled by the computer, is shown at the upper left. A 25.4 mm diameter shaft is one test specimen, and the bearing specimen is loaded on the shaft from underneath to allow the provision of an oil film. At the upper left is a servo-actuator to apply the load through a lever and pivot bearing arrangement. Two load cells are used. The load cell at the end of the load lever (at right) if for normal force and the load cell nearer the bearing specimen (center of the image) measures friction force.

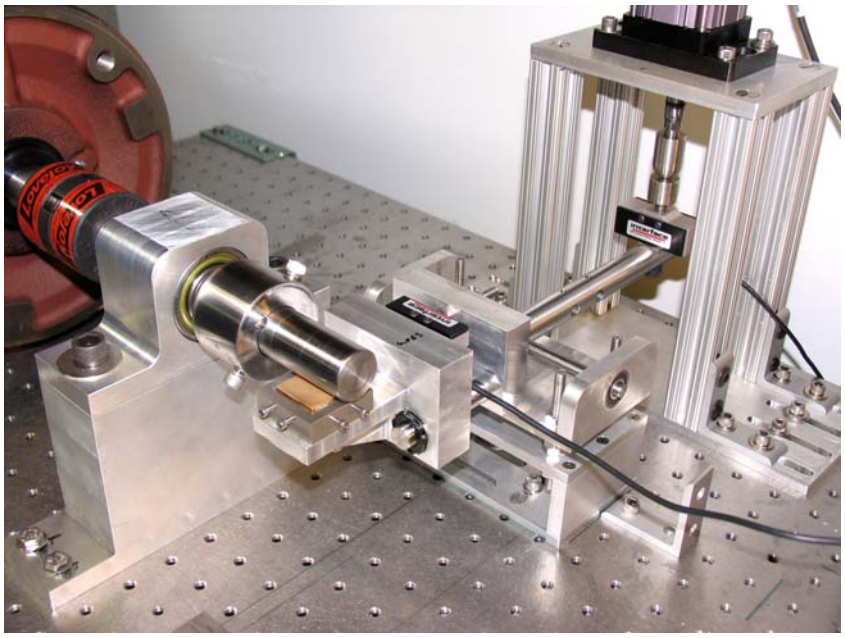

Figure 1. VLBT specimen holding arrangement. The design was modified to simplify specimen mounting and alignment. A bronze specimen is shown mounted below the steel shaft.

Initial sliding experiments were conducted on CDA 932 bronze and Ti-6Al-4V alloy, lubricated with Mobil 15W40 oil. After only 4 minutes of contact, the titanium alloy exhibited significant wear (see Figure 2a) compared with equal sliding time on the bronze (Figure 2b) under similar load and 1.0 m/s speed. While there are still remnants of the initial surface finishing marks on the bronze wear scar, the titanium has worn to a depth of about 100 □m in the same period (Figure 3). Clearly, coatings and/or surface engineering processes are required to produce better performance from titanium alloys. Additional baseline tests will be run during the next quarter to characterize the

repeatability of such results and to compare the friction coefficient versus time behavior during running-in. Then work will begin on surface engineered titanium treatments which were found to be most promising during the first phase of this effort.

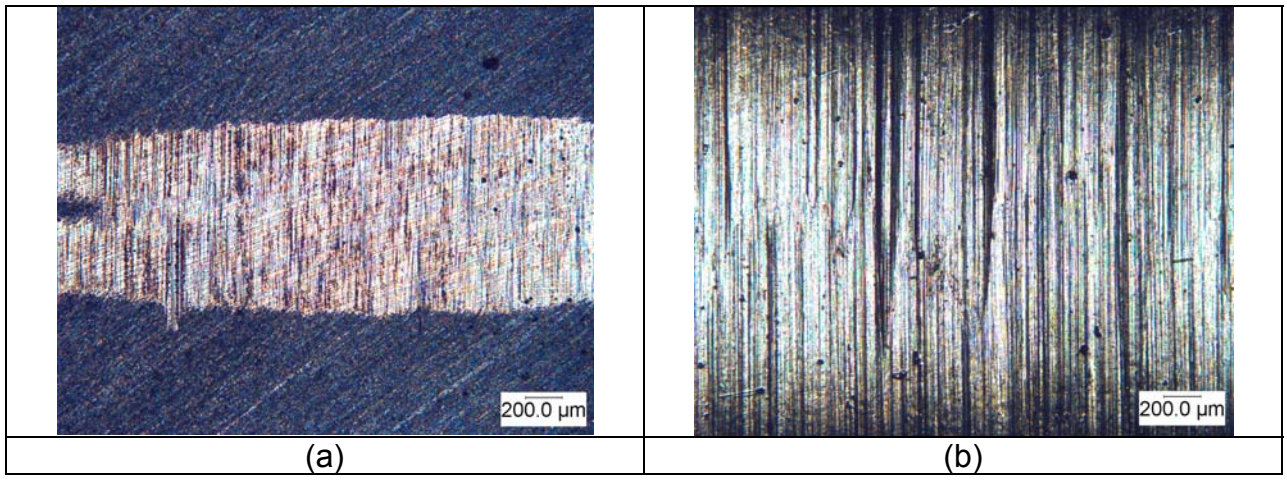

Figure 2. Comparison of (a) the wear scar on bronze CDA 932 wear slid against steel with (b) wear damage on titanium alloy Ti-6Al-4V rubbed under the same conditions.

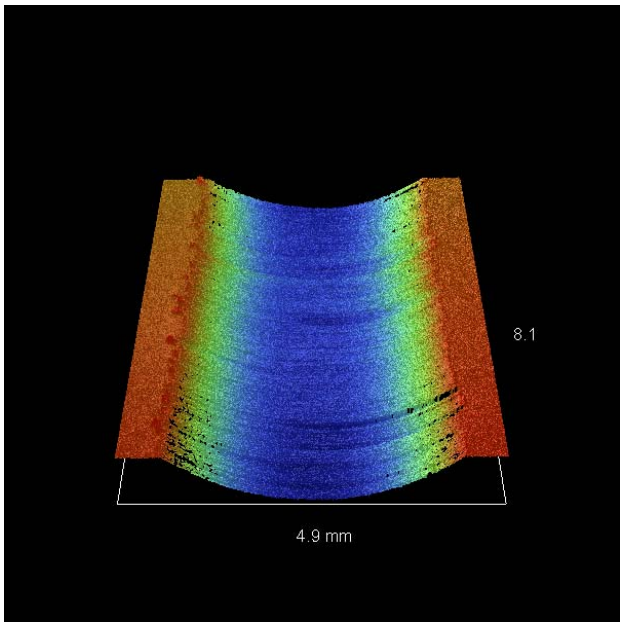

Figure 3. Reconstructed 3D image of the Ti-6Al-4V wear scar after four minutes of sliding. The scar is approximately 0.10 mm deep.

Future Plans. Plans for the upcoming quarter include: (1) to complete bench-mark tests on non-treated titanium and bearing bronze in preparation for evaluating the friction and wear performance of the down-selected candidate surface treatments and coatings.

Status of Milestones

Design friction and wear testing apparatus to simulate connecting rod motions, loads, and speeds, and complete a series of baseline experiments on small test coupons of candidate titanium alloys, with and without surface treatments. **(09/10)** *Status: design completed***.**

Complete construction of a variable-load bearing test system and conduct baseline experiments to establish its operating characteristics. **(03/11)** *Status: completion delayed due to a combination of budget uncertainties and unforeseen alignment issues. Baseline tests underway but not yet complete.*

Complete tests of candidate coatings and multiple surface treatments using the variable-load bearing test system**. (09/11)** *Status: to begin in Quarter 4.*

Communications/Visits/Travel

None this quarter.

Problems Encountered

Problems in achieving the desired alignment of test specimens required a redesign and re-machining of several test fixtures. These issues also delayed calibration of friction and normal force sensors. Further optimization of specimen alignment procedures continues in order to ensure repeatability of friction and wear test data.

References

None

Publications and Presentations

D. Bansal, O. Eryilmaz, and P. Blau, "Surface engineering to improve the durability and lubricity of Ti-6Al-4V alloy," presented at the 2011 International Conference on Wear of Materials (April 3-7, 2011, Philadelphia).

D. Bansal, O. Eryilmaz, and P. Blau, "Surface engineering to improve the durability and lubricity of Ti-6Al-4V alloy," Wear, Vol. 271, pp. 2006-2015.

Agreement 23284: Friction Reduction Through Surface Modification

Peter J. Blau
Oak Ridge National Laboratory
and
Stephen M. Hsu
George Washington University

Objective/Scope

The primary objective of this two-year effort is to improve the fuel efficiency of diesel-powered vehicles by reducing the friction of contacting surfaces by employing specific patterns of micro-scale features. These features function in two ways: (1) to increase the lubricant film thickness, which separates bearing surfaces, and (2) by trapping harmful wear debris in depressions below the contact surface. One bearing surface of particular interest is that between the piston ring and cylinder liner, although other frictional surfaces in engines, like those of bucket lifters and cam lobes are also of interest.

The scope of this effort includes the preparation and testing of textured bearings by various surface engineering methods. During FY 2011, ORNL will select appropriate laboratory-scale friction test methods, prepare textured surfaces on bearing materials, and investigate the effects of specific patterns and feature depths on frictional characteristics as a function of sliding time. Changes in the morphology of the surfaces during the running-in stages will be correlated with the friction coefficient versus time sliding history. Understanding the running-in period is key to separating the contributions of as-finished surface roughness, wear-in, and lubricant conditioning as the bearing system approaches its longer-term, steady-state condition. A university subcontract will complement in-house efforts by developing a new masking technology to enable the surface patterning of curved surfaces like those on piston rings and cylinder bores.

Technical Highlights

Survey of Prior Research on Texturing. A review of previous research on the application of surface patterns to control friction is being prepared. It contains a list of bearing-related applications to which textures have been applied as well as the methods used to produce such patterns. The effectiveness of surface textures on reducing friction and wear varies from significant improvement to a net degradation of behavior, reinforcing the importance of designing specific textures to fit the interfacial conditions of the applications of interest. When completed, this review will be published as an ORNL technical report.

Indentation Array Texturing. Experiments are underway to investigate the effects of indentation array texturing (IAT) on friction of two different materials: bearing bronze and titanium alloy. The purpose of these experiments is to understand to what degree texturing can overcome the limitations of scuffing-prone material combinations under a boundary lubrication regime, as is present in piston rings-on-liners during the direction reversal portion of the stroke. Square (25.4 mm x 25.4 mm), flat coupons of bronze alloy CDA 932 and titanium alloy Ti-6Al-4V are being used for these reciprocating

sliding experiments. A 5 x 8 mm array of Vickers microindentation hardness indentations was placed on polished flat surfaces with a lateral spacing of 150 m along the rows and 75 m between off-set rows (see Figure 1). An array consisting of approximately 3600 impressions was placed on each specimen using an automated hardness testing machine. Indentation loads were adjusted so that the sizes of the impressions on the bronze and titanium were similar despite their difference in hardness. Impressions were then measured using a vertical scanning interferometer (Wyko NT 9100, Brucker Instruments) to determine the rim height around indentations that needed to be removed to produce a flat surface containing pyramidal pockets. A 3D image of several bronze impressions shows the pattern of displaced material around the rims (Figure 2). Prior to friction testing, these rims will be gently polished away so that their 0.6 m-high rims do not affect lubricant flow or abrade the counterface. Results of initial friction experiments on these IAT surfaces will be presented in the next report.

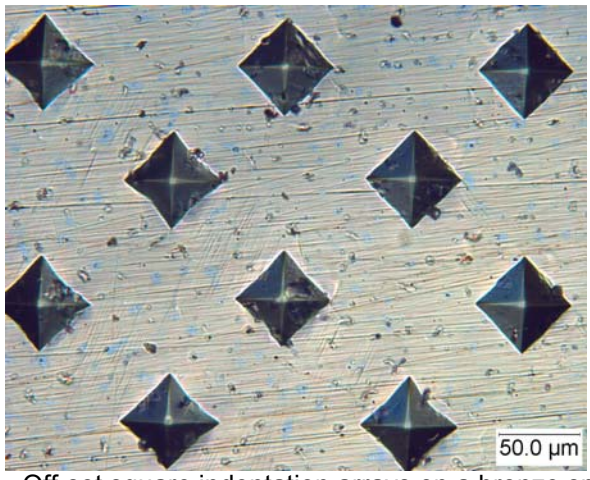

Figure 1. Off-set square indentation arrays on a bronze specimen.

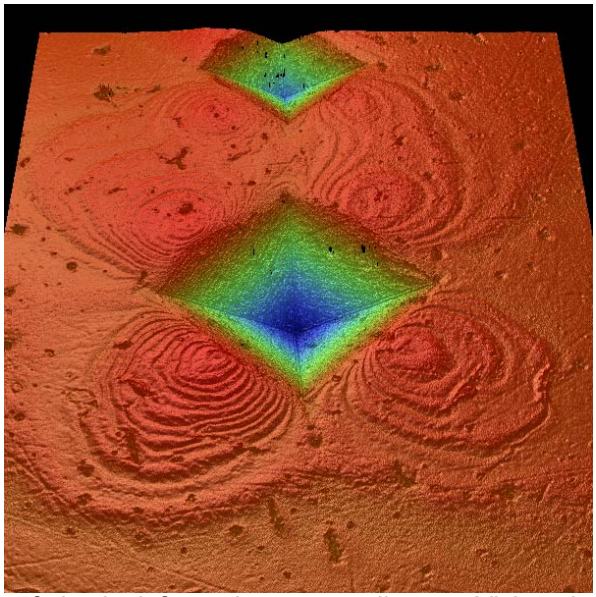

Figure 2. Pseudo-3D image of plastic deformation surrounding two Vickers impressions. Small surface pits are second phase particles within the leaded bronze alloy.

Progress at George Washington University (subcontract). Subcontract Milestone 1 was completed: *"Milestone 1)* A report on ring texture designs and associated test data in simple bench tests and comparison shall be submitted in July, 2011." That report was provided to ORNL separately, and presents a conceptual design which addresses the shapes and aspect ratios of dimples, their depth, their arrangement, their spacing, and their density. Additional progress at GWU is summarized as follows:

Working with Cummins Engine Company, the piston ring contact kinematics was analyzed. The ring material composition and the cross-hatched liner surface specifications were provided under a non-disclosure agreement. Simple bench tests using a pin-on-disk tester and a ball-on-three flats geometry in a four ball wear tester were conducted to examine possible surface texture pattern designs under various contact stresses. The cross-hatched counter-surface posed a potentially disruptive effect when applying an additional texture and will be studied later, in reciprocating tests.

Bench test results suggested that a dual-feature textural pattern might be suitable for initial ring design: small deep elliptical dimples are useful in boundary and elasto-hydrodynamic lubrication regimes, while relatively shallow large dimples are useful in hydrodynamic lubrication regime.

A surface texture fabrication technique for actual ring specimens has been successfully developed. Photolithography was used to develop a large area on soft polymeric masks followed by an electrochemical etching sequence to transfer those patterns onto the ring surface. Adjustments in etching agent, current, and buffer conditions were necessary to cope with the ring metallurgy and composition. Ring segments cut from actual rings were textured. The availability of a scalable, cost-effective fabrication technique is a crucial step in introducing the technology into practice.

The Cameron-Plint reciprocating friction and wear tester was set up and calibrated. Using a preliminary test procedure, a textured patterned ring segment was tested and showed significant friction reduction. This preliminary result, while encouraging, will need to be verified and optimized in the future.

To address a second promising application, studies have begun on the contact kinematics of the cam-roller interface. A ring-on-block tester will be used to study the sliding portion of the contact interface. By adjusting the contact width and pressure, a pre-worn block will be used to provide friction data under various contact pressures.

Status of FY 2011 Milestones

(a) Put in place a university subcontract to produce textured surfaces for further study. (3/31/2011). *Completed*.

(b) Complete baseline lubricated friction tests on flat laboratory test coupons and correlate their frictional running-in behavior with the features of surface textures. (9/30/2011). *In progress.*

Communications/Visits/Travel
None.

Problems Encountered
None.

Publications/Presentations/Awards
None.

References
None.

Agreement 23285: Efficiency Implications of Advanced Materials in Advanced Combustion Internal Engines

Charles E.A. Finney
Oak Ridge National Laboratory

Objective/Scope

This study will examine the efficiency effects of materials changes enabling higher operating cylinder pressures and having altered heat-transfer characteristics. An existing late-model, six-cylinder, heavy-duty diesel engine model, constructed in GT-Power, will be used to examine the effects of increased operating pressures, with both real (cylinder geometry) and effective (elevated boost pressures) higher compression ratios. Additionally, heat-transfer characteristics of the cylinder, piston and valves will be changed to mimic materials differences. Of primary interest will be changing the combustion rates to simulate various high-efficiency combustion modes currently under active industrial R&D.

The result of this study will be to demonstrate potential benefits of operating in higher-efficiency combustion modes achievable with advanced materials, enabling higher operating pressures, and with different fuel burn rates. A partial thermodynamic energy breakdown will be part of the analysis results.

Technical Highlights

In this reporting period (3Q FY 2011), preparations and background research were performed to prepare for analytical and modeling studies in Q4. The preparations included selecting and adapting the simulation model for parametric studies. Additionally, analytical studies were begun to provide insight into boundaries and trends to be seen in the simulation results.

Status of FY 2011 Milestones

This project is on schedule for completion by September 30.

Communications/Visits/Travel

None in this reporting period.

Problems Encountered

Internal model verification and validation can be problematic without experimental data to confirm fidelity. Schemes were devised to account for lack of validation data in some instances.

Publications/Presentations/Awards

None in this reporting period.

References

None.

Agreement 9130: Catalyst Characterization

Thomas Watkins, Larry Allard, Michael Lance, Harry Meyer
Oak Ridge National Laboratory

Krishna Kamasamudram, Alex Yezerets
Cummins Inc.

Objective

The objective of this effort is to produce a quantitative understanding of the process/product interdependence leading to catalyst systems with improved final product quality, resulting in diesel emission levels that meet the prevailing emission requirements.

Goals, Barriers, Relevance & Integration

In the study area of VTP's Materials Technology subprogram, the Propulsion Materials Technology activity provides materials R&D expertise to enable advanced materials and supports the goals of several VTP subprograms.[1] Within the Advanced Combustion Engine subprogram-Combustion and Emission Control R&D activity, one primary R&D direction is to: Develop aftertreatment technologies integrated with combustion strategies for emissions compliance and minimization of an efficiency penalty. [1] Correspondingly, one *goal* is to: by 2015, improve the fuel economy of light-duty gasoline vehicles by 25 percent and of light-duty diesel vehicles by 40 percent, compared to the baseline 2009 gasoline vehicle. In support of these, this project addresses four *barriers*[1] related to the Emission Control: Lack of fundamental knowledge of advanced engine combustion regimes, improving durability and improving market perception. This project is *relevant* to this goal as the understanding of materials changes underlying the Ammonia Oxidation (AMOX) catalyst performance degradation with age increases, efficient and durable AMOX with higher NO_x conversion efficiencies can be attained. This minimizes constraints on engine-out NO_x emissions and allowing engines to be tuned for optimal fuel efficiency, cost and durability. This project also addresses three *barriers*[1] related to the Propulsion Materials Technology activity itself: Changing internal combustion engine combustion regimes, long lead times for materials commercialization and costly precious metal content. This project supports clean diesel, which increases acceptance by the public. Larger acceptance, in turn, results in larger percentages of conversion to diesel, with the resulting reduction in petroleum usage/dependency upon foreign oil. This project is *integrated* within Vehicle Technologies Program as it utilizes characterization tools acquired and maintained by the High Temperature Materials Laboratory (HTML) Program.

Technical Highlights

The main focus in FY2011 is to continue to characterize the ammonia oxidation (AMOX) catalyst characterization of a practically-relevant zeolite catalyst subjected to hydrothermal aging for lifetime prediction model input. The technical approach will be as before: experimentally characterize materials, supplied by Cummins, from all stages of the catalyst's lifecycle: fresh, de-greened, aged, regenerated, on-engine and off-engine,

etc. Determinations include: crystal structure, morphology, phase distribution, particle size and surface species of catalytically active materials; seek the atomic mechanisms and chemistry of adsorption and regeneration processes. Ultimately, an understanding of the thermal and hydrothermal aging processes and other degradation mechanisms is sought throughout the lifecycle of the catalytic material. {Acronyms are used liberally through out this report and are defined in Table I.}

A redesigned portable manifold was assembled and is now ready for testing (see Figure 1). The manifold is capable of delivering gases, such as synthetic exhaust with water vapor, to reaction chambers and stages. This will facilitate in-situ studies with XRD, piezospectroscopic and possibly STEM techniques. High temperature XRD experiments using this manifold are planned for Fall 2011 to study the in-situ hydrothermal aging of samples at elevated temperatures in air with <10% H_2O.

Status of FY 2011 Milestones

In the reporting period, the ORNL team continued characterizing an ammonia oxidation (AMOX) catalyst characterization of a practically-relevant zeolite catalyst subjected to hydrothermal aging for lifetime prediction model input. The milestone is on target.

Travel, Presentation, Personnel

ORNL personnel traveled to Washington DC for the DOE 2011 Vehicle Technologies Annual Merit Review and Peer Evaluation Meeting on May 10, 2011 and made the following presentation:

T. R. Watkins, L. F. Allard, M. J. Lance, H. M. Meyer, K. Kamasamudram and A. Yezerets, “Catalyst Characterization,” presented at the DOE 2011 Vehicle Technologies Annual Merit Review and Peer Evaluation Meeting, Washington, D.C., May 10, 2010.

References

1. Vehicle Technologies Program, Multi-Year Program Plan 2011-2015, Dec. 2010, pp. 2.3-1, 2 ; 2.5-8.

Table I – Acronyms

AMOX	ammonia oxidation
HTML	High Temperature Materials Laboratory
NO_x	Nitrogen and Oxygen containing compounds
ORNL	Oak Ridge National Laboratory
STEM	Scanning Transmission Electron Microscopy
XRD	X-ray Diffraction

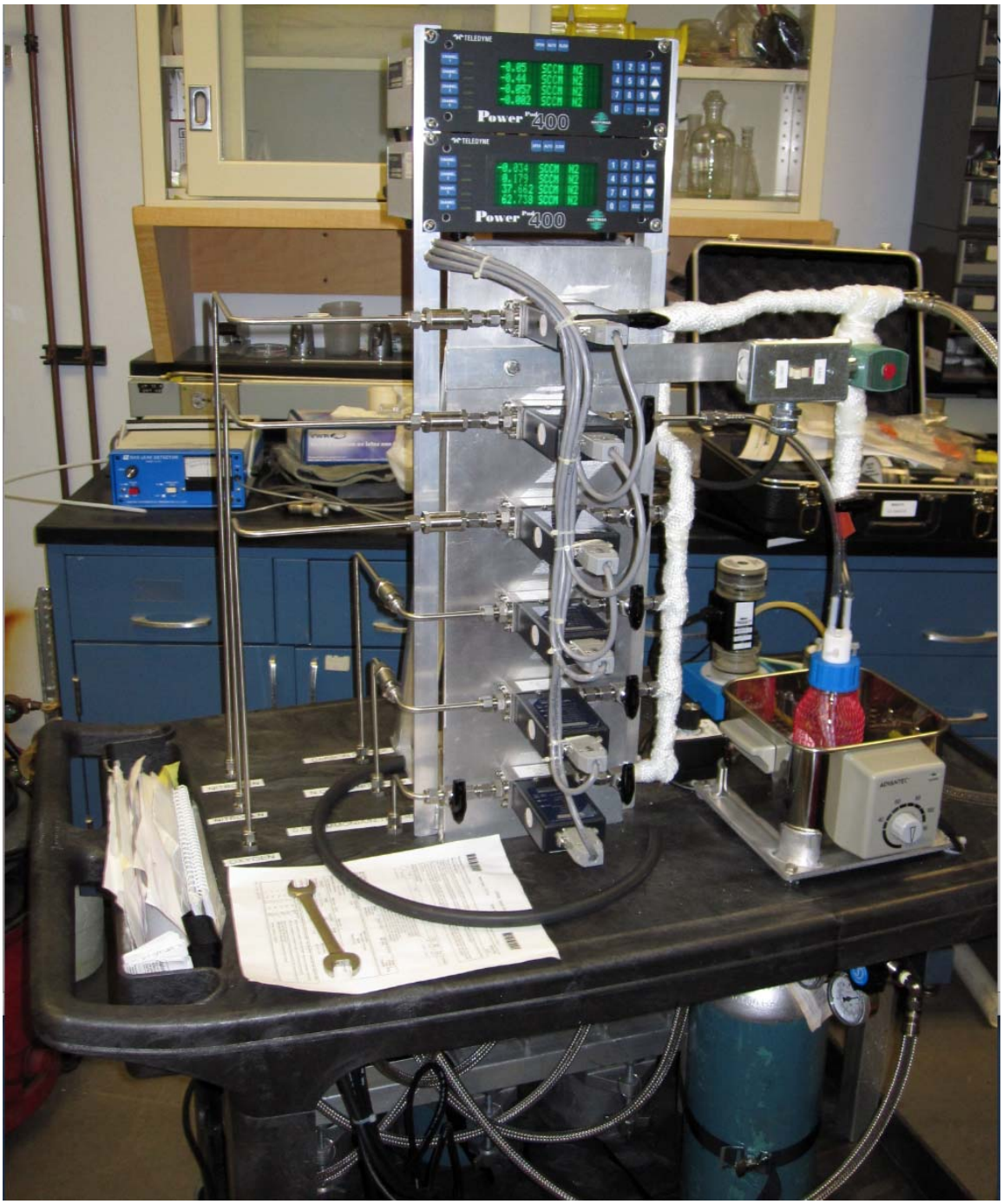

Figure 1 - The assembled and redesigned portable manifold system. The total flow of the system will range from 50 to 400 standard cubic centimeters per minute (sccm) and handle six component gases: N_2, NO, O_2, NH_3, CO_2 and H_2O. The gas lines will be heated to >150°C to prevent water condensation and in-line deposits. Given the corrosive and toxic nature of NH_3 and NO, respectively, these will originate from cylinders with dilute starting mixture of each.

Agreement 10461: Durability of Diesel Engine Particulate Filters

Thomas R. Watkins, Amit Shyam, Hua-Tay Lin and Edgar Lara-Curzio
Oak Ridge National Laboratory

Randall J. Stafford
Cummins, Inc.

Objective

The objective of this effort is to identify and implement test techniques to characterize the physical and mechanical properties of ceramic diesel particulate filters (DPFs), to identify the mechanisms responsible for the degradation and failure of DPFs and to develop analysis tools for predicting their reliability and durability.

Goals, Barriers, Relevance & Integration

In the study area of the Office of Vehicle Technologies' (OVT) Materials Technology subprogram, the Propulsion Materials Technology activity provides materials R&D expertise to enable advanced materials and supports the goals of several OVT subprograms.[1] Within the Advanced Combustion Engine subprogram-Combustion and Emission Control R&D activity, one *goal* is by 2015, to develop materials, materials processing, and filter regeneration techniques that reduce the fuel economy penalty of particle filter regeneration by at least 25 percent relative to the 2008 baseline. This project addresses four *barriers*[1] related to the Emission Control: Lack of cost-effective emission control, lack of modeling capability for emission control, improving durability and costly precious metal content. This project is *relevant* to this goal as the understanding of the relationships of the material properties for the filter (and catalyst) substrates enables optimization of porosity, strength, elastic modulus, thermal conductivity, thermal expansion, etc. leading to improved materials processing and models and optimized regeneration strategies that improve fuel economy and increase DPF life. This project also addresses two *barriers*[1] related to the Propulsion Materials Technology activity itself: Changing internal combustion engine combustion regimes and costly precious metal content. This project supports clean diesel, which increases acceptance by the public. Larger acceptance, in turn, results in larger percentages of conversion to diesel, with the resulting reduction in petroleum usage/dependency upon foreign oil. This project is *integrated* within Vehicle Technologies program as it utilizes characterization tools acquired and maintained by the High Temperature Materials Laboratory (HTML) Program.

Technical Highlights

In the reporting period, the ORNL team continued characterizing a new SiC-based DPF material. The DPF honeycomb monoliths were sectioned, and samples were machined as before.[2] Double torsion fracture toughness testing was performed at 800 and 900°C as described elsewhere.[2,3] The average fracture toughnesses, K_{IC}, are listed in Table I. Unlike the cordierite, the fracture toughness of the SiC-based DPF appears to increase with temperature. As was speculated earlier,[3] the mechanism for this increase in toughness is due to increased ductility of the free Si nodules. It should be noted that

the average value at 800°C incorporates one large value (1.22 MPa√m), which may be an outlier. If this datum is excluded, the average value becomes 0.83 (0.06) MPa√m. Data collection at 800°C continues with collections at 300°C to follow.

The fracture surfaces of successfully tested double torsion samples were examined using the SEM (see Figure 1). In examining these micrographs, it is often difficult to discern pre-fracture/pre-existing surfaces from post-double torsion fracture-related surface features. Machining debris can be seen in Figure 1A, and the absence of same indicates a post machining fracture surface (see center of Figure 1A). Careful inspection reveals a "crust" around the prominent and very flat fracture surface seen (lower center left). The round features are composed of silicon; the block-shaped features are the SiC. Both the SiC grains and Si nodules fracture in a transgranular fashion. In Figure 1B, a close up of a similar region clearly shows the "crust" around a fracture Si nodule, which is most likely a silicate glass. Given the short duration at temperature before fracture (<15 min.), it was felt that the crust had a negligible effect on the fracture toughness values

Status of FY 2011 Milestones

In the reporting period, the ORNL team continued characterizing a new SiC-based DPFs, which is part of the milestone to continue to investigate the interaction and properties of washcoat, soot and substrate on properties of new and field tested DPFs. Later in FY11, we plan to initiate characterization of the dynamic and static fatigue response of SiC DPFs (second milestone).

Travel, Presentation, Personnel

ORNL personnel traveled to Washington, DC, for the DOE 2011 Vehicle Technologies Annual Merit Review and Peer Evaluation Meeting on May 11, 2011, and made the following presentation:

T. R. Watkins, A. Shyam, H.T. Lin, E. Lara-Curzio, R. Stafford, T. Yonushonis, "Durability of Diesel Engine Particulate Filters," presented at the DOE 2011 Vehicle Technologies Annual Merit Review and Peer Evaluation Meeting, Washington, D.C., May 11, 2011.

A summer student, Mr. Kevin Wright, from Clemson has been hired to assist with the fracture toughness measurements.

References

1. Vehicle Technologies Program, Multi-Year Program Plan 2011-2015, Dec. 2010, pp. 2.3-4; 2.5-7, 8.
2. A. Shyam, E. Lara-Curzio, T. R. Watkins and R. J. Parten, "Mechanical Characterization of Diesel Particulate Filter Substrates," *J. Am. Ceram. Soc.*, **91** [6] 1995–2001 (2008).
3. T. R. Watkins et al., "Agreement 10461: Durability of Diesel Engine Particulate Filters," Second Quarter FY2011 Propulsion Materials Quarterly Report (January-March 2011).

4. A. Shyam, E. Lara-Curzio[ζ], T. R. Watkins, K, L. More, "The role of microstructure in determining the thermal expansion, elastic and fracture properties of porous cordierite at elevated temperatures," in preparation.

Table I – Fracture toughness, K_{IC} (MPa√m), of various DPF materials at ambient and elevated temperatures.

Temperature	Cordierite [26]	Al_2TiO_5	SiC
RT	0.38(0.02)	0.13(0.02)	0.42(0.05)
300°C	0.34(0.04)		
500°C	0.31(0.05)	0.16(0.02)	0.55(0.03)
800°C	0.36(0.03)		0.93(0.20)
900°C	0.36(0.02)		0.72(0.20)

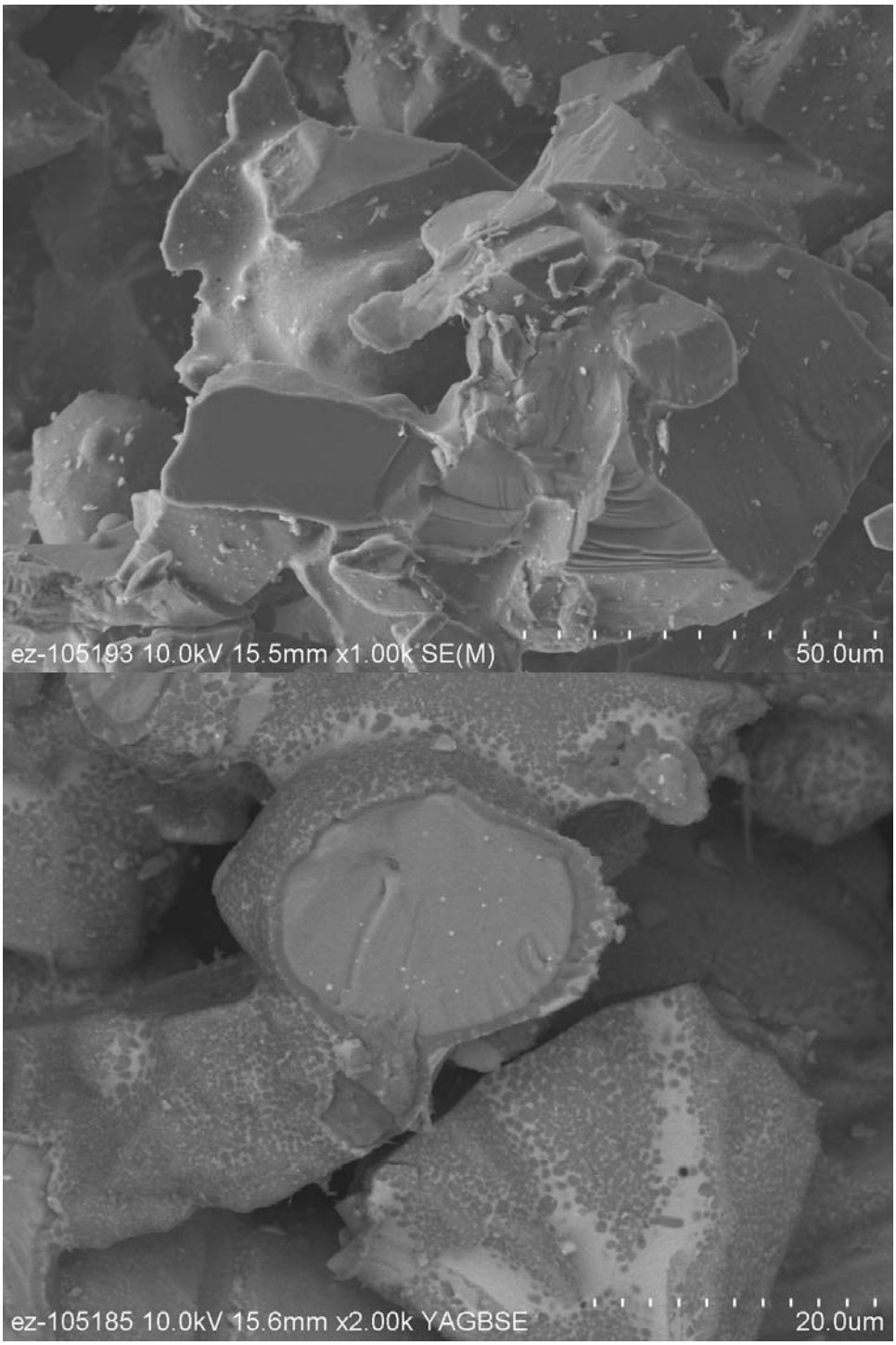

Figure 1 – A). SEM micrograph of the double torsion fracture surface of a SiC-based DPF material tested at 900°C. B). A close up backscattered electron image (BSE) of a silicon nodule and the surrounding area of another region in the sample. Here, the lighter appearing phase indicates a higher atomic number.

Agreement 10635: Catalysis by First Principles

C. Narula, M. Moses DeBusk, Xiaofan Yang
Oak Ridge National Laboratory

Objective/Scope

This research focuses on an integrated approach between computational modeling and experimental development, design and testing of new catalyst materials, that we believe will rapidly identify the key physiochemical parameters necessary for improving the catalytic efficiency of these materials. The results will have direct impact on the optimal design, performance, and durability of supported catalysts employed in emission treatment; e.g., lean NO_x catalyst, three-way catalysts, oxidation catalysts, and lean NO_x traps etc.

The typical solid catalyst consists of nano-particles on porous supports. The development of new catalytic materials is still dominated by trial and error methods, even though the experimental and theoretical bases for their characterization have improved dramatically in recent years. Although it has been successful, the empirical development of catalytic materials is time consuming and expensive and brings no guarantees of success. Part of the difficulty is that most catalytic materials are highly non-uniform and complex, and most characterization methods provide only average structural data. Now, with improved capabilities for synthesis of nearly uniform catalysts, which offer the prospects of high selectivity as well as susceptibility to incisive characterization combined with state-of-the science characterization methods, including those that allow imaging of individual catalytic sites, we have compelling opportunity to markedly accelerate the advancement of the science and technology of catalysis.

Computational approaches, on the other hand, have been limited to examining processes and phenomena using models that had been much simplified in comparison to real materials. This limitation was mainly a consequence of limitations in computer hardware and in the development of sophisticated algorithms that are computationally efficient. In particular, experimental catalysis has not benefited from the recent advances in high performance computing that enables more realistic simulations (empirical and first-principles) of large ensemble atoms including the local environment of a catalyst site in heterogeneous catalysis. These types of simulations, when combined with incisive microscopic and spectroscopic characterization of catalysts, can lead to a much deeper understanding of the reaction chemistry that is difficult to decipher from experimental work alone.

Thus, a protocol to systematically find the optimum catalyst can be developed that combines the power of theory and experiment for atomistic design of catalytically active sites and can translate the fundamental insights gained directly to a complete catalyst system that can be technically deployed.

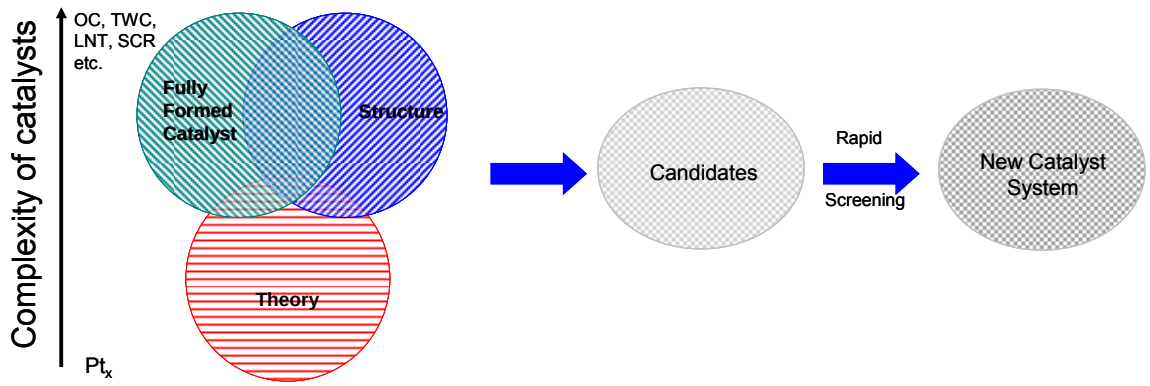

Although it is beyond doubt computationally challenging, the study of surface, nanometer-sized, metal clusters may be accomplished by merging state-of-the-art, density-functional-based, electronic-structure techniques and molecular-dynamic techniques. These techniques provide accurate energetics, force, and electronic information. Theoretical work must be based on electronic-structure methods, as opposed to more empirical-based techniques, so as to provide realistic energetics and direct electronic information.

A computationally complex system, in principle, will be a model of a simple catalyst that can be synthesized and evaluated in the laboratory. It is important to point out that such a system for experimentalist will be an idealized simple model catalyst system that will probably model a “real-world” catalyst. Thus it is conceivable that “computationally complex but experimentally simple” systems can be examined by both theoretical models and experimental work to forecast improvements in catalyst systems.

We have focused on the oxidation catalyst and SCR catalyst to develop and demonstrate catalyst by design protocol as a prelude to developing catalyst by design protocols for complex emission treatment catalysts; e.g., TWCs, NO_x traps, and HC-SCR catalysts. Our goals are as follows:

- Our theoretical goal is to carry out the calculation and simulation of realistic supported Pt nanoparticle systems (i.e., those equivalent to experiment), in particular by addressing the issues of complex cluster geometries on local bonding effects that determine reactivity. As such, we expect in combination with experiment to identify relevant clusters, and to determine the electronic properties of these clusters. In addition, we plan to study zeolite structures with a view to develop an insight on the mechanistic aspects of catalytic process to enable us to develop better catalysts.
- Our experimental goal is to synthesize metal carbonyl clusters, decarbonylated metal clusters, sub-nanometer metal particles, and metallic particles (~5 nm) on alumina (commercial high surface area, sol-gel processed, and mesoporous molecular sieve), characterize them employing modern techniques including Aberration Corrected Electron Microscope (ACEM), and evaluate their CO, NO_x,

and HC oxidation activity. Furthermore, guided by theoretical studies we plant to synthesize new zeolites and characterize them.

- This approach will allow us to identify the catalyst sites that are responsible for CO, NO_x, and HC abatement. We will then address design of new durable catalysts systems that can withstand the prolonged operations.

Technical Highlights

Until recently, our theoretical studies have focused on supported noble metals. We have shown that single platinum atoms supported on θ-alumina slab contain platinum atom is in the zero oxidation state. This result is very different from that reported in literature on single platinum atoms supported on α-alumina or simplified models of γ-alumina where a platinum atom generally has an unpaired electron. This also means that mechanism of CO, NO_x, or HC oxidation on Pt(0) will be different from that on Pt(I) or Pt(II). We plan to carry out first principle studies of CO oxidation on Pt atoms supported on θ-alumina slab.

Since our experimental work has already shown that the distribution of platinum on γ-alumina and θ-alumina is almost identical, and the surface properties and CO oxidation of both catalysts are identical, we propose that Pt supported on θ-alumina is a better model for Pt supported on γ-alumina than Pt supported on α-alumina or simplified models of γ-alumina.

We have also shown that incorporation of palladium in platinum particles at sub-nanometer scale is quite ineffective in improving the durability, however, large Pt-Pd nanoparticles tend to be more hydrothermally durable than pure Pt particles. While efforts are in progress to prepare sub-nanometer Pt-Pd particles to validate the results of theoretical studies, we have initiated theoretical studies of SCR-zeolite-catalysts.

In this report, we describe our theoretical studies on single atoms of Ni, Pt, Pd, Cu, Ag, Au employing Gaussian smearing functions with a width of 0.05 eV to states near Fermi level to facilitate convergence and obtain high quality Density of State data. The experimental work summarizes our efforts to synthesize a complex containing Pt-Pd bond which we plan to employ to synthesize sub-nanometer particles Pt-Pd supported on alumina to validate our theoretical studies.

Theoretical Studies: In the 2nd quarter report, we presented the bonding picture and Density of States analysis of platinum group metal (Ni, Pd, and Pt) and coinage metal (Cu, Ag, Au) atoms adsorbed on θ-alumina (010) surface. All platinum group or coinage metal atoms preferentially adsorbed on a bridging position between 2 oxygen atoms from adjacent layers and were located above aluminum. Moreover, the platinum group atoms showed d^{10} configuration with no associated magnetization.
In this report, we present charge density analysis of these systems. The charge density differences for the metal atom-substrate system were calculated to obtain insight into the differences in surface binding according to the following equation:

$$\Delta\rho = \rho_{M\text{-}Alumina} - (\rho_{Alumina} + \rho_M)$$

The $\rho_{M\text{-}Alumina}$ is charge density of total system, $\rho_{Alumina}$ is the charge density of alumina surface fixed at the adsorbed geometry, and the ρ_M is the electron density of the metal atom fixed at the adsorbate geometry.

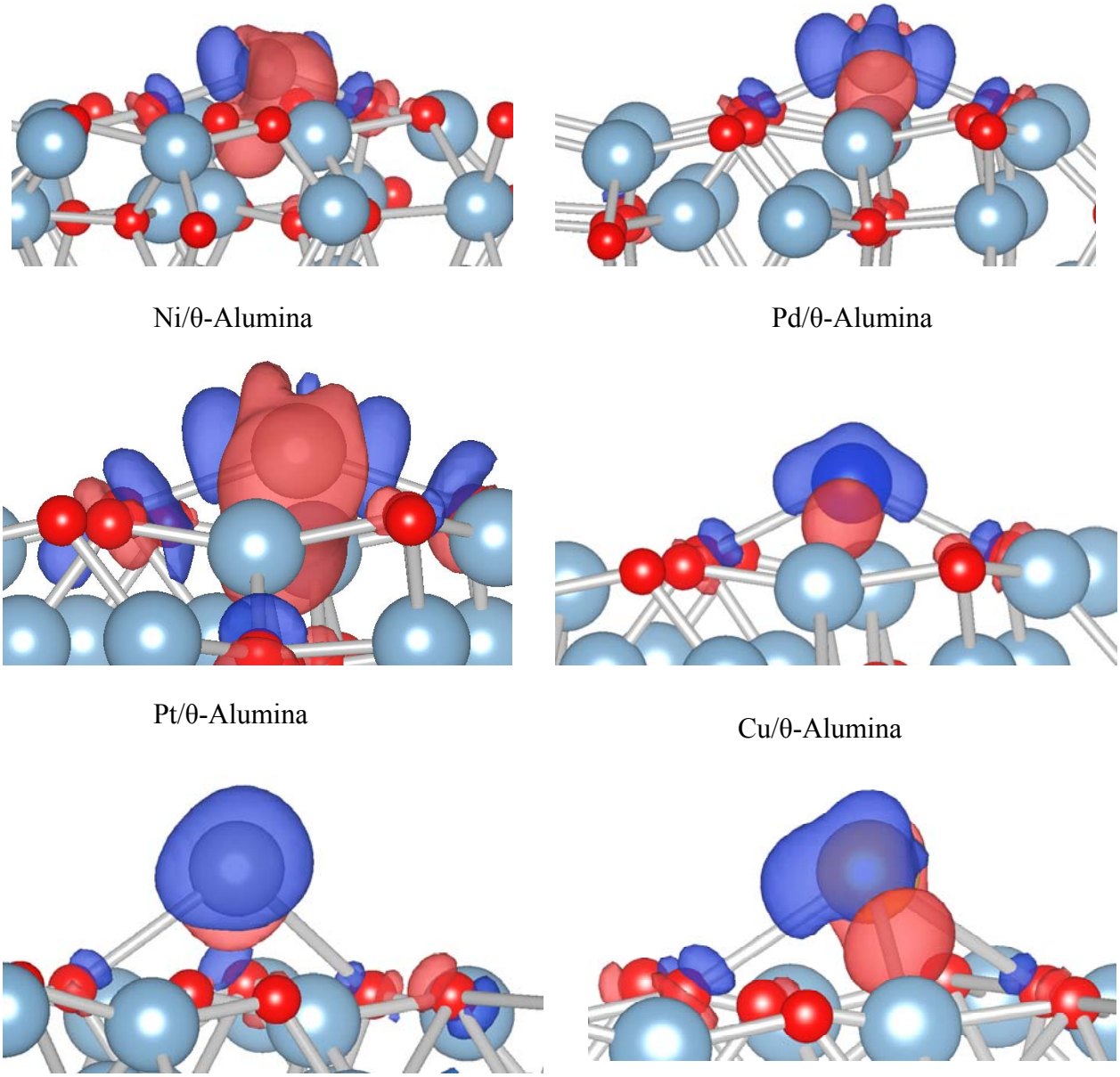

Figure 1: Charge density difference isosurfaces (0.005 e/Å^3 for Pt group atoms and 0.008 e/Å^3 for coinage metal atoms) for metal adsorption on θ-Alumina (010) surface.

The density of state analysis suggested that Ni is in $3d^{10}$ state and Ni s, d and O 2p orbitals are strongly hybridized as a result of mixing of s-d metal hybrids with O2p orbitals. This was further supported by lack of magnetization at Ni. The charge

distribution analysis also supports this bonding picture and shows charge depletion (blue color in Figure 1) Ni and O atoms despite covalent bonding and charge accumulation near Ni atoms. This net charge shift away from Ni to oxygen results from interaction between Pt atom and surface oxygen ions. The Ni atom – surface bonding interaction appears to be localized to the adsorption site. Since GGA tends to exaggerate electron delocalization due to incomplete treatment of self-interactions, the localization of bonding can be considered to be robust to the GGA approximation. The charge density plots for Pt and Pd adsorbed on θ-Alumina (010) surface are very similar to adsorbed Ni atom reflecting similar bonding interactions.

The coinage metal requires high excitation energy to go from ground state to excited state. As such, their configuration does not easily change form ground to excited state. While the coinage atoms also favor the location between two surface oxygen atoms, their bonding picture is somewhat different from those of platinum group atoms. The coinage atom exhibits filled d orbitals and occupied s-orbital with magnetization primarily associated with s orbitals. The charge density plots for coinage atoms adsorbed on θ-Alumina (010) surface are superficially similar to adsorbed platinum atoms reflecting similar underlying bonding interactions. The charge transfer can be seen on subsurface oxygen atoms also while there is no charge transfer to aluminum atoms.

Thus, the charge density calculations complete the picture of bonding of platinum group and coinage atoms adsorbed on θ-Alumina (010) surface, presented in the previous report.

Experimental Studies: In the previous report, we have shown that PdPt nanoalloy samples, i.e., PVPPdPt14, PVPPdPt11, and PVPPdPt41, synthesized employing PVP polymer as a template, exhibit ~ 2.5 nm Pd-Pt particles regardless of Pd:Pt. Hydrothermally aging of PVPPdPt41 results in particle size growth to 3.5 nm, 4.5 nm, 13 nm, and 20 nm at aging temperature of 500°C, 600°C, 750°C, and 900°C, respectively. In this report, we summarize our results on PVPPdPt14 and PVPPdPt11 samples.

Hydrothermal Aging of PVPPdPt14: We employed hydrothermal aging protocol reported by researchers at Ford Motor Company (Catalysis Letters, 2007, 116, 1-8). A typical procedure is as follows: 0.7 g of PdPt nano alloy was treated under a flow (5L/min) of N_2, O_2 (5%) and H_2O (10%) for 3 hours at a series of temperatures (500°C, 600°C, 750°C and 900°C). The temperature ramp up and down was carried out under pure N_2. TEM studies of resulting samples show particle size growth to 3.5 nm, 4.5 nm, 7.5 nm, and 30 nm at aging temperatures of 500°C, 600°C, 750°C and 900°C, respectively.

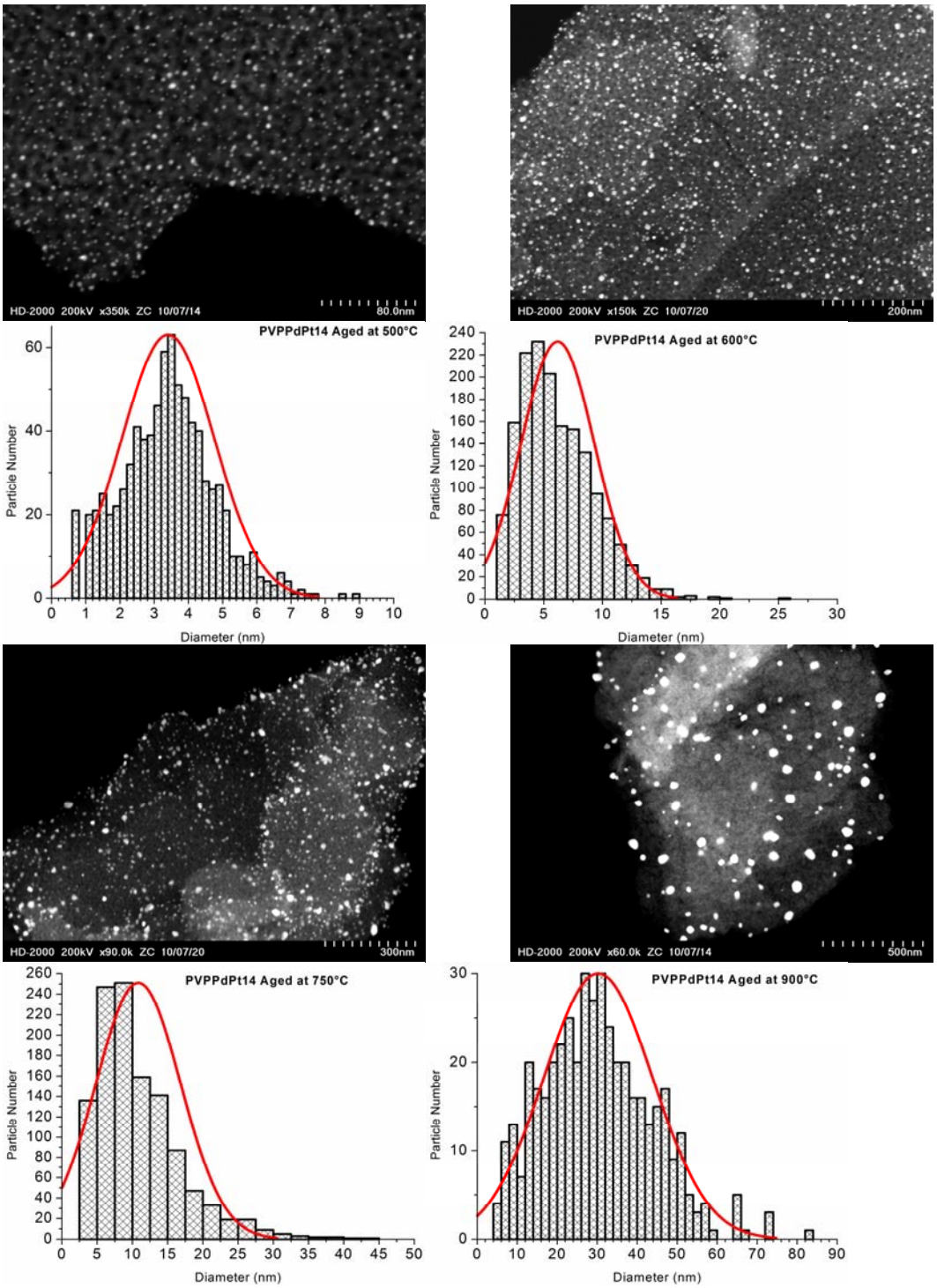

Hydrothermal Aging of PVPPdPt11: A 0.7 g of PdPt nano alloy was treated under a flow (5L/min) of N_2, O_2 (5%) and H_2O (10%) for 3 hours at a series of temperatures (500°C, 600°C, 750°C and 900°C). The temperature ramp up and down was carried out under pure N_2. TEM studies of resulting samples show particle size growth to 3.0 nm, 4.5 nm, 12.5 nm, and 30 nm at aging temperatures of 500°C, 600°C, 750°C and 900°C, respectively.

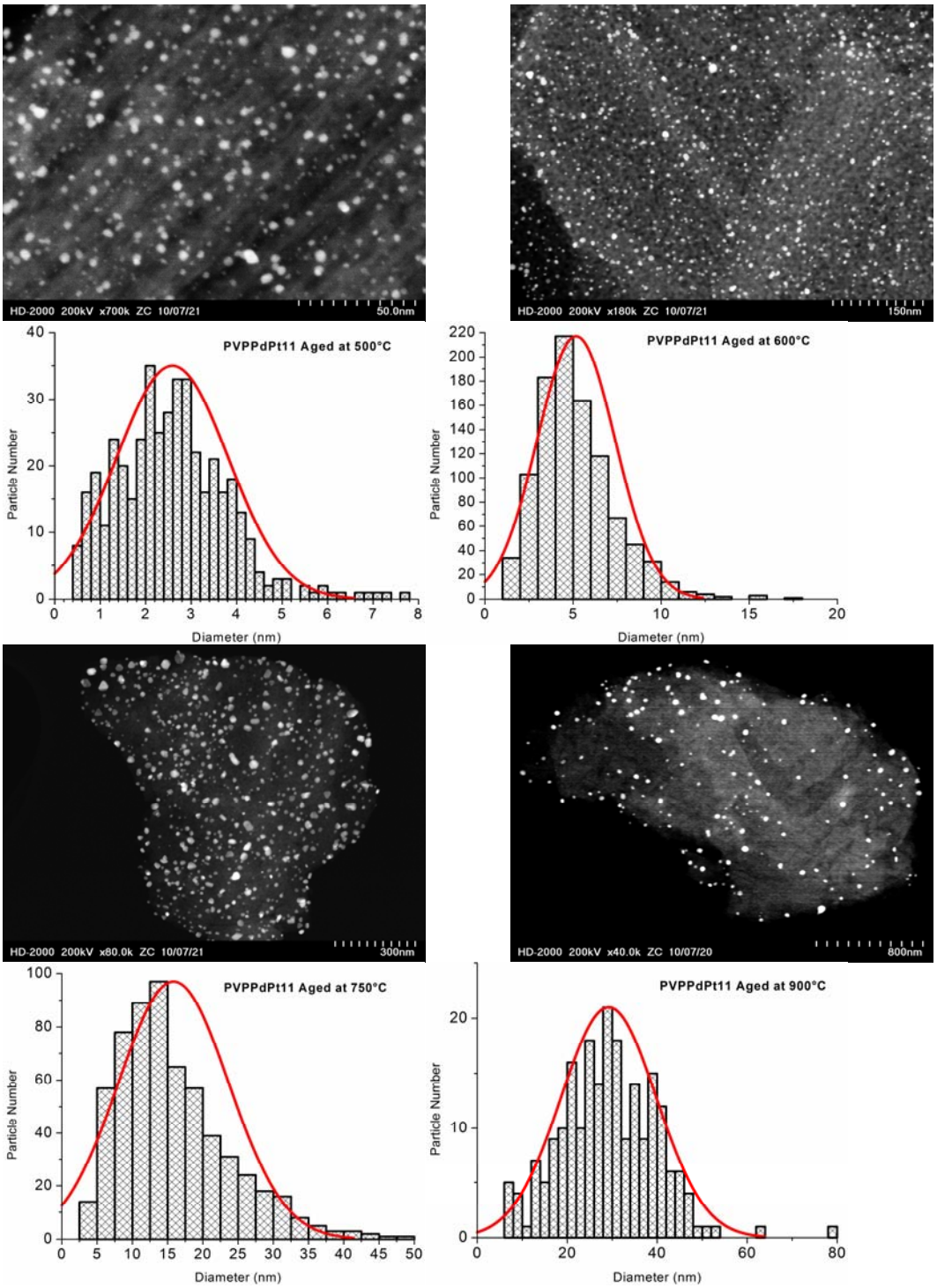

<u>Size Distribution Comparison:</u> The following table is to summarize the particle size change of three samples PVPPdPt14, PVPPdPt11, and PVPPdPt41 at different aging temperatures. It is clear that alloying Pd into the Pt nanoparticle dramatically restrains the size growth under hydrothermal aging. For example, the size of pure Pt nanoparticle reported in literature (Catalysis Letters, 2007, 116, 1-8) grows to 9 nm after aging at 500°C. The Pd/Pt samples developed in this study show enhanced hydrothermal

stability compared to the literature results, 3.5 nm vs. 5 nm after aging at 500°C. The ratio of Pd to Pt in the nanoalloy shows no difference in controlling particle size growth when the samples are aged at low temperatures, i.e., 500°C and 600°C, and under extreme condition at 900°C, whereas less amount of Pd seems to better stabilize the particle at 750°C.

Table 1. Size distribution comparison among PVPPdPt14, PVPPdPt11, and PVPPdPt41 after different aging conditions.

	500°C	**600°C**	**750°C**	**900°C**
Pd : Pt = 1 : 4	3.5	4.5	7.5	30
Pd : Pt = 1 : 1	3.5	4.5	12.5	30
Pd : Pt = 4 : 1	3.5	4.5	13	30

Sub-nanometer Pt-Pd supported on γ-alumina: In the previous report, we described the synthesis of *trans*-[$(NH_3)_2$Pt(1-methylcytosine)PdCl]NO_3, a precursor for controlled deposition of Pt-Pd in 1:1 ratio. Since the pure samples of this compound could not be prepared, we used its mixture with trans-[Pt$(NH_3)_2$(1-methylcytosine)]$(NO_3)_2$ (parent compound) for the deposition of Pt-Pd clusters. The TEM of the resulting material shows sub-nanometer particles which are essentially agglomerates of single atoms (Figure 2).

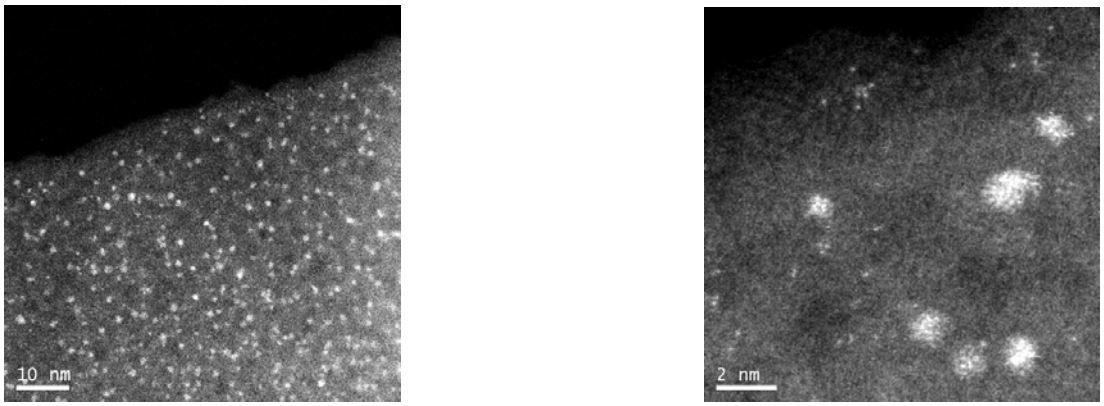

Figure 2: TEM of Pd-Pt on γ-alumina. The low-magnification (left) suggest ~1 nm particles which exhibit agglomerate features at high magnification (right).

Further characterization employing aberration corrected electron microscope is in progress and will be presented in a future report.

Status of FY2011 Milestones:

1. We will complete theoretical modeling of large supported Pt clusters and carry out mechanistic studies of CO, NO_x, and HC oxidation.

   Theoretical modeling of large supported Pt clusters is ongoing. We will initiate mechanistic studies after obtaining data for ~10 atom clusters.

2. We will also explore bimetallic subnanomenter supported Pt-Pd clusters to determine lowest energy system, synthesize them, and determine their stability under CO, NOx, and HC oxidation conditions. The results will facilitate the search for optimum catalyst systems for CO, NO, and hydrocarbon oxidation and NO_x reduction.

   We have synthesized subnanometer Pt-Pd supported on γ -alumina are attempting to characterize them employing ACEM.

Communication/Visits/Travel

We have prepared a manuscript titled "Density Functional Studies of Adsorption of Transition Metal Atoms on θ-Al_2O_3(010) Surface" for Physical Review.

PI is lead organizer of a symposium on emission treatment for energy production and utilization at ACS meeting, Denver, August, 2011. There will be three sessions at the symposium addressing chemistry of emission treatment catalyst.

A joint project on lean NO_x treatment is ongoing with John Deere Co under work for others arrangement.

Problems Encountered

The characterization of Pt-Pd subnanometer catalysts supported on γ–alumina is pending due to ongoing repair of ACEM.

Publications

1. C.K. Narula, M.G. Stocks, "Density Functional Studies of Adsorption of Transition Metal Atoms on θ-Al_2O_3(010) Surface" Physical Review.
2. C.K. Narula, "Catalyst by Design – Bridging the Gap between Theory and Experiments at Nanoscale Level" Encyclopedia of Nanoscience and Nanotechnology, Vol. II, Taylor & Francis, New York, 2008, pp 771-782 (invited).
3. C.K. Narula, L.F. Allard, D.A. Blom, M. Moses-DeBusk, "Bridging the Gap between Theory and Experiments – Nano-structural Changes in Supported Catalysts under Operating Conditions" SAE-2008-01-0416, SAE Int. J. Mater. Manu., 1(2008) 182-188.
4. C.K. Narula, L.F. Allard, D.A. Blom, M.J. Moses, W. Shelton, W. Schneider, Y. Xu, "Catalysis by Design - Theoretical and Experimental Studies of Model Catalysts", SAE-2007-01-1018 (invited).

5. C.K. Narula, M.J. Moses, L.F. Allard, “Analysis of Microstructural Changes in Lean NO_x Trap Material Isolates Parameters Responsible for Activity Deterioration” SAE 2006-01-3420.
6. Y. Xu, W.A. Shelton, and W.F. Schneider, “The thermodynamic equilibrium compositions, structures, and reaction energies of Pt*x*O*y* (*x* = 1-3) clusters predicted from first principles,” *Journal of Physical Chemistry B,* 110 (2006) 16591.
7. Y. Xu, W. A. Shelton, and W. F. Schneider, “Effect of particle size on the oxidizability of platinum clusters,” *Journal of Physical Chemistry A*, 110 (2006) 5839.
8. C.K. Narula, S. Daw, J. Hoard, T. Hammer, “Materials Issues Related to Catalysts for Treatment of Diesel Exhaust,” *Int. J. Amer. Ceram. Tech*., 2 (2005) 452 (invited).

Presentations (last 12 months)

1. Narula, C.K. Stocks, G.M., Density Functional Studies of Adsorption of Transition Metal Atoms on θ-Al_2O_3(010) Surface” American Chemical Society Meeting, Denver, CO, August 28, 2011.
2. Narula, C.K.; Chen, X.; Stocks, G.M., DeBusk, M.M.; Allard, L.F.; “First-Principles and Experimental Studies of the Sub-Nanomenter Platinum Atoms Supported on θ-Alumina” 230th American Chemical Society Meeting, Boston, MA, August 22-26, 2010
3. Narula, C.K.; Chen. X.; Stocks, M.G.; “First-Principles Studies of the Structure and Bonding of Metal Atoms Supported on θ-Alumina,” 229th American Chemical Society Meeting, San Francisco, CA, March 21-25, 2010.
4. Moses-DeBusk, M.; Narula, C.K. "Catalyst by design: Combining the power of theory, experiments, and nanostructural characterization for catalyst development," 227th National American Chemical Society Meeting, March 2009 (invited).

References

1. Moore, C.E. *Atomic Energy Levels*: Natl. Bur. Stand. U.S. Circ. No. 467; GPO: Washington, DC, 1952.
2. Yudanov, I; Pachhioni, G.; Neyman, K.; Rosch, N.; J. Phys. Chem. B **1997**, *101*. 2786.
3. Hosmane, R.S.; Leonard, N.J.; Synthesis **1981**, 118-119.
4. Lipper, B.; Lock, C.J.L.; Speranzini, R.A.; Inorg. Chem. **1981**, *20*, 808.

Agreement 19214: Effects of Biodiesel Fuel on Diesel Particulate Filter Materials

M. J. Lance, A. A. Wereszczak, and E. E. Fox, and T. J. Toops
Oak Ridge National Laboratory

Objective/Scope

To characterize changes in the microstructure and material properties of commercial diesel particulate filters (DPFs) in exhaust gas produced by biodiesel blends.

Technical Highlights

Three considered DPF materials are being examined and are shown in Fig. 1. One is a cordierite and the other two are silicon carbides (SiCs) with different porosity contents. For each material, three specimen geometries are being harvested out of the DPFs for the mechanical evaluations: O-ring specimens, biaxial flexure disks, and sectored flexure specimens.

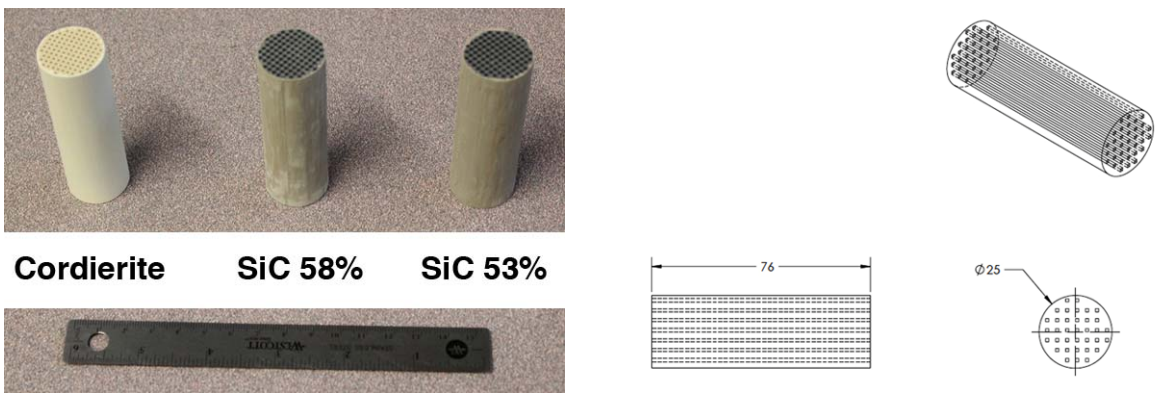

Figure 1. The mechanical properties of three DPF materials (left) are being evaluated. The nominal dimensions (right) of the DPF are 25-mm diameter and 76-mm-length.

Preliminary mechanical testing of DPF specimens was completed in Q3 for the estimation of the materials (tensile) failure stress as a function of tensile-stress-direction and location. Table 1 shows the failure stress for the three DPF materials being studied in this project under biaxial flexure. The SiC samples clearly had more than 10 times the strength as the cordierite sample even at the same porosity. The higher porosity SiC sample (58% porosity) similarly had a fracture stress 10% below the lower porosity SiC (52% porosity). The end cap of the DPF which had alternating channels filled with ceramic was also tested and had a fracture stress 50 to 130% higher than the sample extracted from the interior. These results constitute baseline measurements that will be compared in the future to DPF samples aged in different conditions to simulate operation in biodiesel and ULSD fuels.

Table 1: Fracture strength of DPF materials under biaxial flexure

Material	Location	Failure Stress (Mpa	StDev
SiC 52% Porosity	Interior	2.18	0.40
	End Cap	3.66	1.31
SiC 58% Porosity	Interior	1.95	0.44
	End Cap	2.92	0.41
Cordierite 59% Porosity	Interior	0.18	0.09
	End Cap	0.42	0.23

Status of FY2011 Milestones

1. Measure the chemical composition and pH of condensate and PM generated by a diesel engine running with ULSD and biofuel blends. (12/10) *On Schedule.*
2. Age filter samples (cordierite, SiC and possibly mullite) in solutions identical to condensate composition. (9/11) *On Schedule.*
3. Monitor microstructural and mechanical property changes in DPF substrates following chemical ageing. (9/11) *On Schedule.*

Communications/Visits/Travel

None.

Problems Encountered

None.

Publications/Presentations/Awards

None.

References

None.

Agreement 20091: Electrically Assisted DPF Material

M. J. Lance, A. A. Wereszczak, J. E. Parks, W. P. Partridge, and E. E. Fox
Oak Ridge National Laboratory

Objective/Scope

In this CRADA project with General Motors (GM), two research objectives are being pursued:

1. Measure of substrate temperatures during DPF regeneration with optically based techniques that are not susceptible to conductive interferences that are problematic for common thermocouple technologies.
2. Analysis of diesel particulate filter (DPF) substrate materials to understand crack and failure mechanisms and resolve current differences in simulation and experimental results.

Technical Highlights

Research in this quarter focused on engine-based studies of the electrical-assisted regeneration method as compared with the traditional fuel-based regeneration method. Problems encountered with temperature measurement of the electrical heater in earlier work were addressed in collaboration with GM by adding isolators to the data acquisition system; this allowed more accurate control of the heater temperature which enabled the studies to be performed reproducibly. The procedure for the studies basically consisted of loading the DPF with particulate matter (PM) under a defined protocol then regenerating the DPF with either the electrical-assisted or fuel-only based regeneration methods. The DPF system was weighed before and after regeneration to determine the mass of PM collected on the DPF and oxidized during regeneration.

A sample result is shown here for demonstration. An electrical-assisted regeneration ("E Regen") technique was used with a target heater temperature of 900ºC for 1 minute duration per heater element. For comparison, a fuel-based regeneration ("Fuel Regen") was also conducted using the same loading protocol. Both methods utilized post-injection for adding fuel to the exhaust for exothermic heating of the DPF. However, the E Regen required a shorter time frame for extra fuel consumption due to the acceleration of PM oxidation produced by the electric heater temperature rise. The difference in time results in a fuel penalty reduction for the E Regen case (shown in relative units in Table 1).

Table 1. Data showing regeneration efficiency and fuel penalty for the E Regen and Fuel Regen methods.

	E Regen	Fuel Regen
DPF Mass Loading (g)	14.7	11.4
Regeneration Efficiency	67%	69%
Fuel Penalty (relative units)	85	100

Analysis of the temperature distribution in the DPF during regeneration is being conducted for the engine-based studies to better understand the parameters affecting regeneration efficiency. Figure 1 shows histograms of temperature for both E Regen and Fuel Regen methods; both heater and DPF temperature histograms are shown for the E Regen technique. Note that only a slight variation in the temperature histogram is observed between the E Regen and Fuel Regen techniques. The 900ºC heater temperature excursions accelerate the oxidation processes but only slightly change the average DPF temperatures shown. Localized temperature increases in the DPF due to the heater processes are also being analyzed for further characterization of the regeneration process.

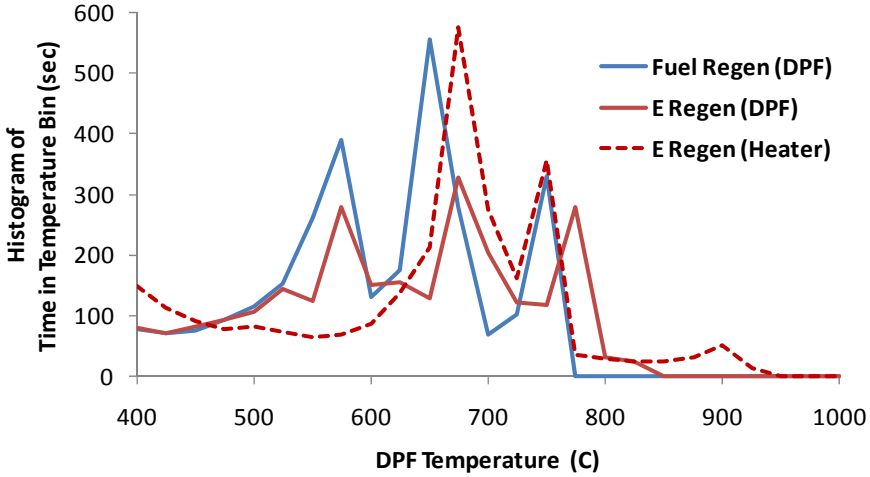

Figure 1. Histogram of temperatures experienced by the DPF and Heater during E Regen and Fuel Regen techniques (25ºC temperature bin).

Studies similar to the data shown here will be continued in the next quarter with a focus on refining the operational parameters to provide the best comparison between the electrical-assisted and fuel-based techniques.

Status of FY 2011 Milestones

1. Measurement of the fuel penalty for both Electrically-Heated DPF and conventional fuel-heated approaches (September 2011). On Schedule
2. Optimization of the fiber-optic temperature measurement technique and a rigged DPF system with fiber-optic and thermocouple probes ready for engine use (September 2011)
3. Database of strength-size-scaling statistics of ceramic used in EHDPF (September 2011) On Schedule.
4. Rank properties and geometrical parameters that most affect tensile stresses in EHDPFs (September 2011) On Schedule.
5. Rules of design for EHDPF regenerators (September 2011) On Schedule.
6. Recommendations for the best commercial alloy for this application (September 2011) On Schedule.

Communications/Visits/Travel

None.

Problems Encountered
None.

Publications/Presentations/Awards
Andrew A. Wereszczak, Michael J. Lance, and Ethan E. Fox, “Failure Stress and Apparent Elastic Modulus of Diesel Particulate Filter Ceramics,” abstract submitted to 2011 Directions in Engine-Efficiency and Emissions Research (DEER) Conference.

A. A. Wereszczak, E. E. Fox, and M. J. Lance, “Failure Stress and Apparent Elastic Modulus of Diesel Particulate Filter Ceramics,” abstract submitted to the 36th International Conference and Exposition on Advanced Ceramics and Composites in 2012.

Andrew A. Wereszczak, Ethan E. Fox, and Michael J. Lance, “Failure Stress and Apparent Elastic Modulus of Diesel Particulate Filter Ceramics,” abstract submitted to the SAE 2012 World Congress.

References
None.

Agreement 9105: Characterization of Catalyst Microstructures

L.F. Allard, C.K. Narula, W.C. Bigelow, D.P. Nackashi and J. Damiano
Oak Ridge National Laboratory

Objective/Scope

The objective of the research is to understand fundamental processes in catalytic systems with applications to transportation technologies, such as those used for the treatment of NO_x emissions, and for the production of biomass-derived liquid fuels. The research heavily utilizes new capabilities and techniques for ultra-high resolution transmission electron microscopy with the HTML's aberration-corrected electron microscope (ACEM). The research is ultimately focused on understanding the effects of reaction conditions on the changes in morphology of heavy metal species on "real" catalyst support materials (e.g. oxides and carbon materials), and the understanding of the structures of model mono-, bi- and multi-metallic catalyst systems of known particle composition. A major thrust of these studies has been to develop methods of *in situ* microscopy at elevated temperatures and under controlled gas compositions. This work has expanded with the collaboration with Protochips Inc. (Raleigh, NC), which provides a novel heating technology utilizing MEMS-based heating devices that we have shown to be stable enough to provide sub-Ångström imaging capabilities at high temperature in the ACEM. Model samples of nanoparticulates of controlled composition on carbon or oxide supports are also being studied in collaboration with the catalysis group at the University of Texas-Austin (Prof. P. Ferreira), the University of Texas-San Antonio (Prof. M. Jose-Yacaman), the University of Missouri-St. Louis (Prof. J. Liu), and University of New Mexico (Prof. A. Datye). Studies of the behavior of platinum group metal (PGM) species on oxide substrates are also being conducted with Drs. S. A. Bradley of UOP Co., and C. H. F. Peden of PNNL, and Prof. F. H. Ribiero at Purdue University. NOx trap catalyst materials BaO/Al_2O_3 are being studied with Dr. Peden and Dr. Ja Hun Kwak at PNNL and Pt-Re/C catalysts on model carbon nanotube materials are being studies with Dr. L. Zhang, also of PNNL. We have also initiated a new study of "intelligent catalysts" for automotive emission control applications, based on the self-regenerative phenomenon of heavy metal species such as Pd and Rh in Ca- and La-based perovskite crystal structures. This work is being conducted in collaboration with Prof. Xiaoqing Pan of the University of Michigan, and Ford Research Laboratory colleague Dr. Andrew Drews.

Technical Progress

Initial tests of the Gen 3 E-cell were conducted, after a number of operational difficulties were encountered and overcome, and the baseline results are shown in this report.

One issue of importance in doing reliable reactions under gaseous environments is the necessity to have an accurate knowledge of the temperature of the sample when at pressures above high vacuum levels. Typically, the Aduro heater devices are calibrated under vacuum, and a set of devices is received with an accompanying .xls file showing the calibration current vs. temperature values, as shown in Fig. 1. A number of devices were also calibrated at increasing pressures, to show how pressure (i.e. increased

conduction/convection effects) affected the heater membrane temperature. The device we used in the present experiments, Device 6 in Box 2 as shown in Fig. 1, showed the current variations seen in Table 1, and plotted in Fig. 2. This table shows the rapid increase in current required to heat to the various temperatures, with increase in pressure. It's clear that at even 10 Torr, the current increase is significant, and by 50 Torr the current required is almost the amount that would be needed at a full atmosphere. What have not yet been determined are the effects of high pressure inside the cell, with a vacuum on the external surface of the heater membrane, and also on the outside of the lower window, which is 30nm thick amorphous SiN.

In the present experiment, we were able to get useful images with a low pressure in the cell (0.71 Torr) and atmospheric pressure of air (~750 Torr). The air was admitted simply by removing the pump (supply) line from the end of the E-cell holder, which left the cell exposed to the atmosphere. Because of an unavoidable small leak in the connections to the supply line, it was not possible to control the pressure (i.e. hold it constant) at any intermediate level; it was observed that any pressure change during imaging caused significant drift in the specimen Z position (height), causing a loss of focus.

As seen in Fig. 1, a current of 2.52mA through the membrane produced a temperature of 400°C when the cell was held at a nominal 0.71 Torr (the lowest pressure reached with the external scroll pump continuously pumping on the holder, given the leak situation). Figure 3 shows an image of Au nanoparticles recorded at 2Mx direct magnification, at 0.71 Torr and a nominal 400°C. Both a high-angle annular dark-field (HA-ADF) and a bright-field (BF) image are shown. After opening the cell to a full atmosphere of air, the current in the heater membrane was increased to 5.09mA, as indicated in Fig. 1, which would give a temperature of 825°C with the heater in vacuum. However, as can be determined from the results shown in the data of Table 1 and plotted in Fig. 2, if the heater were in full atmosphere, we would expect a temperature in excess of 400°C, since the current increase needed is near a factor of 2 (e.g. at 600°C, and 400 Torr, the factor is 6.798/3.506 = 1.94. Figure 4 shows a similar area at an atmosphere of air, and at 2Mx direct magnification and (nominally) 400°C. We could detect no appreciable diminishment of signal in either the HA-ADF or BF image. The HA-ADF image clearly shows particles smaller than 1nm in size. Figure 5 shows an image pair recorded at 5Mx direct magnification, in which the 2.35Å lattice from {111} closest packed planes is resolved. <u>To our knowledge, this is the first time lattice resolution has been achieved at a significantly elevated temperature, and at a full atmosphere pressure.</u>

The ability to achieve high resolution at an atmosphere pressure in the cell can be explained by understanding that the resolution in the scanning transmission image is governed primarily by the diameter of the electron beam as it is incident on the crystal of interest, and is not affected by subsequent scattering of the electrons by the gas in the cell after the beam exits the sample. As noted in the last quarterly, in the geometry achieved in the Protochips E-cell, the electron beam path is controlled primarily by the thickness of the contact pads microfabricated onto the heater chip, and to some extent

by the pressure in the cell. An atmosphere pressure in the cell caused the membranes to balloon so that the gas path grew to a measured 13 microns. This path length is still small enough (especially compared to the 10 mm gas paths in a full "environmental TEM" that uses differential pumping to isolate the cell region from the remainder of the electron optical column) so that virtually all of the electrons that exit the sample are collected by the HA-ADF and BF detectors, thereby producing images that are not affected by the pressure. Further work is needed to quantify this capability, and to determine the ultimate limits of image resolution in the environmental cell. Results of these new studies will be reported in the next quarterly.

Status of Milestones

On schedule

Communications/Visits/Travel

1. Larry Allard visited GM Tech Center, Warren, MI, to discuss potential future collaborations in catalyst studies, grapheme materials, and novel magnet materials studies.
2. Larry Allard presented an invited talk entitled "Recent Developments in *In Situ* Heating and Gas-Reaction Studies of Catalytic Materials via STEM Imaging in an Aberration-Corrected Electron Microscope," at the Argonne National Laboratory Annual User Meeting, Workshop on "*In Situ* Catalysis Studies," May 2-4, 2011.

Publications

1. "Characterization of alumina-supported Pt and Pt–Pd NO oxidation catalysts with advanced electron microscopy," O.K. Ezekoye, A.R. Drews, H.-W. Jen, R.J. Kudla, R.W. McCabe, M. Sharma, J.Y. Howe, L.F. Allard, G.W. Graham and X.Q. Pan, J. Catalysis, **280**(1), 16 May 2011, p. 125-136

Table 1. Calibration table for current vs. pressure for 4 temperatures (600, 700, 800 and 900°C, showing effects of atmosphere on temperature of a heater membrane.

Table 1

Device 6 box 2					
Pressure	VAC	10Torr	50Torr	100Torr	400Torr
600	3.5062358	5.47849344	6.37433669	6.58471083	6.79859122
625	3.65476573				
650	3.80958764				
675	3.97096806				
700	4.13918481	6.20877722	7.45053266	7.76097152	7.91619095
725	4.31452751				
750	4.49729801				
775	4.68781097				
800	4.88639438	7.27584123	8.83460104	9.35255884	9.5626738
825	5.09339011				
850	5.30915451				
875	5.53405906				
900	5.76849093	8.19125711	10.2967563	10.9197533	11.3293162

TEMP	DEVICE #1	DEVICE #2	DEVICE #3	DEVICE #4	DEVICE #5	DEVICE #6
200	1.86	1.85	1.85	1.72	1.84	1.81
225	1.94	1.93	1.93	1.80	1.92	1.88
250	2.02	2.01	2.01	1.89	2.01	1.96
275	2.11	2.09	2.10	1.98	2.09	2.04
300	2.20	2.17	2.19	2.07	2.19	2.13
325	2.29	2.26	2.29	2.17	2.28	2.22
350	2.39	2.35	2.39	2.27	2.38	2.32
375	2.49	2.45	2.49	2.38	2.48	2.41
400	2.59	2.55	2.60	2.50	2.59	2.52
425	2.70	2.65	2.71	2.61	2.70	2.62
450	2.82	2.76	2.83	2.74	2.82	2.73
475	2.94	2.87	2.95	2.87	2.94	2.85
500	3.06	2.98	3.08	3.01	3.07	2.97
525	3.19	3.10	3.21	3.15	3.20	3.10
550	3.33	3.23	3.35	3.30	3.34	3.23
575	3.47	3.36	3.49	3.46	3.49	3.36
600	3.61	3.50	3.65	3.62	3.64	3.51
625	3.77	3.64	3.80	3.80	3.80	3.65
650	3.93	3.78	3.97	3.98	3.96	3.81
675	4.09	3.94	4.14	4.17	4.13	3.97
700	4.27	4.10	4.32	4.37	4.31	4.14
725	4.45	4.26	4.51	4.58	4.50	4.31
750	4.64	4.43	4.70	4.80	4.69	4.50
775	4.83	4.61	4.91	5.02	4.90	4.69
800	5.04	4.80	5.12	5.26	5.11	4.89
825	5.25	4.99	5.34	5.52	5.33	5.09
850	5.47	5.20	5.57	5.78	5.56	5.31
875	5.71	5.41	5.82	6.06	5.80	5.53
900	5.95	5.62	6.07	6.34	6.06	5.77
925	6.20	5.85	6.33	6.65	6.32	6.01
950	6.46	6.09	6.60	6.97	6.59	6.27
975	6.74	6.33	6.89	7.30	6.88	6.53
1000	7.02	6.59	7.19	7.65	7.18	6.81
1025	7.32	6.86	7.50	8.01	7.49	7.10
1050	7.63	7.13	7.83	8.39	7.81	7.40
1075	7.95	7.42	8.17	8.80	8.15	7.71
1100	8.29	7.72	8.52	9.22	8.51	8.04
1125	8.64	8.03	8.89	9.66	8.87	8.38
1150	9.01	8.36	9.27	10.12	9.26	8.73
1175	9.39	8.70	9.68	10.60	9.66	9.10
1200	9.79	9.05	10.10	11.11	10.08	9.49

Aduro devices are temperature-calibrated

2.52mA = 400°C in vac

5.09mA = 825°C in vac

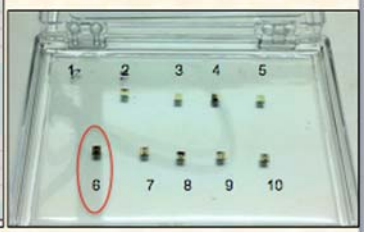

Fig. 1. Table of temperature vs. current in the heater membrane, calibrated for 6 of the Aduro heater devices shown e.g. inset in a 'gelpack' box. The temperatures are calibrated in a test chamber for each device, using infrared camera techniques. Currents for temperatures of 400°C and 825°C are indicated, see text for details.

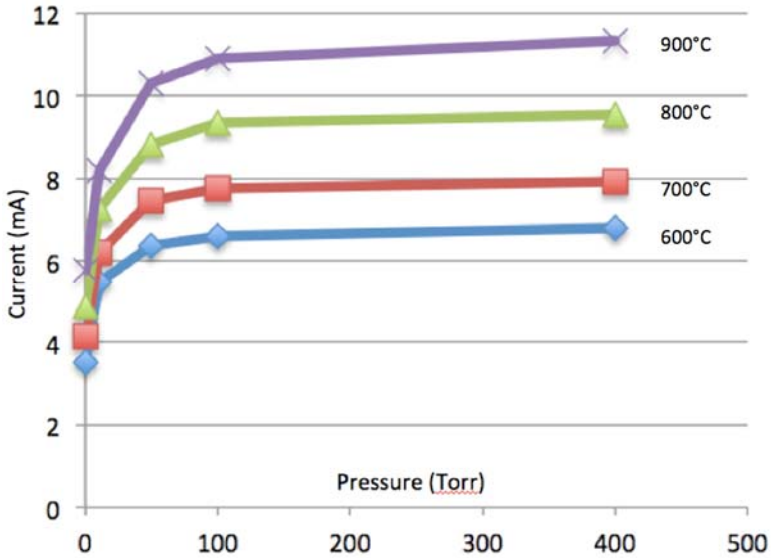

Fig. 2. Plot of current vs. pressure for 4 temperatures, showing the effects of increasing pressure on the temperature of heater membranes.

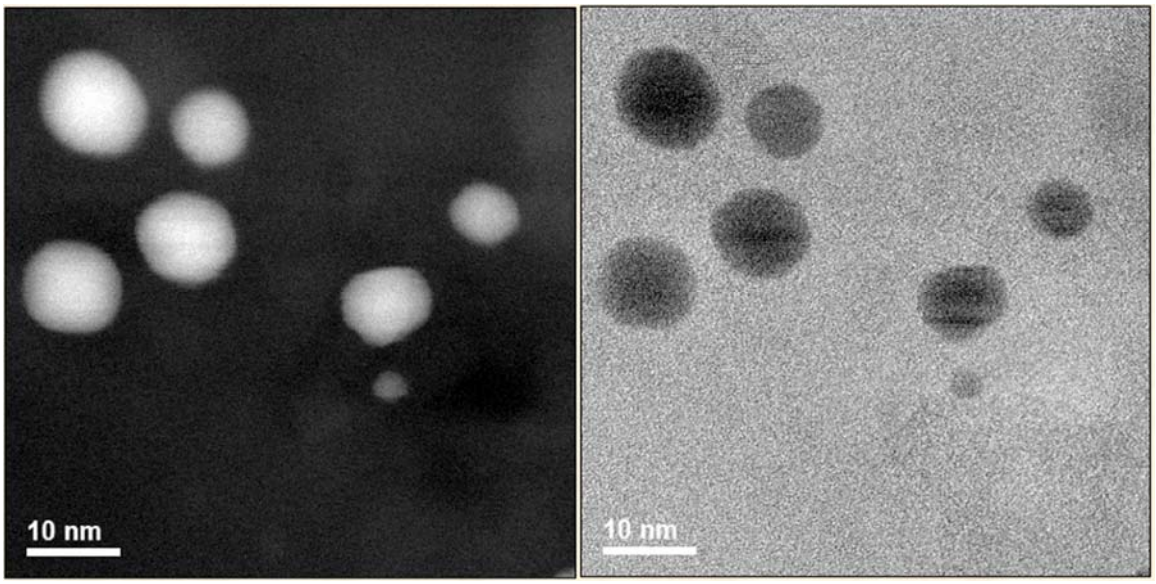

Fig. 3. HA-ADF and BF images of Au nanoparticles on the amorphous SiN heater window, at a nominal pressure of 0.71 Torr and temperature of 400°C. Images recorded at 2Mx direct magnification. Compare to Fig. 4.

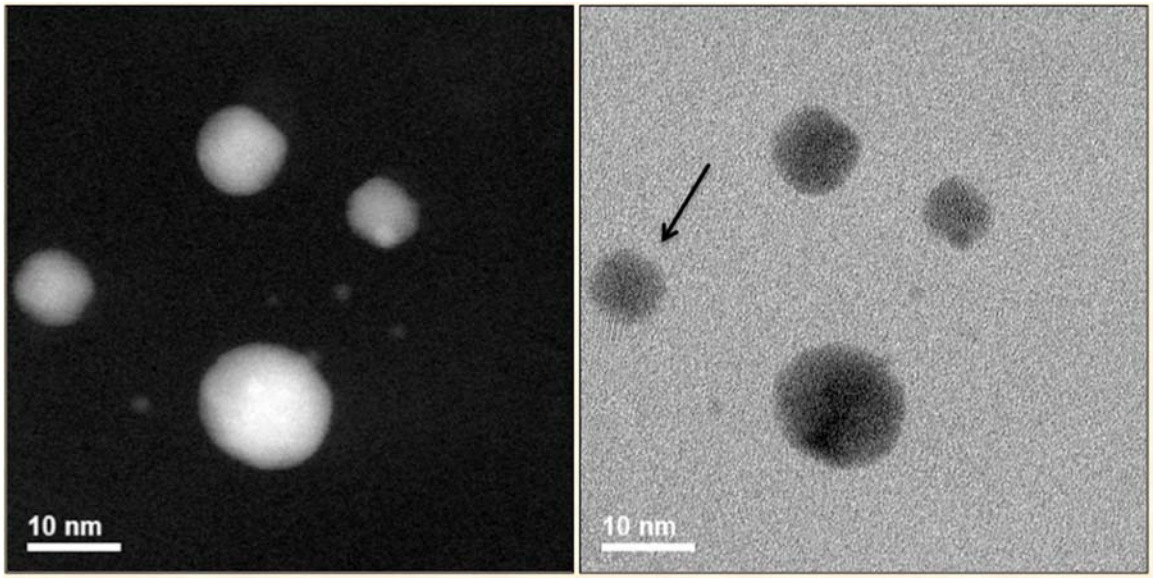

Fig. 4. HA-ADF and BF images of Au nanoparticles on the amorphous SiN heater window, at a full atmosphere of air, and a nominal temperature of 400°C. Note the signal level apparently unchanged by the presence of air in the cell. Images recorded at 2Mx direct magnification. Particle arrowed is shown in Fig. 5. Compare to Fig. 3.

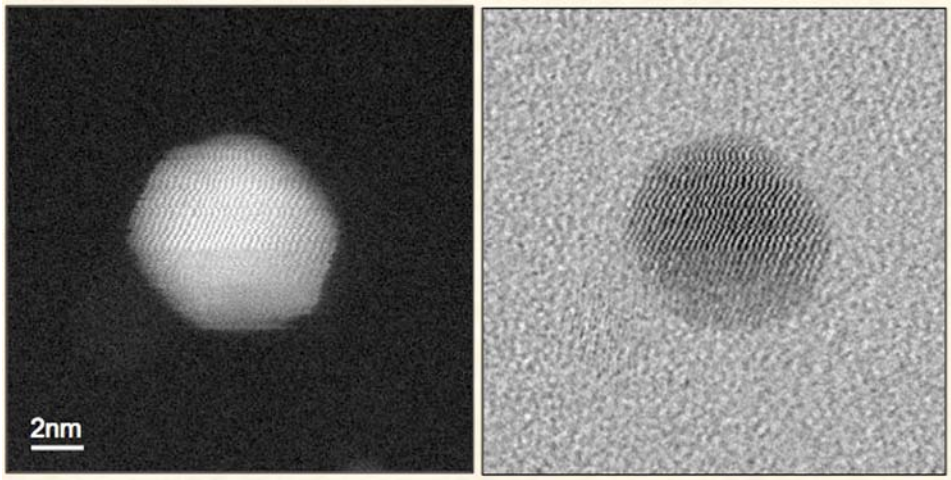

Fig. 5. HA-ADF and BF images of Au nanoparticles on the amorphous SiN heater window, at a full atmosphere in air, and a nominal temperature of 400°C. Images recorded at 5Mx direct magnification, showing 2.35Å lattice resolution of Au {111} planes.

Agreement 14957: High Temperature Thermoelectrics

A. A. Wereszczak, H. Wang, R. McCarty,* A. Thompson,* and J. Sharp*
Oak Ridge National Laboratory
***Marlow Industries, Inc.**

Objective/Scope

Two-thirds of the chemical energy in automotive fuel is rejected to the atmosphere as waste heat. Thermomechanical stresses must be managed and TE material strength must be improved to fully exploit TE devices for waste heat recovery. Toward that, needed thermomechanical and thermophysical properties of candidate thermoelectric (TE) materials are measured in this project and then used with established probabilistic reliability and design models to optimally design automotive and heavy vehicle TE modules. Thermoelectric materials under candidacy for use in TE modules tend to be brittle, weak, and have a high coefficient of thermal expansion (CTE); therefore, they can be quite susceptible to mechanical failure when subjected to operational thermal gradients. A successfully designed TE module will be the result of the combination of temperature-dependent thermoelastic property and strength distribution data and the use of the method of probabilistic design developed for structural ceramics.

Technical Highlights

Mechanical Property Measurements

A new test fixture was conceived and fabricated because of the need to strength test a very large number of Marlow-fabricated, small-sized Bi_2Te_3 bend specimens up to 250°C and achieve valid testing (i.e., fixture-specimen alignment). Its schematic representation is shown in Fig. 1. Completion of the large test matrix should occur early in Q4.

Residual stresses in the metallization used in Marlow thermoelectric devices continue to be estimated using a combination of finite element analysis and surface stresses measured using optical fluorescence on alumina substrates.

Residual Stress and Transport Property Measurements

Residual stress of a prototype skutterudite 4 x 4 leg-array TE module was evaluated at the High Flux Isotope Reactor (HIFR) in the May 2011 cycle. This study was based on preliminary earlier residual stress analysis runs on p-type and n-type elements. The strongest diffraction peak was selected to monitor d-spacing changes as a function of location within the TE module. The sampling volume was a pancake-shaped-slice with dimensions of 0.5 x 3 x 3 mm. Up to 12 measurements were carried out in the z-direction (i.e., parallel to heat and current flow direction). The same gauge volume was used with two stress free elements to obtain baseline values that were then subtracted from the measured d-spacing values. During the course of the testing, it was learned there was a slight composition change in the stress-free elements and the elements used in the module. Therefore, another test has been scheduled to re-evaluate the TE module in the August HFIR cycle. However, this test showed the neutron diffraction technique could be used to assess residual stress in the skutterudite-containing TE module.

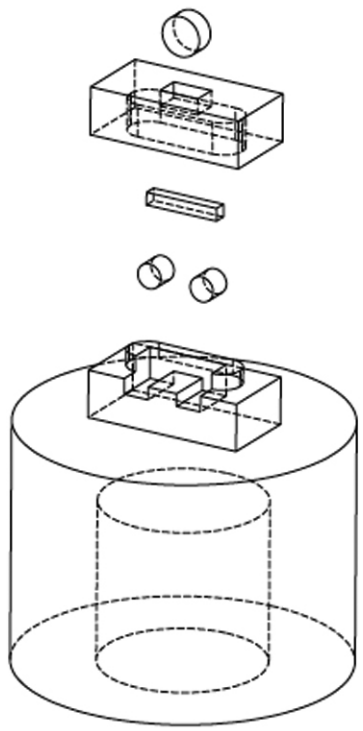

Figure 1. Exploded view of three-point-bend fixture designed and fabricated for temperature testing of TE materials up to 250°C. The shown bend specimen has nominal dimensions of 2 x 2 x 12 mm.

The thermal diffusivity, Seebeck coefficient, and electrical conductivity of a Mg-Ag-Sb system were measured.

Marlow skutterudite materials prepared by melt-spin and spark-plasma-sintering (SPS) were tested for thermal diffusivity, Seebeck coefficient and electrical conductivity as a function of temperature.

Hall effect measurements on Bi_2Te_3 and MgAgSb were conducted. A commercial system made by ECOPIA was used for preliminary study. Disk shaped samples about 1-2 mm thick were used. The results showed dependence on sample geometry. A second Hall effect system made at ORNL was used to compare the results. Marlow has provided a series of Bi_2Te_3 specimens with varying thickness to carry out a more detailed study on Hall effect measurements on thermoelectrics.

<u>Status of FY 2011 Milestones</u>

1. Generate thermoelastic and mechanical property database as a function of temperature on candidate p- and n-type TEMats fabricated by Marlow Industries as part of CRADA. [Sep11] *On schedule.*
2. Refine in-situ thermal-gradient-strength test method for TEMats. [Sep11] *On schedule.*

3. Transport properties measurements of selected thermoelectric materials. [Sep11]
   On schedule.

Communications/Visits/Travel

- A presentation describing this project's progress was made on 11 May 2011 at the DOE Annual Merit Review, Arlington, VA.
- Semi-annual CRADA review with Marlow was held on 25 May 2011 at Marlow (Dallas, TX).

Problems Encountered

None.

Publications/Presentations/Awards

J. R. Salvador, J. Yang, A. A. Wereszczak, H. Wang, and J. Y. Cho, "Temperature Dependent Tensile Fracture Stress of n- and p-Type Filled-Skutterudite Materials," Science of Advanced Materials, 3:1-10 (2011).

References

None.

Agreement 16308: MBD Thermoelectrics Theory and Structure

David J. Singh
Oak Ridge National Laboratory

Objective/Scope

We will use modern science based materials design strategies to find ways to optimize existing thermoelectric materials and to discover new families of high performance thermoelectrics for waste heat recovery and cabin climate control applications in vehicles. The emphasis will be on the thermoelectric figure of merit at temperatures relevant to waste heat recovery and vehicular climate control, as well as on other properties important for these applications, especially anisotropy, cost and mechanical properties.

Technical Highlights

Vehicular applications of thermoelectric materials for waste heat recovery, as well as climate control in vehicles (needed in particular for hybrid and electric vehicles) necessitate the study and identification of high performance materials comprised of elements that are low in cost and abundant. We continued our recent studies of such materials and in particular we have performed a detailed theoretical analysis (based on calculations done with the WIEN2K[1] and the in-house developed transport code BoltzTrap[2]) for the Zintl compound $CaMg_2Sb_2$. A closely related, isostructural and isoelectronic material (Mg_3Sb_2) has already achieved a ZT of 0.55 at 650 K[3] and based on our calculations the band structure of the Ca compound is more favorable.

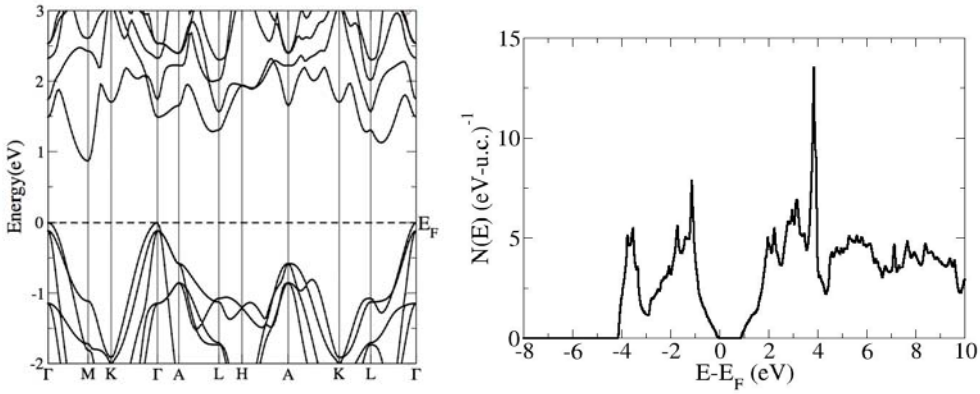

Figure 1: The calculated band structure (left) and density-of-states (right) of $CaMg_2Sb_2$. Note the comparatively small dispersions in the valence and conduction bands (left) and the large density-of-states just below the valence band maximum (right) and above the conduction band minimum, favorable for large thermopower.

This material is entirely comprised of inexpensive abundant materials, and in addition there are a substantial number of Zintl compounds, such as $CaMg_2Bi_2$ with similar structure and electronic properties whose alloying with this compound can be expected to result in additional increments to the ultimate performance (i.e., ZT) via lowering of

the lattice thermal conductivity. Samples of $CaMg_2Bi_2$ have been synthesized at Oak Ridge and tests of their thermoelectric properties are planned.

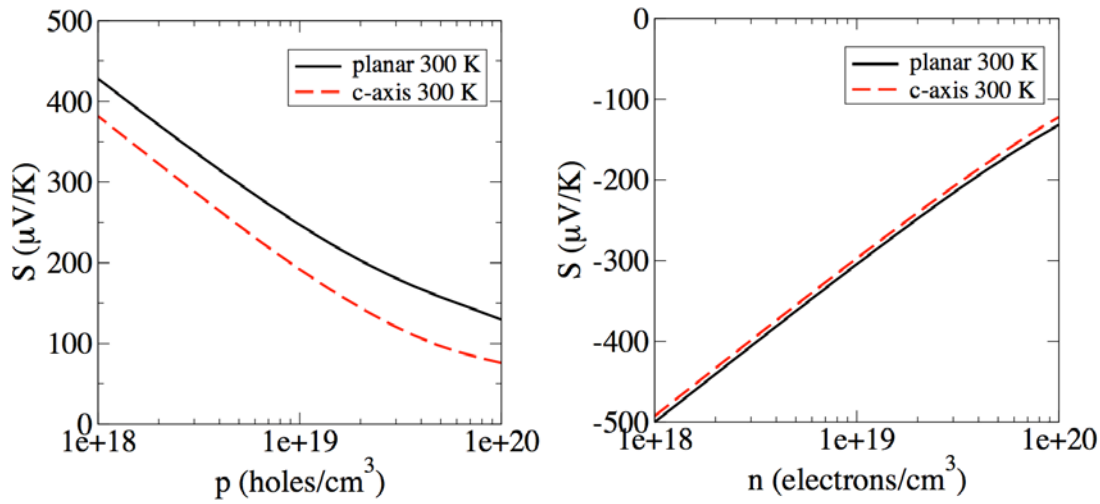

Figure 2: The thermopower (S) at various hole concentrations (left) and electron concentrations (right) of $CaMg_2Sb_2$ at 300 K. Note the thermopowers approaching -300 μV/K in the planar and c-axis calculations for electron concentrations near $10^{19}/cm^3$. High thermopowers at these concentrations generally bode well for thermoelectric performance. In addition, good thermopower is also present for hole-doping, with values above 200 μV/K at the hole concentration of $10^{19}/cm^3$. Materials showing good performance for both electron and hole doping are of particular value for applications such as (in this case) vehicle climate control, which require both p-type and n-type materials.

As reported at the Annual Merit Review Meeting, last year we did a number of calculations aimed at determining whether the performance of PbTe and PbSe were optimized, with the finding that they are not.[4,5] We predicted that those materials can have substantially higher figures of merit that were known if the carrier concentration were optimized. We found that ZT values as high as 2 may be achievable. Recent work by G.J. Snyder of Caltech[6] on an alloyed PbTe/PbSe system has come close to our prediction, with a ZT of 1.8 at 850 K reported in this system, and it is likely that additional optimization will raise this value still further.

Status of FY 2011 Milestones

We are making progress towards our milestone of successfully predicting new thermoelectric compositions. We plan to study Bi_2Se_3 as a possible low-cost replacement for Bi_2Te_3 in the temperature range 300-600 K, appropriate to vehicular thermoelectric refrigeration as well as a bottoming material in an exhaust heat recovery system. Specific studies will include first principles calculations of the electronic structure and transport. We also will perform calculations of the lattice dynamics of $CaMg_2Sb_2$ in order to better assess the potential of this material.

Problems Encountered

No significant problems encountered this quarter.

Publications/Presentations/Awards

1. D. Parker and D.J. Singh, "Transport properties of hole-doped $CuBiS_2$", Phys. Rev. B **83**, 233206 (2011).

2. D. Parker, M.H. Du and D.J. Singh, "Doping dependence of thermoelectric performance in Mo_3Sb_7: First-principles calculations", Phys. Rev. B **83**, 245111 (2011).

References

1. P. Blaha, K. Schwarz, G. K. H. Madsen, D. Kvasnicka and J. Luitz, WIEN2k, An Augmented Plane Wave + Local Orbitals Program for Calculating Crystal Properties (Karlheinz Schwarz, Techn. Universitat Wien, Austria), 2001. ISBN 3-9501031-1-2.

2. G.K.H Madsen and D.J. Singh, "BoltzTraP: a code for calculating band-structure dependent quantities," Computer Physics Commun. **175**, 67 (2006).

3. Takenobu Kajikawa, Naoyuki Kimura and Takahiro Yokoyama, "Thermoelectric Properties of Intermetallic Compounds: Mg_3Bi_2 and Mg_3Sb_2 for Medium Temperature Range Thermoelectric Elements", Proceedings of International Conference on Thermoelectrics 2003, IEEE.

4. D. Parker and D. J. Singh, "High-temperature thermoelectric performance of heavily doped PbSe," Physical Review B **82**, 035204 (2010).

5. D. J. Singh, "Doping-dependent thermopower of PbTe from Boltzmann transport calculations," Physical Review B 81, 191527 (2010).

6. Yanzhong Pei, Xiaoya Shi, Aaron LaLonde, Heng Wang, Lidong Chen and G. Jeffrey Snyder, "Convergence of electronic bands for high performance bulk thermoelectrics," Nature **473**, 66 (2011).